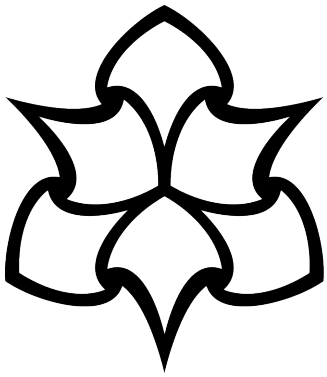

Investigation into the Electrochemical *N*-dealkylation of Tertiary Amides

MANDEEP KAUR

MPhil 2021

Investigation into the Electrochemical *N*-dealkylation of Tertiary Amides

MANDEEP KAUR

A thesis submitted in fulfilment of the requirements of the of the Manchester Metropolitan University for the degree of Master of Philosophy

Department of Natural Sciences

Division of Chemistry and Environmental Science

Manchester Metropolitan University

2021

Abstract

This thesis reports a novel reagent-less dealkylation of benzylic amides with varying steric effects and electronic properties of an attached group. Complex drug structures are explored to probe the feasibility of the reaction. Electrosynthetic experiments were performed at room temperature in an undivided cell using tetrabutylammonium perchlorate (TBAP) as an electrolyte. Reticulated vitreous carbon (RVC) was used as both the working and counter electrode. The constant current method was employed for the reactions. An optimisation survey found that changing the electrochemical process from controlled voltage to controlled current conditions led to deethylation. Methanol was found to be essential for *N*-deethylation to occur. Using the controlled current method *N*-deethylation of *N,N*-Diethylbenzamide (**106**) was achieved with an isolated yield of 86%. The proposed reaction mechanism indicates the reaction proceeds *via* one of the two pathways, pathway A dominates and proceeds *via* the typical Shono α-methoxylation initiation.

Chapter 1 introduces and includes examples of general electrochemical concepts that apply to organic electrosynthesis. The chapter consists of electrochemical methods and techniques for the analysis of small molecules. The literature review compares the emerging trends using electrochemistry coupled to LC-MS to detect the presence of *N*-dealkylated drug metabolites and current trends for the *N*-dealkylation of amides, including conventional methods.

Chapter 2 reports the optimisation survey of **106** for electrochemistry and purification method, LSV of the compounds is discussed, and the reaction mechanism is proposed.

Chapter 3 reports the electrosynthetic dealkylation survey of amides. LSV survey of the selected compounds were analysed and indicated that stronger electron-donating substituents did not give dealkylation. The use of electrochemistry to study the *N*-dealkylation of drug and herbicides molecules are also described. The LSV of molecules were examined, and HPLC was explored to purify the products. *N*-dealkylation of complex compounds requires further probing using electrochemical methods and optimisation to obtain the final product. Finally, the chapter summaries key research findings for the work. The Chapter also explores future work and the

diverse approaches for further research, such as; use of flow cells for the oxidation of the amides.

Chapter 4 presents the procedures for the synthesis of amides and electrochemical methods used during the thesis. It contains compound characterisation using the following methods: LC-MS, ^{1}H-NMR and C^{13}-NMR.

Academic Aims of the Investigation

Academic Aims:
The work aimed to investigate the viability of *N*-dealkylation of tertiary amides when applied to various tertiary amide structures.

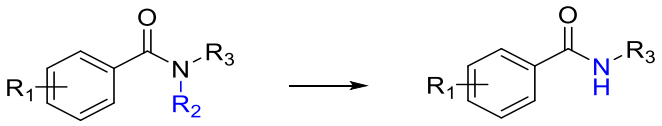

Objective:

1. Synthesis of benzylic amides with varying steric effects, electronic properties and the electron-withdrawing ability of an attached group on the amide-donating compound.
2. Optimisation of electrochemical parameters using *N,N*-Diethylbenzamide (**106**).
3. Hypothesis and inference of reaction mechanism.
4. Application of the data collected from optimisation to the selected drugs and herbicides.

Abbreviations

Abbreviation	Definition
MeCN	Acetonitrile
A	Amps
CE	Counter electrode
CV	Cyclic voltammetry
Cy	Cyclohexane
CYP-450	Cytochrome P-450
ECE	Electron transfer, chemical reaction and electron transfer
EDG	Electron Donating group
Et	Ethyl
EtOAc	Ethyl acetate
EWG	Electron withdrawing group
Flash Column Chromatography	FCC
GCE	Glassy carbon electrode
g	Grams
HPLC	High performance liquid chromatography
HOMO	Highest occupied molecular orbital
HLM	Human liver microsomes
iPr	Isopropyl group
LSV	Linear sweep voltammetry
LC-MS	Liquid chromatography-mass spectrometry
LUMO	Lowest unoccupied molecular orbital
MS	Mass spectroscopy
MHz	Megahertz
MeOH	Methanol
Me	Methyl
mL	millilitre
mmol	millimolar
mV	Millivolts
M	Moles
NBZ	Nitrobenzene
NMR	Nuclear magnetic resonance
Ppm	Parts per million
RLM	Rat liver microsomes
RE	Reference electrode
RMM	Relative molecular mass
RVC	Reticulated vitreous carbon
TBAP	Tetrabutylammonia perchlorate
WE	Working electrode

Content

List of Schemes

List of Figures

List of Tables

Chapter 1: Organic and Metabolites Synthesis using Electrochemistry

1. Introduction

Volta Pile's[1] innovation of an electric battery observed the continuous movement of electrons and is considered the first electrochemistry experiment that can be traced back to the 1800s.[2] Terms such as electrolysis, anode, cathode were introduced in the infancy of electrochemistry and have formed an essential part of the vocabulary.

Faraday's endeavours in the 1830s generated curiosity in using the electric current to initiate nonspontaneous organic reactions. Faraday's application of potential led to the observation of movements of ions through a solution, hence, leading to the current application of ionic salts as electrolytes to increase the conductivity of an organic system.[3]

The first organic electrochemical experiment was Faraday's electrolysis of acetic acid. This inspired the Kolbe electrolysis in 1847, where anodic oxidation of a prevalent carboxylic acid gave a favourable way to access alkyl radicals.[4] The first electrochemical cathodic reduction of an organic compound was Schoenbein's dehalogenation of trichloromethanesulfonic acid.[5]

The use of electrochemistry is being explored in several areas of chemistry; one such area of interest is using electrochemistry to study metabolites of drugs. Detection of possible toxic metabolites of drugs is a vital step in the development of new drugs. It is imperative to comprehend how these drugs will behave in the body. Current techniques for testing new drugs include the use of *in vivo* or *in vitro* methods. The process of performing experiments with cells outside their standard biological settings is known as *in vitro,* and these types of experiments are usually conducted in petri dishes or test tubes*. In vitro* drug metabolism studies are used for screening and characterising drug metabolites. They provide information regarding drug pathways and make suggestions for further *in vivo* testing.[6]

The use of living organisms such as animals or human models for testing the drugs is known as *in vivo,* which includes hepatic (metabolism of drugs in the liver using numerous enzymes) and non-hepatic microsomes.[7] The breakdown of Eukaryotic cells in the laboratory to produce endoplasmic reticulum pieces and from this vesicle-like artefacts are reformed to microsomes.[8]

Liver cells or subcellular segments from animals and humans are easily accessible and therefore are generally utilised to investigate drugs *in vivo* at the initial stage of drug discovery. [9] The most widely used microsomes from an animal are the rat liver microsomes (RLM) as they contain high concentrations of cytochrome P450 (CYP450) (Scheme 2)[7] The bulk of drug-metabolizing enzymes, predominantly CYPs, are primarily found in liver cells but also originate in the intestines and lungs.

Liver microsomes containing vesicles are derived from the hepatocytes endoplasmic and therefore include a complete set of drug metabolising enzymes and are often employed to study enzyme induction processes. However, the isolation of hepatocytes can be difficult as cell damage may occur, and the procedure is more complex than using liver cell homogenate.[10]

However, these methods of testing drugs have several disadvantages, including the development of reactive metabolites or intermediates, which have short half-lives. These are difficult to detect, and the replication of reaction conditions *in vitro* procedures is challenging. These short-lived species tend to covalently bond to cellular macromolecules, such as proteins and DNA. [7, 11]

Scheme 1 is an example of oxidative metabolism of aminophenol or phenylenediamines, where dehydrogenation by CYP produces quinones, quinone imines, or quinone diimines and eventual binds to glutathione or cellular macromolecules. Apart from the complicated testing methods, the cost and time associated with testing drugs is extensive.[11]

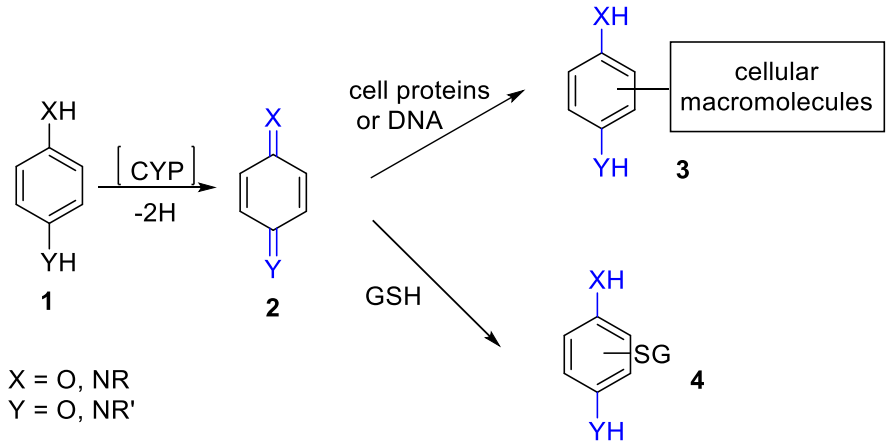

Scheme 1: Oxidative metabolism of aminophenol or phenylenediamines.[11]

An alternative method for detecting metabolites is to use electrochemistry. Electrochemistry consists of the addition or removal of electrons from the electrostatic pull between electrons and nuclei when an electrical potential is applied.[12] It is the simplest way of interacting with molecules. Applications of electrochemistry can be found in various fields of chemistry, including analytical[13-15] and synthesis of organic compounds [2, 12, 16-18]

As an alternative to toxic and potentially dangerous oxidising and reducing chemicals, electricity is used. Therefore, electrochemistry is considered an environmentally favourable procedure for performing oxidations and reductions of compounds. The electroactive substances can be examined by applying the following methods: differential pulse, cyclic voltammetry, direct and indirect electrolysis (Section 1.4).[12]

Electrochemistry methodology can imitate the major redox reactions that take place in the human body.[19, 20] There are several advantages to using electrochemistry compared to the classical method for studying metabolism. Metabolites with short half-lives and stable species can be detected quickly and cleanly (i.e. organ extraction and animals).

Mechanistic insight into a drug's metabolism pathway could be gained by using cyclic voltammetry and spectroelectrochemistry methods to detect transient metabolites. The drugs are analysed in a non-cellular environment, which makes scalability, reproducibility and purification easier.[7] Drug metabolism data is

replicated faster and is more effective when compared to the widely used techniques.

Although the literature is filled with various methods of testing and detecting drugs using electrochemistry coupled with LC-MS[21-24], there are scarce examples of isolated drug metabolites.

A typical functional group found in drugs is the amide bond. In 2017 it was present in 60% of newly approved drugs.[25] It is nature's most fundamental connecting group (e.g., peptides and proteins) and is predominant in naturally occurring and synthetic compounds. [26] [27-29] Amides are crucial in the development and composition of biological and chemical systems.[30] They play a vital role in the construction of pharmaceuticals, agrochemicals, and polymers (Figure 1).[27-31] Drugs containing amide bonds can lead to the formation of *N*-dealkylated metabolites.[32-36]

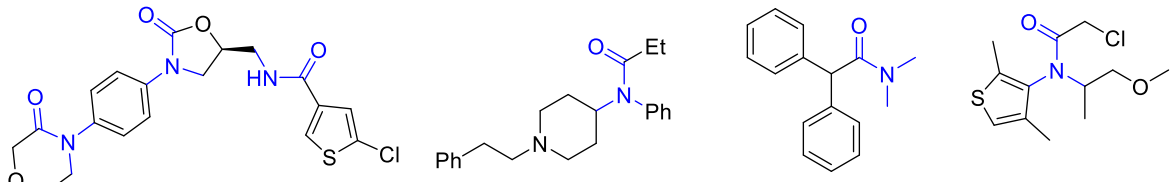

Figure 1: The amide bonds present in pharmaceuticals and agrochemicals compounds.

The sections below explore the essential concepts that are required in organic electrosynthesis. The sections Include current trends in *N*-dealkylation of amides, use of electrochemistry to study drug metabolism and the scope of using electrochemistry as a method in a wider area of organic chemistry.

1.1. Introduction to drug metabolism

For a drug to metabolise, it needs to be converted into a more polar form during metabolism before it is eliminated from the body.[37] For drugs to be approved, a balance is required within the absence of metabolism (drug build-up, preferred metabolism, e.g. pro-drug release) and rapid metabolism (short half-life/duration of action) dependent on the drug target.[38]

Drugs are metabolised in the body in two stages: Phase I and Phase II metabolism. Phase I metabolism involves oxidative, reductive, or hydrolytic reactions that either expose a previously masked polar group in the drug or add a polar group. The majority of phase I metabolisms proceed *via* the CYP-450 family of enzymes. CYPs can stimulate other forms of oxidative transformations, for example, heteroatom-dealkylation, dehalogenation, and dehydrogenation.[39] The hydrolysis of an ester to a carboxylic acid, the addition of a hydroxyl group to a C-H bond and reduction of a nitro group to an amine is a typical example of phase I metabolism.[40]

There are numerous CYP isoforms due to the variation found in the protein sequence. The CYP450 class of enzymes are monooxygenases that utilise an essential haem group to oxidise their substrate (Scheme 2). Scheme 2 shows the catalytic cycle of CYP450 and the mechanism of action for the drug.

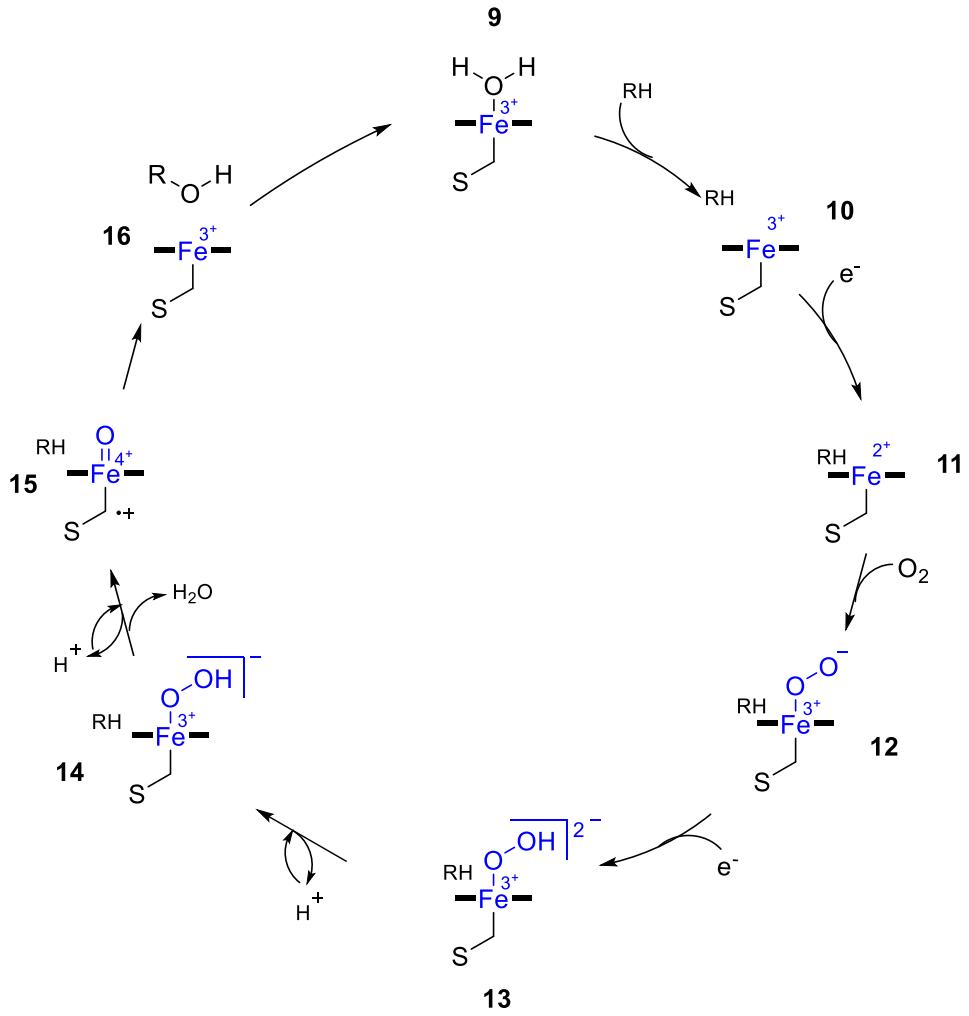

Scheme 2: Catalytic cycle of cytochrome p450.[41]

9 Ferric (Fe^{3+}), a 6-coordinate low spin heme iron axially coordinated by cysteine thiolate (S) and a feebly attached water molecule (H_2O), is the start of the reaction order where p450 is in an inactive state. A 5-coordinate high spin heme iron (**10**) is formed when restraining of a substrate (RH) eliminates the water ligand. Ferric-superoxo (**12**) complex is produced when a redox partner reduces **10,** and the ferrous iron binds to dioxygen. The ferric-peroxo intermediate (**13**) was created via a single electron reduction by the redox partner. **13** is then protonated to produce a transient ferric-hydroperoxo species (**14**). **14** undergoes additional protonation and dehydration to fabricate compound **15,** the ferryl-oxo porphyrin radical cation species. **15** is thought to be the key oxidant in CYP450 reactions and abstracts hydrogen from RH to form **16** substrate radical before "recovering" the hydroxyl to the substrate to form hydroxylated product and to restore the resting state **9**.[42, 43]

Phase II metabolism includes reactions on the exposed or added polar group via conjugation to further increase the polarity of the drug metabolite, which enables clearance from the body. Phase II conjugates include reactions with carbohydrates (glucuronidation) and peptides (in particular glutathione) and the addition of sulphate groups.[37]

An additional method of predicting a metabolite is to use *in silico* methods.[44] This is a computer-based approach that is divided into various sub-sections. Based on the data collected on the knowledge of CYP-active sites, calculations can be made using *in silico* method to optimise studies using a lead structure towards its metabolic stability.[44] This could result in a more efficient drug discovery and development process.

1.2 Preparative Electrosynthesis of drug metabolites

The review "Metabolism Inspired Electrosynthesis" was published in *ChemElectroChem* by the group in 2019.[37] There are numerous advantages to using mass spectrometry (MS) directed electrosynthesis. This enables the avoidance of laborious synthetic development. The combination of MS and electrochemistry has led to the prospect of isolating potential drug metabolites on a preparative scale.

Paci and colleague[45] (Scheme 3) reported a method to isolate the analogous α-methoxy metabolites with equipotent activity to the natural α-hydroxy metabolites using the controlled current method. The anodic oxidation was conducted in current-controlled conditions in an undivided cell with graphite rod as electrodes. Ifosfamide **17** gave two stereoisomers and is metabolised to 4-hydroxy-ifosamide **(19**) at 48%, and Cyclophosphamide (**21**) at 36%. **18** is metabolised to 4-hydroxycyclophosphamide**. 17** and **18** are examples of alkylating agents used in sarcoma and cerebral tumours. A single product for *Cyclophosphamide* was observed and gave **22** at 40% isolated yield (**20** was not detected).

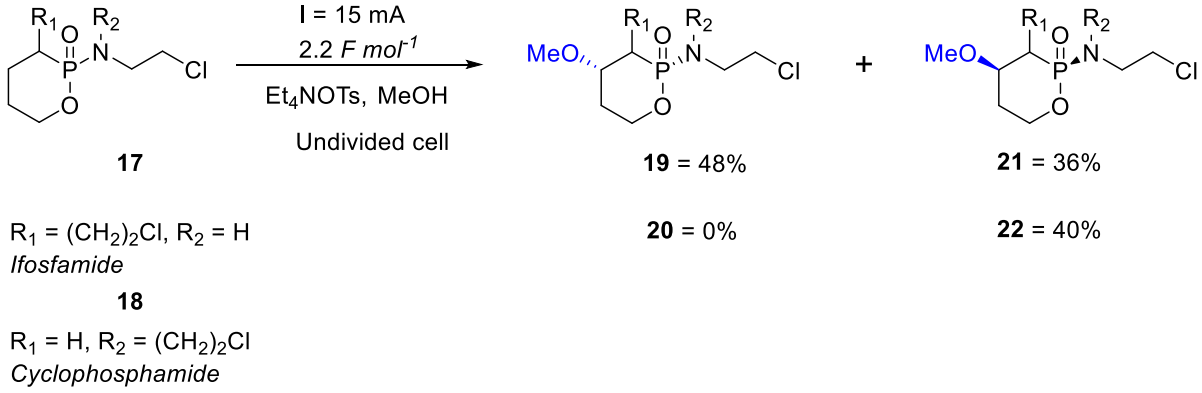

Scheme 3: Electrochemical oxidation of Ifosfamide (**17**) and Cyclophosphamide (**18**).[45]

Nouri-Nigjeh and co-workers[46] synthesised an aromatic hydroxylation of Lidocaine (**23**, a local anaesthetic) using electro-Fenton conditions (Scheme 4) and a square wave pulse sequence (between 0.2 – 12.0 s). This improved the selectivity of hydroxylation (**24**) and dealkylation (**25**) by 50-fold, and a yield of 10% for **24** and **25** were recorded. In comparison, a potential of +5000 mV resulted in low yields of both aromatic hydroxylation (**24**) and dealkylated (**25**) products.

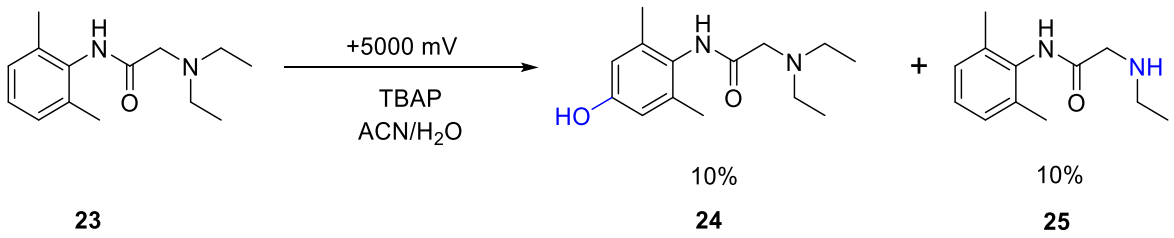

Scheme 4: Lidocaine (**23**) electro-oxidation using a square wave pulse sequence.[46]

A modified method for the dealkylated metabolites for Fesoterodine (Scheme 5) was reported by Torres and colleagues at Pfizer.[47] **26** was used as a reference compound for the chromatographic observation of the deterioration of the antimuscarinic drug in biological systems. 89% conversion yields were reported for the mono amine dealkylation (**27**) and deamination (**28**).

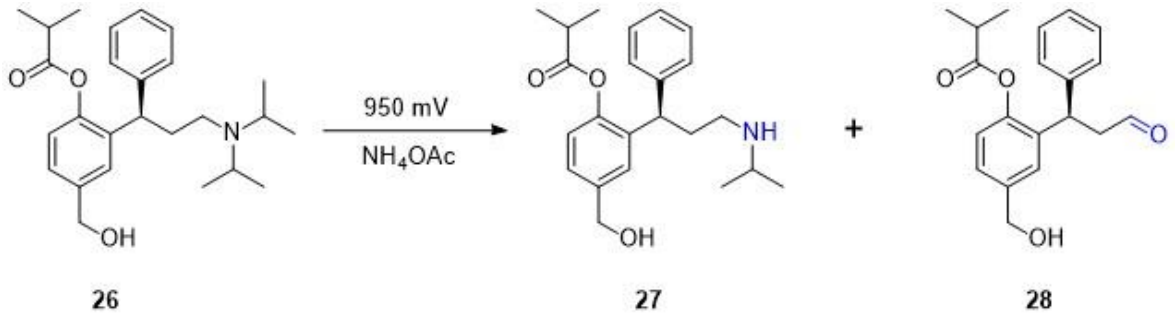

Scheme 5: Electrochemical oxidation Fesoterodine (**26**).[47]

Roth and colleagues employed a combination of preparative, potentiostatic or galvanostatic electrosynthesis in flow. [48] Their work highlighted that it is possible to accomplish a clean late-stage electrosynthesis of drug metabolites. The *Peri*-oxidation of the methylene next to an amide or urea to the imide moeity and *S*-oxidation from sulphide to sulfoxide (no over oxidation to sulfone). Scheme 6 shows the corresponding products of the drugs were achieved using a mixture of these methods. Tolbutamide **29** (a hypoglycaemic medication) using the potentiostatic method led to **30** with an isolation yield of 19%. Primidone **31** (an anticonvulsant medication) gave **32** at 24%. Albendazole **33** (anthelminthic drug) led to **34** at 38%, and finally, chlorpromazine **35** (an antipsychotic drug) gave **36** at 51%. Prepared oxidation products for **29** are recognised biological metabolites of the drug molecule.

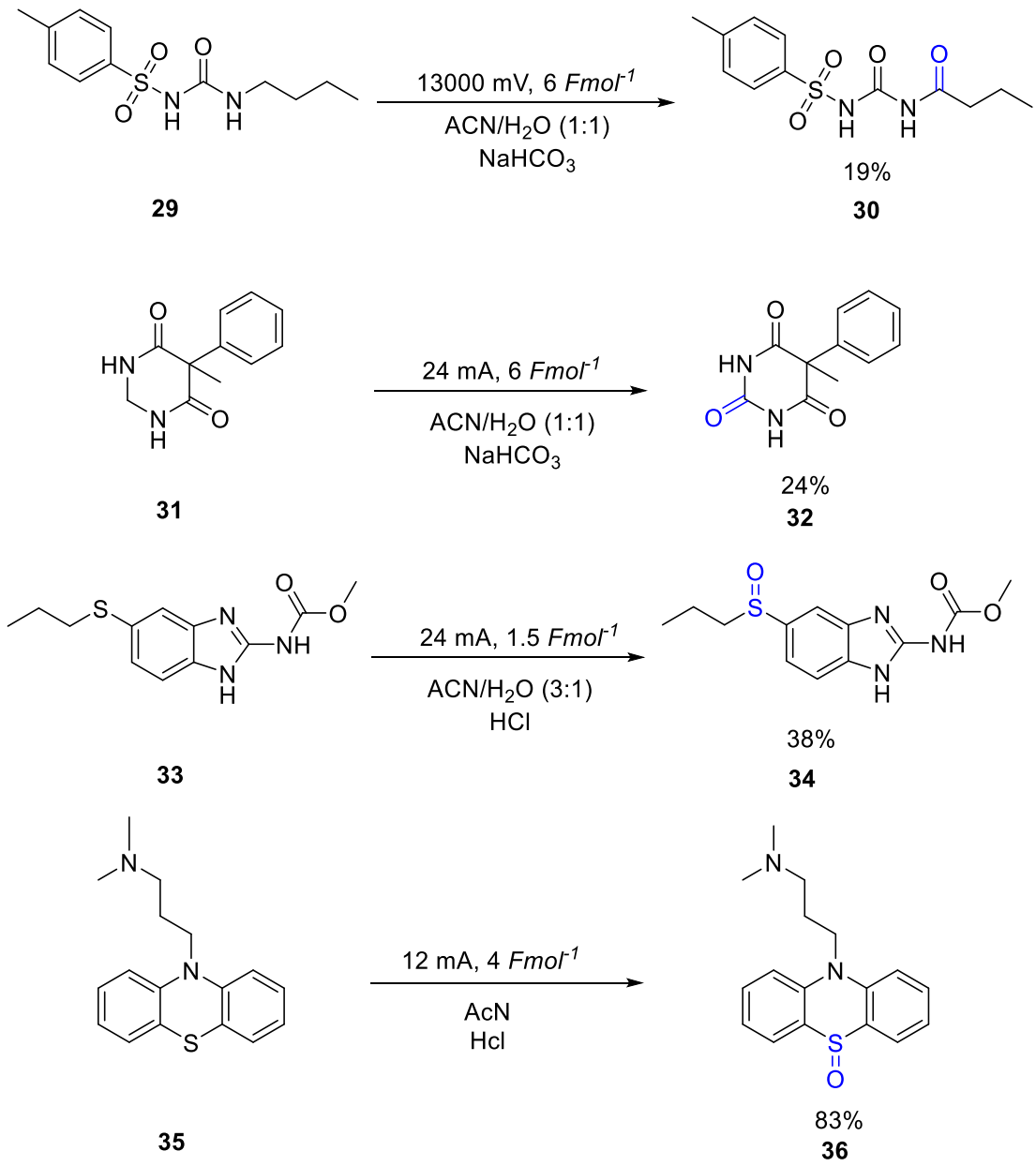

Scheme 6: Oxidation of sulphides and methylene groups on drug molecules.[48]

1.3 Brief review of the method for *N*-dealkylation

The *N*-acyliminium ion is mandatory in developing the carbon-carbon bond in an amide-containing compound.[49, 50] The formation of an intermediate *N*-acyliminium ion can lead to *N*-dealkylation and other C-X bonds. This substantial characteristic is seen in the formation of cyclic and heterocyclic ring systems, such as the Pictet-Spengler and Diels–Alder reactions.[51, 52]

Shono-oxidation is a reaction of electrochemical anodic oxidation of an unfunctionalised amide. It contributes a complementary approach to the C-H activation of a low reactivity intermediate. Yoshida[53], Jones and Banks[54] have extensively reviewed Shono oxidation.

Some examples precede Shono's work in anodic oxidation/alkylation of amides.[55, 56] However, Shono *et al.*[57, 58] demonstrated the synthetic value of linking an electroorganic step with a vital carbon-carbon bond-forming reaction needed in organic chemistry. Scheme 7 shows the first recorded direct electrochemical anodic oxidation of an α-methylene group (**38**). **39** was isolated with a yield of 70-80% using anodic oxidation, further treated with Lewis-acid, and subsequent addition of a nucleophile to produce a novel carbon-carbon bond.

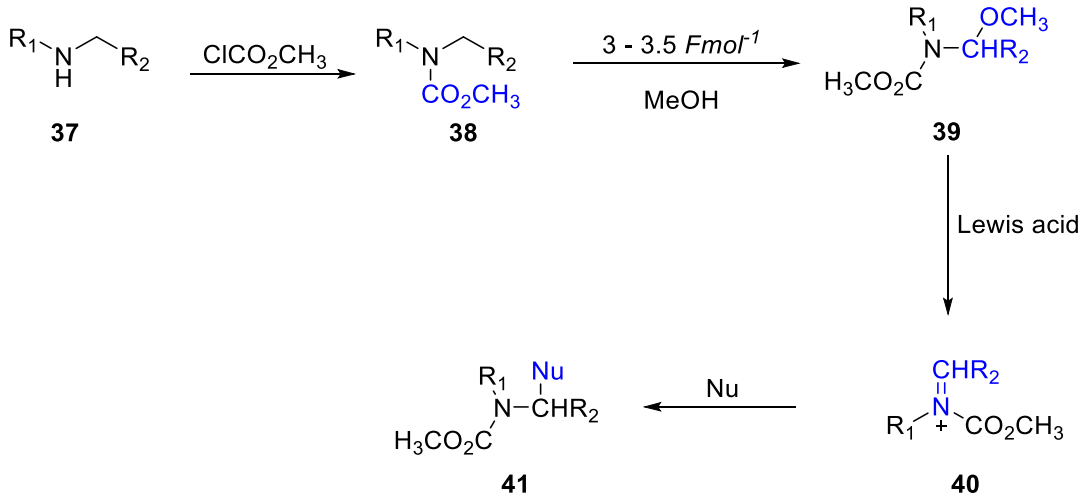

Scheme 7: Chemical and electrochemical combined reaction for the Shono oxidation.[58]

Hall *et al.*[59] 1990 suggested that a substantial change in the rate of a chemical reaction for *N*-dealkylation by CYP-450 led to hydrogen atom abstraction in amides and electron abstraction in amines (Scheme 8). This is perhaps due to the significant change in the kinetics and selectivity of *N*-dealkylation of amides vs amines.

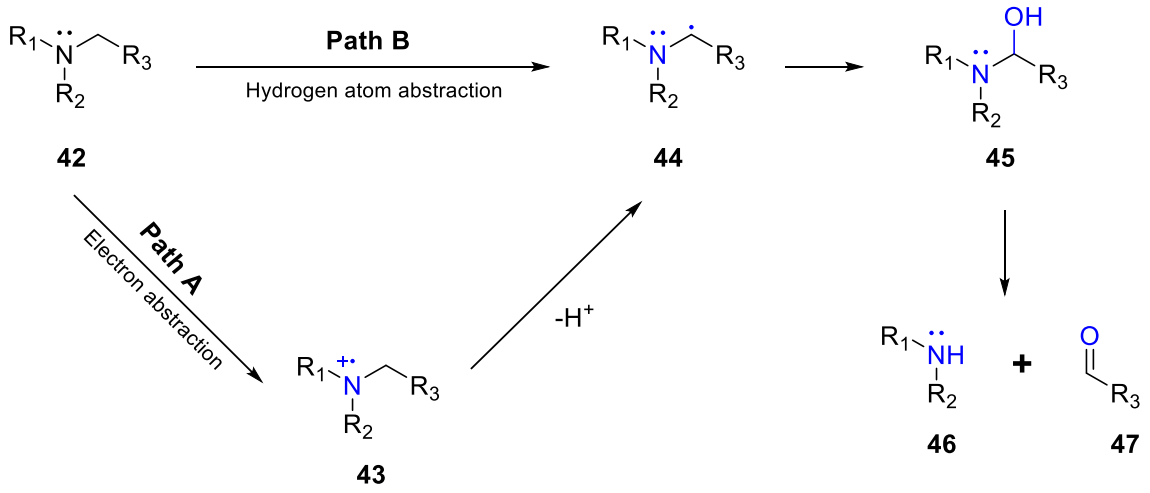

Scheme 8: **Path A**: electron abstraction mechanism for the amine during metabolism. **Path B**: Hydrogen atom-abstraction mechanism for amide metabolism.[59]

To understand the *N*-dealkylation of amides, Hall *et al.*[60] in 1991 conducted mechanistic studies and the impact of *N*-substituents on rates and selectivity. Amides (Scheme 9) were incubated *in vitro* with liver microsomes from phenobarbital-induced rats and went through mono-*N*-dealkylation. The amide nitrogen of the substrate with two different alkyl substituents leads to the duo producing mono-*N*-dealkylated products.

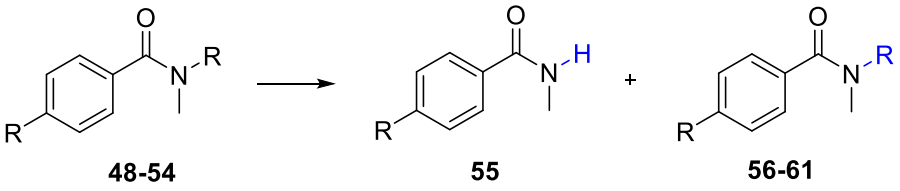

R = Me Et nPr nBu $PhCH_2$ isoPr cycloPr
48 49 50 51 52 53 54

Scheme 9: Amides selected for the mechanistic study.[60]

Scheme 10 shows the possible reaction pathways when one-electron oxidation by CYP-450 takes place. Rather than α-carbon deprotonation, the iminium cation radical reacts through fragmentation of the cyclopropyl ring and covalent modification of the enzyme (pathway d, R = alkyl, benzyl). *N*-dealkylation of amines by p-450 has a low kinetic deuterium isotope effect and is more selective towards removing a methyl group rather than a primary or secondary alkyl group.

Compared to the amines, amides have higher oxidation and a substantial intramolecular deuterium isotope effect. Hence, *N*-dealkylation of amides is instigated by α-hydrogen atom abstraction instead of electron abstraction (pathway a & f) and, therefore, the greater inclination for *N*-demethylation of **54** and the apparent absence of general suicide substrate activity by **54**.

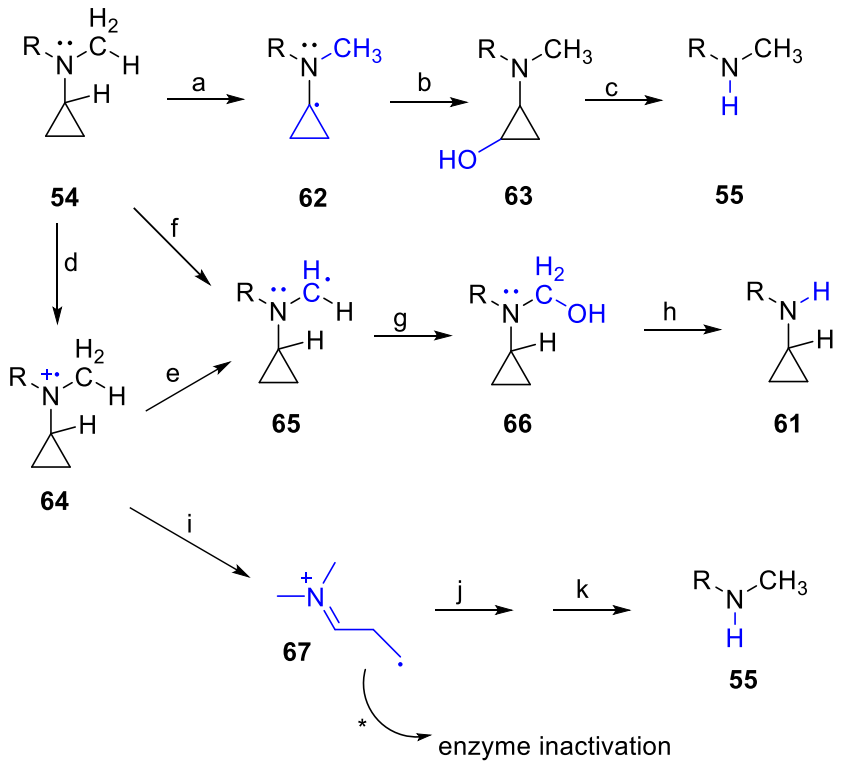

Scheme 10: Reaction mechanism pathway for microsomal and anodic oxidation.[60]

Anodic oxidation of **54** (Scheme 10) [61] was conducted using methods previously reported by Hall *et al.*[61] 1989. The intermediates involved in the reactions were observed, and the overall kinetic deuterium (reaction rate) was studied. Initial experiments were conducted in the conditions reported by Shono *et al.*[57] for anodic oxidation. However, these conditions (+1.1-1.2 V, 4 *Fmol*$^{-1}$, methanol as solvent) did not affect the selected amide dealkylation. Controlled potential electrolysis (+2.0 V) was conducted in a cell with two chambers, an anode and cathode separated with a glass frit. 2 *F*mol^{-1} was used as electron transfer wire mesh. A platinum electrode was used as a working and sodium perchlorate as an electrolyte.

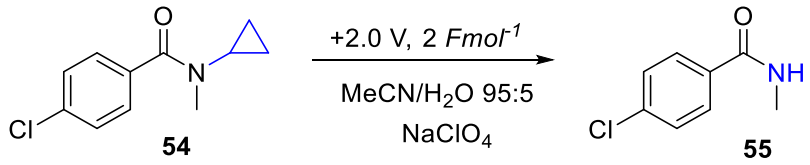

Scheme 11: Anodic oxidation of **54** using electrochemistry.[61]

The anodic oxidation reactions gave a clean product (**55)** via *an* electron abstraction mechanism (isolated yields are not reported). The ratios between demethylation/dealkylation in microsomes (43:1) vs anodic oxidation (1:35) varied significantly. **56** is the primary product of anodic oxidation as electron abstraction. **54** (pathway i) is preferred to the opening of the cyclopropyl ring with the simultaneous release of strain energy instead of deprotonation of a methyl group (pathway e).

Iley *et al.*[34] investigated regioselectivity and stereoselectivity of amide dealkylation using chemical and microsomal methods. Chemical oxidation used 5, 10, 15, 20-tetraphenylprophyrinatoiron (III)/ tert-butylhydroproxide (TPPFe/ButOOH). TPPFe/ButOOH was selected because they are involved in hydrogen atom abstraction mechanisms involving the *tert-butoxyl* radicals. Phenobarbital-induced rat liver microsomes were used for the microsomal method.

Microsomal dealkylation is regioselective for *Z*-alkyl groups, and the selectivity comes from protein substrate interactions in the enzyme active site instead of any fundamental chemistry of the haem unit. To gain insight into how regioselectivity of the dealkylation proceeds, conformationally, rigid lactams **68-70** were chosen (Scheme 12). Under chemical and microsomal conditions, ring oxidation **71, 74, 77** demethylation **72, 75, 78** and both ring oxidation and oxidative demethylation **73, 76,** and **79** were produced. The noticeable difference between chemical and microsomal is that during microsomal conditions, **68** reacts readily, and demethylation is favoured to ring oxidation.

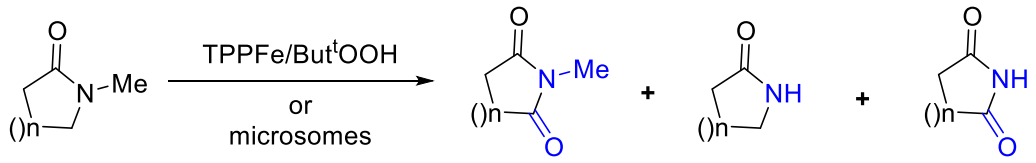

68 n = 1
69 n = 2
70 n = 3

71 n = 1
74 n = 2
77 n = 3

72 n = 1
75 n = 2
78 n = 3

73 n = 1
76 n = 2
79 n = 3

Scheme 12: The products of microsomal oxidation of lactams biometric.[34]

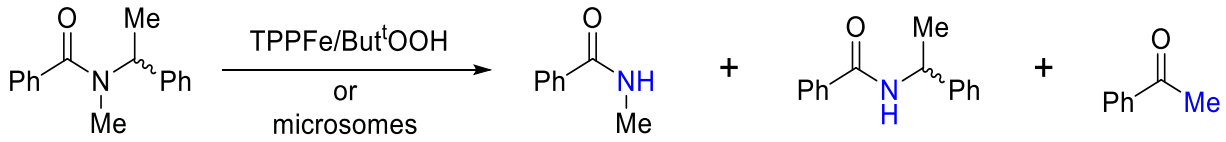

80 **81** **82** **83**

Scheme 13: Products of oxidative dealkylation of **80**.[34]

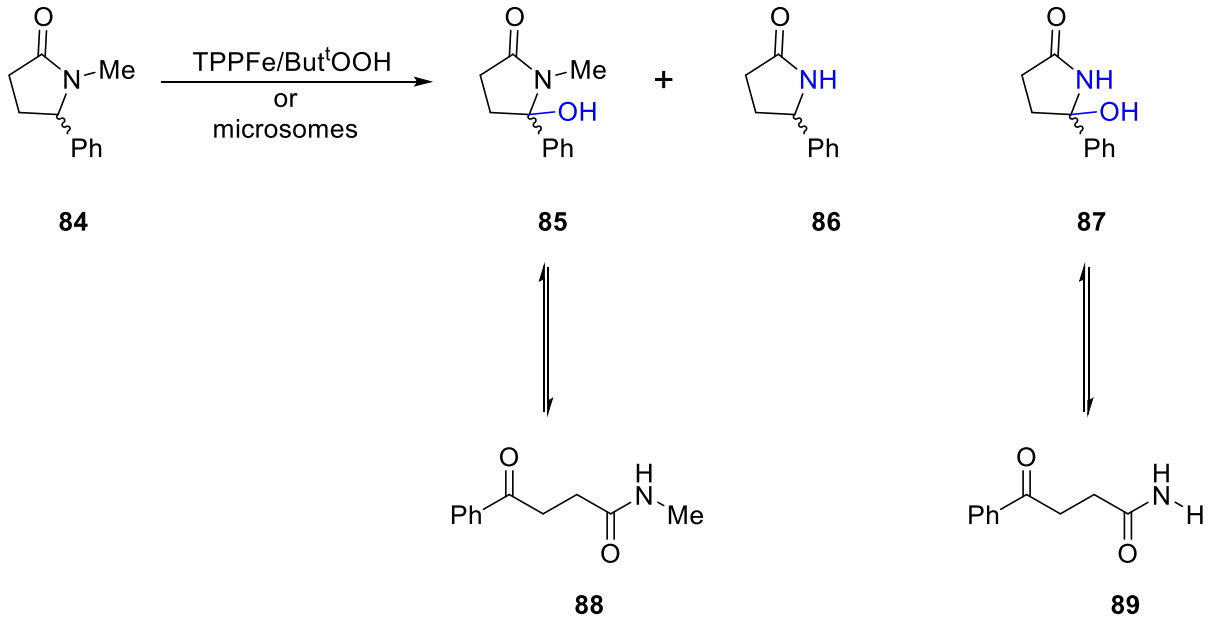

84 **85** **86** **87**

88 **89**

Scheme 14: Dealkylation of **84**.[34]

To examine the stereo-selectivity of the dealkylation, the following compounds were selected **80** (acyclic amide), where the rotation (Scheme 13) about the C-N bond is permitted, and **84** (cyclic amide) where amide conformation is static (Scheme 14) were selected. For **80**, loss of the secondary alkyl group is preferred, and in **84,** ring-oxidation is favoured over demethylation when using the chemical method. In microsomal (*R*)-**80,** dealkylation is preferred over demethylation, whereas (*S*)-**80**

demethylation is preferred. Microsomal oxidation of (*R*)-**84** and (*S*)-**84** ring oxidation at the 5- position of the pyrrolidone ring is favoured over demethylation. The (*S*) enantiomer goes through ring oxidation 2-3 times more readily than the (*R*)-enantiomer. [34]

Lorenc *et al.*[62] *r*eported deprotection of tertiary amides containing the *N*-isopropyl group (Scheme 15). The reactions were conducted using 90º C, methanesulfonic acid (MsOH). When alkyl carboxamides with 0, 1, or 2 hydrogens to the carbonyl group were present, the isopropyl group was removed selectively in the company of alkyl and aryl groups. The study noted that the reaction time increased as the size of groups attached to the nitrogen decreased. This could be due to electronic effects or the liberation of steric strain for the substrates with larger groups.

Lorenc *et al.*[62] proposed a mechanism of deprotection (Scheme 16). The amide carbonyl group **90** undergoes protonation to give **91**. This undergoes SN1-type ionisation to give **92** and isopropyl cation **93**. The secondary amide **95** is generated from the tautomerism of **92**. **93** undergoes elimination to give propene **94**. **96** can be formed directly when **93** undergoes fragmentation.

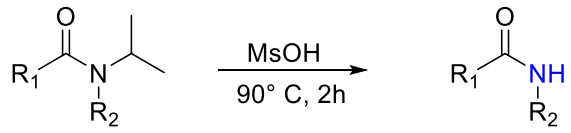

90 **95**

R_1: Adamantane, Cy, n-C_9H_{21}, PhH, Anisole, NBZ
R_2 = iPr, methyl, ethyl, CH_2PH, Ph,

Scheme 15: Reaction conditions for deprotection of **90**.[62]

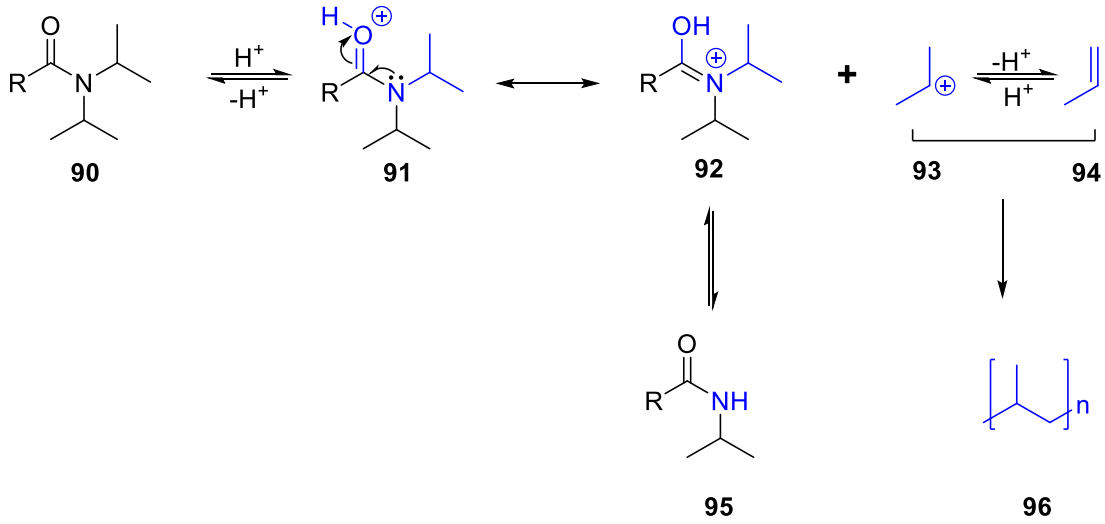

Scheme 16: Proposed mechanism for deprotection by Lorenc *et al*.[62]

Using Shono's approach, the C-H group adjacent to the amide can be transformed into C-X bonds (e.g. C-C, C-O, C-N, C-S, C-P, etc.). Suárez *et al.*[63] demonstrated C-C bond is generated *via* an anodic methoxylation step.

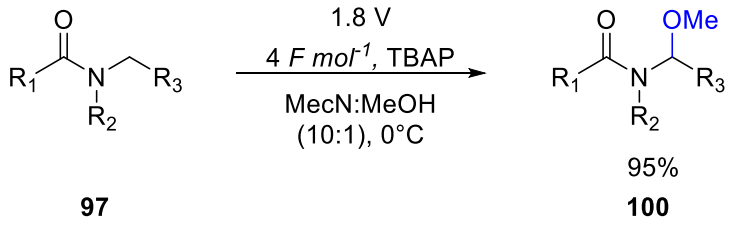

Scheme 17: Overall reaction conditions for Shono oxidised tertiary amide.[63]

Shono oxidation and cyclic voltammetry behaviour of the selected amide and numerous parameters such as optimisation of the applied voltage were investigated by Suárez *et al.*[63] using the potentiostatic method (Scheme 17). Optimisation studies regarding the voltage parameter concluded that the potential between +1.8 V and +2.0 V gave the optimum conversion. Tetrabutylammonium perchlorate (TBAP) was used as a suitable electrolyte as it gave the highest conversion rate to the electrosynthesised product compared to the other electrolytes such as tetraethylammonium *p*-toulenesulfonate, sodium tetrafluoroborate, among others. The amount of charge required was investigated, and 4 *Fmol*$^{-1}$ was ideal and gave the highest conversion.

Scheme 18 shows that a radical cation intermediate **98** is formed at the working electrode as the tertiary amide undergoes single electron oxidisation. The loss of a proton at the α-position and electron forms an α- *N*-acyliminium ion **99**, this *N*-acyliminium ion undergoes a nucleophilic attack from the solvent (methanol), losing a proton to form an α-methoxy amide. This is the Shono-oxidised product **100**. 99% conversion and 51% isolated yields were recorded.

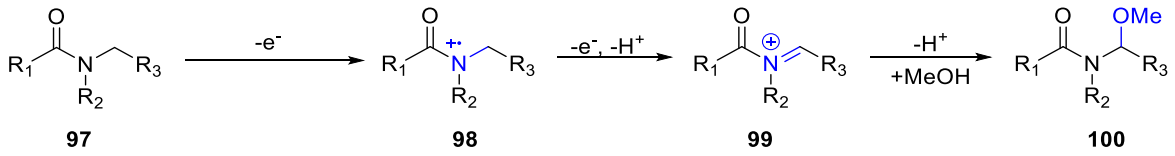

97 **98** **99** **100**

Scheme 18: A possible mechanism for the Shono oxidation by Suárez *et al*.[63]

1.4. Electrochemical Techniques

The section below gives a brief overview of indirect, direct, flow electrolysis, cyclic voltammetry, galvanostatic and potentiostatic methods used in electrochemistry.

1.4.1. Basic Principles

Electrodes are required to transfer charge and electrons for the compound to change when using electrochemical methods. Electrodes are always submerged in a solution and have an anode and a cathode. Electrolytes are salts that supply ions and facilitate the current conduction from one electrode to the other. Depending on the reaction method, two or three electrodes can be involved in the setup (Section 1.4.6).

Generation of a reactive intermediate for the downstream functionalisation takes place at the working electrode (WE). Depending on the substrate's reaction, the WE can be either an anode or cathode, excluding paired electrolysis. An electrode with a constant and established potential (i.e. Ag/Ag+ or saturated calomel electrode) is exploited as a reference (RE). A counter electrode (CE) is utilised to complete the electrical circuit; the current flows through the WE, which has a fixed, stable potential to the CE where the opposite reaction occurs.

Oxidation of a substrate occurs at the working electrode in anodic oxidation, while the reduction occurs at the cathode. The electrons donated by the substrate at the anode move around the circuit to decrease solvent molecules/protons or other species cathodically. Hence, individual electrochemical reactions are a mixture of two half-reactions.

Chemical reaction (C) takes place in a solution, and a heterogeneous electron transfer (E) process with the molecule develops at the electrode surface and cumulates to the creation of a radical-cation or radical-anion (reactive intermediate).[64] The combination of these two can be repeated to allow various kinetic sequences in terms of electrochemical (E) and chemical (C) steps, e.g., EE, EC, ECE.

A feature that makes electrochemistry innovative for synthesising a complex molecule is the reversal of the reactivity of a functional group (umpolung), which is not easily attainable by traditional chemistry.[65] When an electron transfer occurs, an umpolung is formed during an electrochemical process.[64] Nucleophiles are transformed to electrophiles when oxidised, and electron-rich compounds become electron-poor. Electron-deficient centres are transformed to electron-rich centres when reduction occurs, therefore, forming nucleophilic reactive sites.[64]

An organic compound can take many pathways during electrochemical reactions depending on the experimental circumstances. Nonetheless, in all routes, the preferred product (Scheme 19) is formed when electron transfer transforms the initial molecule (RX) into a reactive intermediate.[66, 67]

The reduction ($RX^{\bullet-}$) of a compound develops at the cathode when an electron is removed from the electrode surface (S_{ox}) and moves to the lowest unoccupied orbital (LUMO) of the compound. Oxidation of a molecule arises when an electron is removed from the highest occupied molecular orbital (HOMO) at the anode. Depending on the electrolytic conditions, the intermediates at this stage can react readily with other compounds, as they are highly volatile.[66, 67] Leaving group (X) is replaced by a nucleophile at the anode (nucleophilic substitution) or electrophile at

the cathode *via* electro oxidation in the presence of superfluous radicals leading to dimerization *via* radical addition taking place.

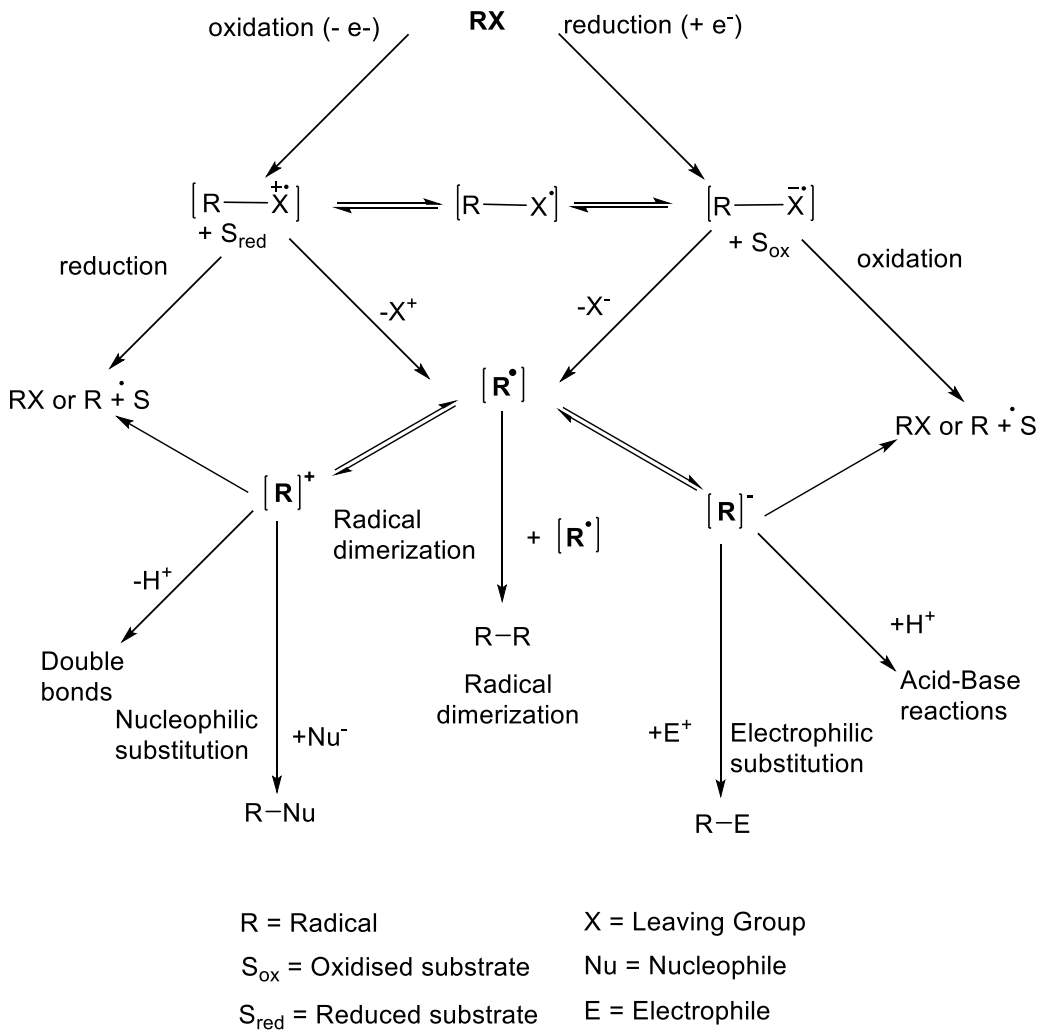

Scheme 19: The electrochemical pathways for the interconversion of functional groups.[66, 67]

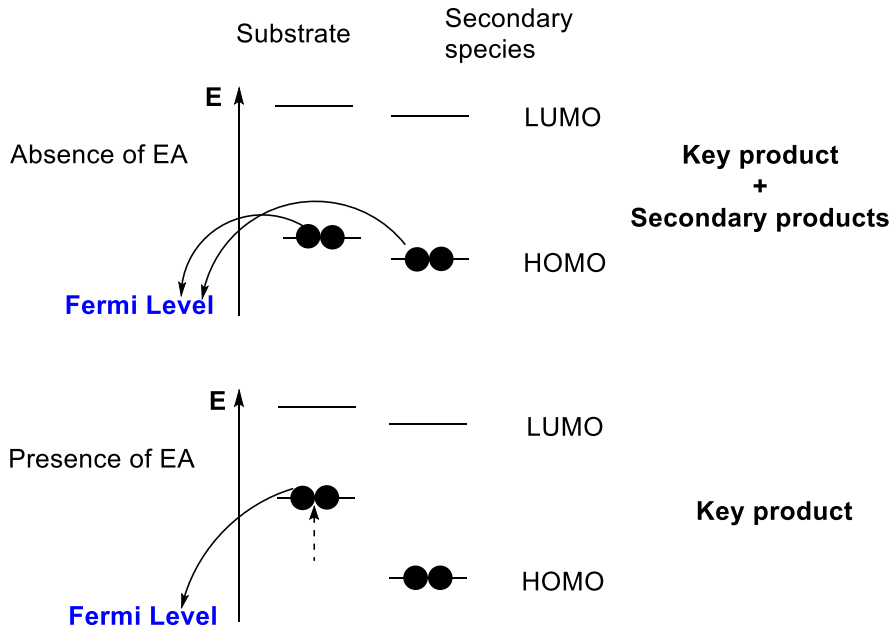

Figure 2: Selective and non-selective transfer of the Substrate.[53, 68]

However, if the HOMO levels of the species are close in energy, it becomes challenging to oxidise a substrate. The electroauxiliary (EA) functional group can be utilised to attain a more selectivity and selective electron-transfer route for the oxidation, thus overcoming this difficulty (Figure 2).[68] This boosts (increases fundamental substrate HOMO level) a desired selective oxidation in a reaction.

1.4.2. Electrode Material

For this project, reticulated vitreous carbon (RVC) electrodes were used. RVC are suitable electrodes for electrosynthesis due to the inertness and stability of the electrodes. It can be used in an extensive range of acids and bases and has low electrical resistance and high current densities.[63]

Vitreous carbon is a form of pure carbon created by the thermal decay of a three-dimensionally cross-linked polymer (i.e. polyurethane and phenolic resins) and is the primary component of RVC.[69, 70] RVC has a high surface area, rigid structure, and low resistance to fluid flow. This is the result of the open-pore foam component of its honeycomb structures which gives it empty space.[71] However, this vacant space makes it brittle, so the electrodes need to be handled carefully.

There are several articles[72-74] regarding the properties of RVC; they include a review by Friedrich *et al.*[71], which highlighted its current applications, where RVC is used as an electrode material both in fundamental and applied electrochemistry. This includes organic synthesis[63, 73], sensors[74], hydrogen peroxide production[75], use in batteries[76] and fuel cells[77] and metal ion removal.[78]

1.4.3. Divided and Undivided

An undivided (Figure 3A) cell is the most straightforward set-up of electrochemistry. There is no physical separation (low internal resistance) between the two electrodes (counter and working). Therefore, both reduction and oxidation take place in the same vessel.

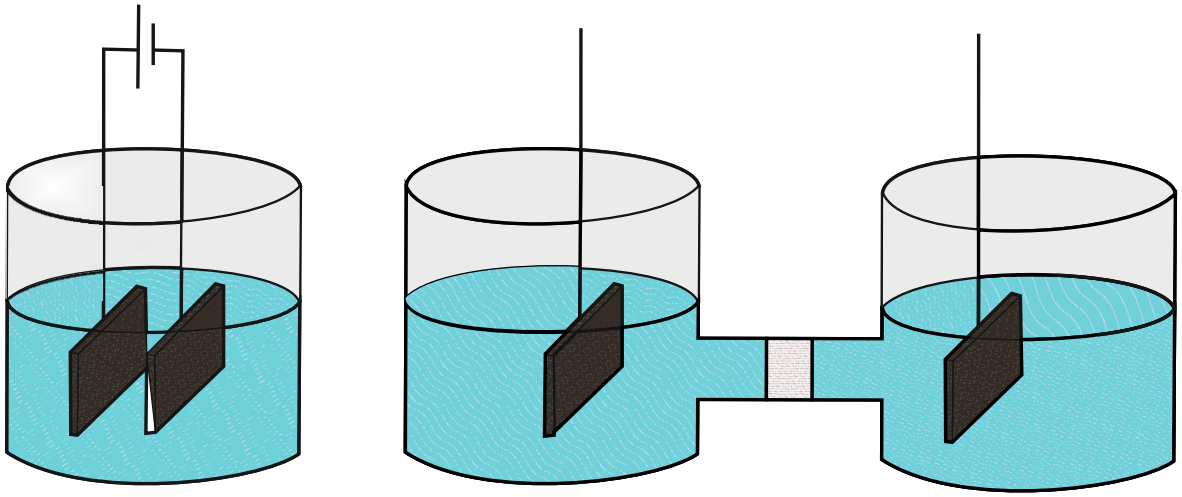

A: Undivided cell

B: Divided cell

Figure 3: Diagram of typical undivided [**A**] and divided [**B**] electrochemical cells.

Occasionally it is necessary to conduct experiments in separate compartments. A divided cell is required when high-energy intermediates spawned at the working anode are reduced too early at the cathode and vice versa. Divided cells (Figure 3B) have a membrane or ion-permeable barrier between the analyte and catholyte solutions (providing higher internal resistance of the configuration) that prevents them from mixing.[16, 79] Although the membrane permits the current to pass through both cathodic and anodic sections, to preserve a high conductivity and low working voltage between the electrodes when applying high currents. The separator easily transports ions and maintains an essential exchange of solvents and impartial

molecules.[64] The ion-permeable barrier should be stable under solvents and organic molecules involved in the process.

Waldvogel *et al.*[80] recently reported the anodic oxidation of oximes to Nitriles-*N*-oxides using flow type reactors. They conducted the experiments in both divided and undivided cells Scheme 20. In an undivided cell oxime, **101** was oxidised to nitrile-*N*-oxide **102** at the anode. **102** diffuses at the cathode and undergoes another transformation to give the nitrile **103**. The desired nitrile **103** had an isolation yield of 63% in flow-type reactions, compared to the batch method, where the yield was 41%. In the divided method of the flow cell, a similar reaction was studied. However, **102** from the analyte was not reduced. In its place, **101** reacted with methyl acetoacetate **104** to perform a condensation and gave product **105**.

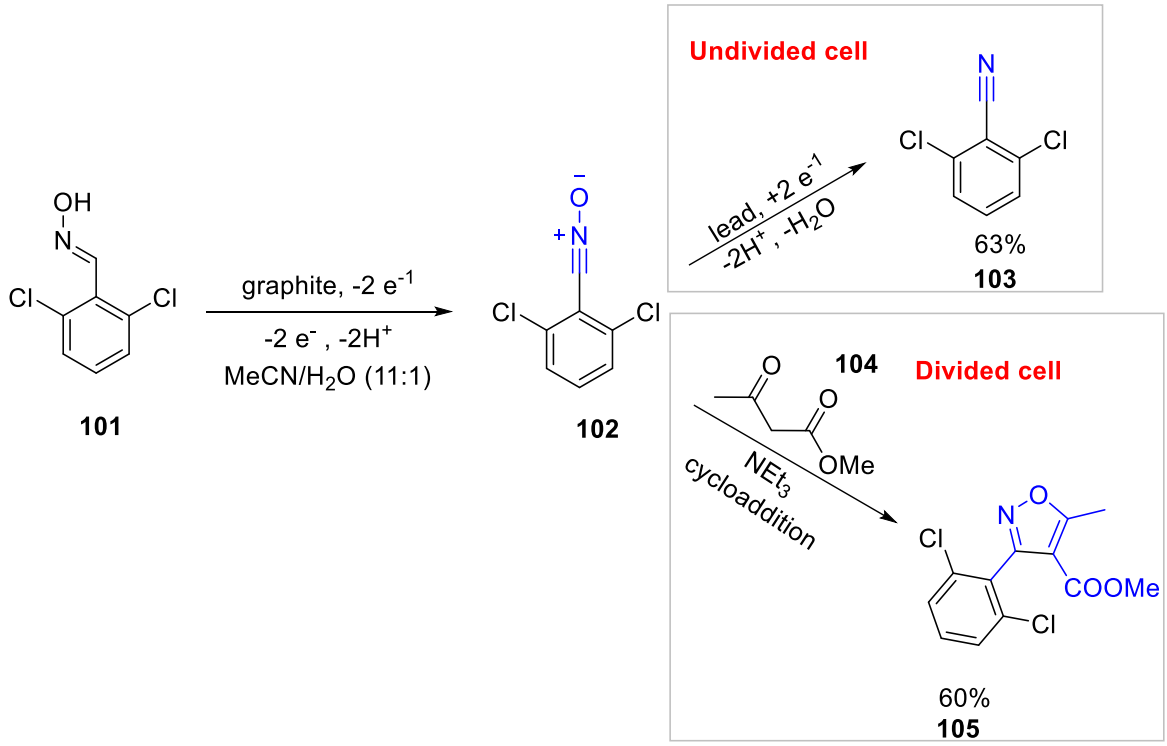

Scheme 20: Oxidation of **101** using flow-type reactors in divided and undivided cells.[80]

1.4.4. Cyclic voltammetry

The redox characteristics of a substance and the behaviour of the product created during the electrochemical reaction are studied by using cyclic voltammetry (CV). Understanding a reaction's heterogeneous rate kinetics, coupled chemical reactions and other interesting chemical properties can be achieved quickly using CV. [81, 82]

Voltammetric measurements are two dimensional, where the potential is linked to the qualitative behaviour of the substance, and the current is linked to quantitative.[81, 83] In CV, consecutive potential sweeps are conducted in both directions, i.e., oxidation and reduction, between two potential values.[83] Among other parameters, the importance of this procedure largely relies on the number of electroactive compounds in the potential range applied.[67] The rate of experiments can be controlled; it makes studying species with short-half lives easier.

Linear sweep voltammetry (LSV) is employed in this thesis. LSV uses the same ramp process as a CV. However, the potential is not reversed and is used to observe the one-half reaction of a cell.

1.4.5. Interpreting Voltammetric data

When CV is used to study the electroactive species, the majority of the solution remains unchanged. Nevertheless, the compound of interest oxidises or reduces at the electrode surface according to the potential applied.[82] Figure 3 shows the potential waveform. Fixed potential (onto the working electrode) is swept linearly with time from the starting potential, E_1, to the more negative potential, E_2, at which the electron transfer between the species and the electrode occurs and the species being detected is formed.

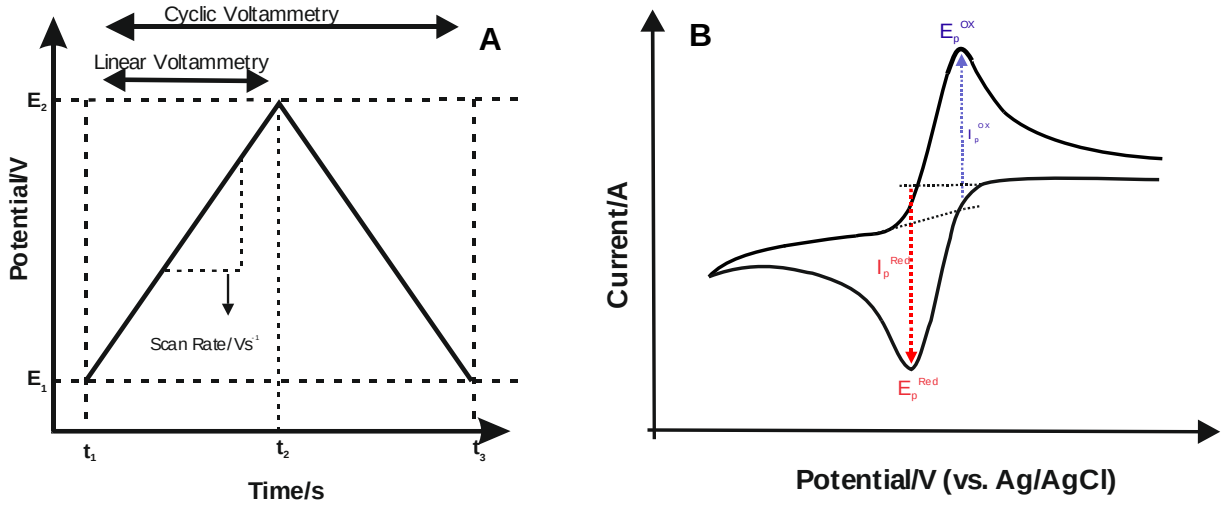

Figure 4: The triangular potential waveform (**A**) used within cyclic voltammetry and linear sweep voltammetry. The application of the potential waveform produces a typical cyclic voltammogram (**B**).[83]

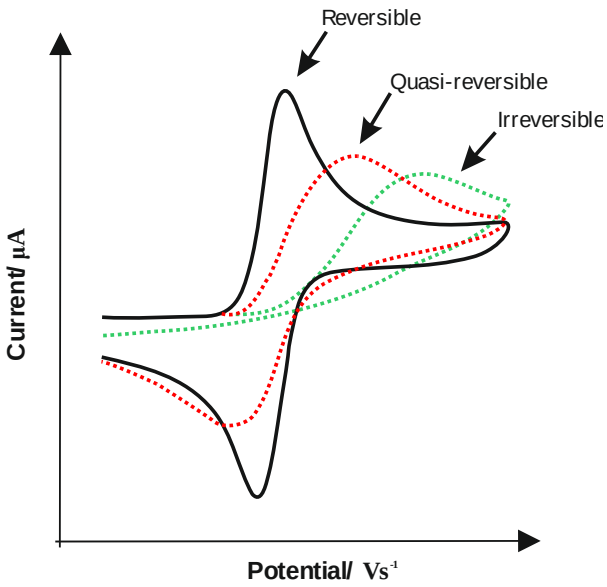

Figure 5: Cyclic voltammetry for the different types of electron transfer.[83]

A distinctive peaked cyclic voltammogram of macroelectrode Figure 5 is achieved when the current and potential are plotted. The current, I_p (proportional to the rate of electron transfer), is documented.[81, 83] The characteristics of the electrochemical process and the chemical species themselves can be calculated by examining the peaks' position and shape.[83] The scan rate, v, in Vs^{-1}, is the constant rate at which the voltage sweeps from the initial potential, E_1, to the vertex potential, E_2, and back again. The scan rate is the rate of change of potential (the slope) and is defined as:

$$v = \left(\frac{\partial E}{\partial t}\right) \qquad (1.4.5.1)$$

Whenever t is on the forward sweep, the potential, E, is given by

$$E = E_1 - vt \qquad (1.4.5.2)$$

At time $t = t_{switch}$, the potential reaches E_2, and the potential sweep reverses direction. For $t > t_{switch}$,

$$E = E_2 + (t - t_{switch}) \qquad (1.4.5.3)$$

Or

$$E = 2E_2 - E_1 + vt \quad (1.4.5.4)$$

Since

$$t_{switch} = \left|\frac{E_1 - E_2}{v}\right| \quad (1.4.5.5)$$

The constants used in the equations below are described as such; peak separation (ΔE_p), n is the number of electrons within the half-reaction. E^0 is the standard electrode potential measured at 1-atmosphere pressure, 1 molar solution at 25° C. F is the Faraday constant, n is the number of electrons transferred in the redox process, and A is the electrode area (cm^2). K0 ($cm\ s^{-1}$) is the standard heterogeneous rate constant, and α is the transfer coefficient. D is the diffusion coefficient of the electroactive species ($cm^2\ s^{-1}$), C is their concentration ($mmol\ cm^3$), and v is the applied scan rate (Vs^{-1}).

The distance between the two peaks indicates if the redox process upon the electrode of choice is reversible, irreversible, or quasi-reversible (Figure 5). For an electrochemically reversible reaction, the peak separation (ΔE_p) between the two peak potentials at 298 K is indicated as:[84]

$$\Delta E_P = E_{pa} - E_{pc} = 0.057/n \quad (1.4.5.6)$$

Using equation (1.4.5.7), the ideal ΔE_p for a reversible electrochemical system must be 57 mV at 298 K and independent of the scan rate. The value of the scan rate controls Quasi-reversible redox systems; hence, the ΔE_p of larger than 57 mV is recorded for these systems.[83] The formal potential is connected to the peak position and for a reversible system is located in the middle of E_{pa} – E_{pc} and is described as the following:

$$\Delta E^0 = \frac{E_{pa} - E_{pc}}{2} \quad (1.4.5.7)$$

When electron-transfer is much slower (irreversible) than that of the mass transfer process, the peak potential is calculated by the following relationship:

$$E_P = E^0 - \frac{RT}{\alpha n' F}[0.78 - \ln\frac{k^0}{D^{\frac{1}{2}}} + \ln\left(\frac{\alpha n' F}{RT}\right)^{\frac{1}{2}}] \quad (1.4.5.8)$$

The *Ep* has a much higher potential than the E^0, with the overpotential related to the k^0 and the α value. The value of E_p becomes larger when the value of *αn* is decreased, causing the CV to become more irreversible.

The peak position is not the only source of quantitative data expressed within a voltammogram. According to the Randles-Ševčik equation (1.4.5.9), the peak current can be obtained and is proportional to the concentration within the bulk solution. For a reversible system, the Randles-Ševčik equation is [82, 83, 85, 86]

$$i_P = 0.446FA[C]_{bulk}\sqrt{\frac{FDv}{RT}} \quad (1.4.5.9)$$

At standard conditions and 298 K leads to

$$i_P = 2.99 \times 10^5 AD^{\frac{1}{2}}[C]_{bulk}v^{\frac{1}{2}} \quad (1.4.5.10)$$

For a quasi-reversible system, the constant is replaced with the value of 2.65 x 10^5. In the case of an irreversible system, the constant changes, however, the introduction of the charge transfer coefficient occurs, which at standard conditions and 298 K leads to:

$$i_P = 2.99 \times 10^5 \sqrt{\alpha AD}^{1/2}[C]_{bulk}v^{\frac{1}{2}} \quad (1.4.5.11)$$

The shape and size of the CV graph can be affected by many factors, including the conductivity, the type of electrode material and the solvent used. Though conduction always occurs during the experiment. The oxidation and reduction peaks would not be visible if higher conductance occurred.

1.4.6. Potentiostatic and Galvanostatic setups

In 1942, Hickling's creation of the potentiostat changed the way electrosynthesis was conducted.[87] This unlocked new possibilities in the area, as the reactions could be realised under constant potential and the current decreases over time. When using the potentiostatic method, the CV of the compound is necessary to determine the oxidation potential. Potentiostatic setup is a three-electrode system containing WE, CE and RE. The potentiostatic method is accomplished by controlling the potential of the WE concerning that of a RE.

Potentiostatic electrolysis can produce a selective transformation by attacking a functional group while leaving others with a different standard potential intact. By controlling the potential at the working electrode, the preferred molecular alteration can be achieved. This method is generally used on a small scale or in research laboratories as it is inexpensive. However, it is impractical on a larger industrial scale due to the cost associated with it.

The galvanostatic electrolysis is a current control method that is more suitable for industrial scale-up as it only requires a two-electrode setup and is cost-effective than potentiostatic oxidation. Since the 19th-century, electrosynthesis has relied heavily on galvanostatic conditions.[12] The setup is a two-electrode system containing a WE and CE. The reaction mixtures are exposed to a constant flow of current, and the potential increases over time. The potentiostatic and galvanostatic processes produce a similar transformation during the start of the reaction. However, as the reaction proceeds, the selectivity of a galvanostatic process is often sub-par to the potentiostatic method since the potential is not fixed. The galvanostatic method is relatively straightforward, but it may lead to over-oxidation of the compound, as the voltage will fluctuate during the reaction.

1.6. Summary

This Chapter gave an overview of the basic concepts of electrochemistry. Such as the methods (types of electrolysis) and techniques (CV, galvanostatic, potentiostatic) need to be considered before performing electrosynthesis. Chemical *N*-dealkylation of amides was reported by Lorenc *et al.*[62], and a single example of electrochemically *N*-dealkylation of amides has been reported by Hall *et al.*[61] 1989.

Analysis of the literature concluded that although this area of chemistry is expanding in both organic and drug discovery, there remains a gap for isolating drug metabolites at a preparative scale. Several unanswered questions still exist in the overall synthetic application of these reactions. These include the effects of electron-withdrawing substituents on the compounds. The conversion of an analyte to *N*-dealkylated or *N*-demethylation, alongside the effects of electrolytes, needs to be investigated. Electrochemistry methods lack a universal application element for easier replication of a reaction method. A thorough understanding of this method is needed for its application to drug discovery and organic synthesis. When compared to the traditional methods, replication of drug metabolites is easily achieved. This method is time-saving and cost-effective, two factors that are imperative in drug discovery.

The work reported in this thesis takes a step towards understanding reactions conducted using electrochemistry when applied to the amide functional group. Results reported in Chapters 2 and 3 have been published.[88] The aim of the project was *N*-dealkylation of an amide compound using a constant current and applying the method to study drug metabolites.

Phase I (Chapter 2) investigates the scope of a method using *N,N*-Diethylbenzamide (**106**) as a model compound. The compound is subjected to several electrochemical optimisation studies, including the effect of current and electrolyte concentration, the inclusion of additives, and changes in the atmosphere. Purification methods were optimised for both removing the electrolytes and improving the isolated yield of the product. Flash column chromatography optimisation regarding the flow rate, solvent rate and recrystallisation method was

examined. The reaction mechanism for the method is hypothesised after observing the data collected.

Chapter 3 includes amides that were purchased and synthesised in-house to probe the reaction scope. LSV of selected amides was conducted to probe electroactivity. The behaviour of amides containing ethyl vs methyl group adjacent to the nitrogen bond was investigated. The steric hindrance, EWG, EDG and rigidity of compounds are explored. The chapter also reports the results collected when the electrochemical methods are applied to drugs and herbicides. Propanidid (**169**), a general anaesthetic, was synthesised, while the rest were purchased. The LSV of the compounds is reported. Additionally, high-performance liquid chromatography (HPLC), divided and undivided cells are explored.

Chapter 2: Optimisation and reaction mechanism

2.1. Introduction

The data reported in this Chapter was published in *ChemElectroChem* 2019 (Metabolism Mimicry: An electrosynthetic method for the selective deethylation of tertiary benzamide).[88] *N,N*-Diethylbenzamide (**106)** has been previously investigated by the group where Súarez *et al.*[63] produced Shono-oxidised product (Scheme 18) [63] when constant potential and TBAP was used as an electrolyte.

Amides were selected because of their stability compared to other functional groups. The stability of the amide bond is explained by looking at the resonance structure of the group. In resonant structure **A**, the amide nitrogen is sp^3 hybridised with pyramidal configuration. However, it is sp^2 because of the conjugation. In **B**, a partial double bond character (rotation about the C-N bond is no longer free) for the C-N bond is due to the sp^2 hybridisation. This explains the characteristic planarity of amides and their inherent stability. [89, 90] The lone pair on nitrogen is shared between nitrogen and oxygen. The electrons are unevenly distributed over the three atoms in the π system with a greater electron density on the oxygen (Scheme 21). Oxygen is more electronegative than nitrogen and hence has a greater share of the electrons in this π system.

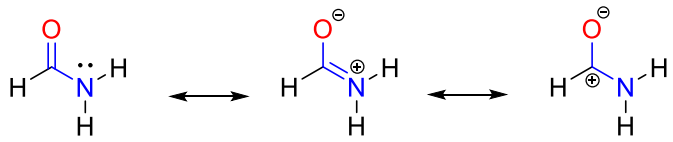

A **B** **C**

Scheme 21: Resonance structure of the amide bond.[89]

This chapter reports the electrosynthesis of **106** using a constant current. The amide structure meets the criteria for Shono-oxidation type reactions, where the C-H group adjacent to the amide could potentially be transformed into an *N*-acyl iminium ion. **106** was synthesised from acyl chloride and a secondary amine using the method described in Chapter 4 (section 4.2.1).[54]

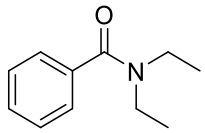

106

91%

Figure 6: *N,N*-Diethylbenzamide (**106**) as a model compound to optimised electrosynthectic and purification methods.

2.2. Linear sweep voltammetry

LSV was used for the characterisation of **106**, and the voltammetric response was explored over the scan rate range 5 to 250 mVs^{-1}. Glassy carbon electrode (GCE) was used as WE, the platinum wire used as CE and Ag/Ag^{+} was used as RE for LSV studies. LSV was selected as only oxidation of the compound was of interest for this project. Increasing scan rates can provide information regarding chemical changes with time, and it can determine the diffusion coefficient and the presence/absence of adsorptive behaviour of a species and the electroactive area of an electrode.

To determine the electrode process, analysis of log_{10} peak current (ip, μA) versus log_{10} scan rate v (mVs^{-1}) is performed to ensure the semi-infinite diffusion model is governed by the Randles–Ševčik equation (Equation 1.4.5.9). The ip value is selected from the highest point of the LSV (i.e. where the maximum oxidation current is recorded). The slope of the graph can determine the type of process. If the slope value is closer to 0, the process is considered diffusional, while a value of 1 is surface adsorption.[91] A value in-between states that the reaction is governed by adsorption and diffusion, where a value of around 0.5 is considered normal for diffusional processes.

To determine if a reaction has a fast electron transfer rate (reversibility) or a slow electron transfer rate (irreversibility), a graph of peak potential E_p (V) vs log i_p (Vs^{-1}) is plotted. The slope value indicates if the process is reversible or irreversible, a value nearing 0 (*i.e.* 0.005) is considered reversible, whereas a value nearing 0.5 is irreversible. However, a value between (0 - 0.5) is considered a quasi-reversible reaction (in-between fast and slow electron transfer rate).

A qualitative approach can be applied where the ΔEp values can be compared over a range of scan rates. The reversible reaction will have the same ΔE_p value at an increasing scan rate, for irreversible ΔE_p will drift to more extreme positive potentials with increased scan rate and are generally accompanied by wider, more broad peak shapes and lower comparable current values.

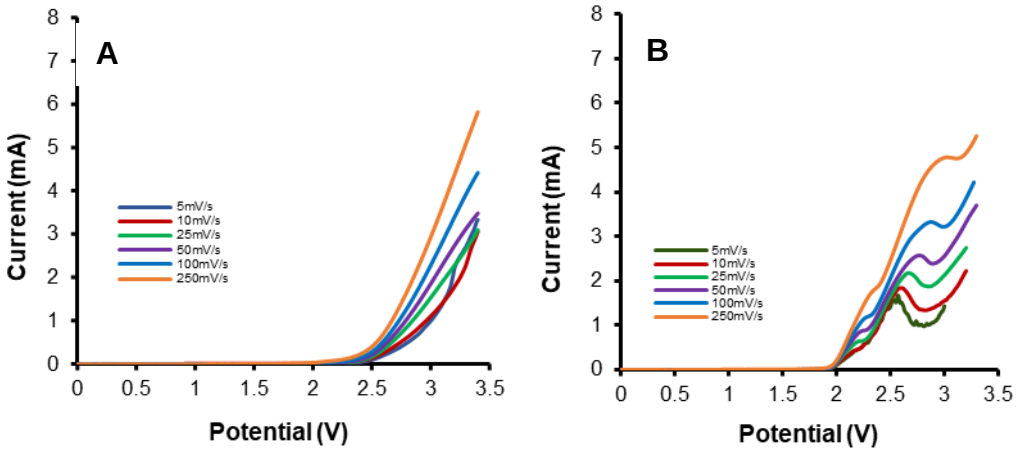

Figure 7: A: Background profile for the solvents, TBAP (0.5 M), MeCN: MeOH (10:1), **B**: scan rate survey for **106** (22.0 mmol). The electrode system consisted of GCE as WE, platinum as CE, and silver wire as RE.

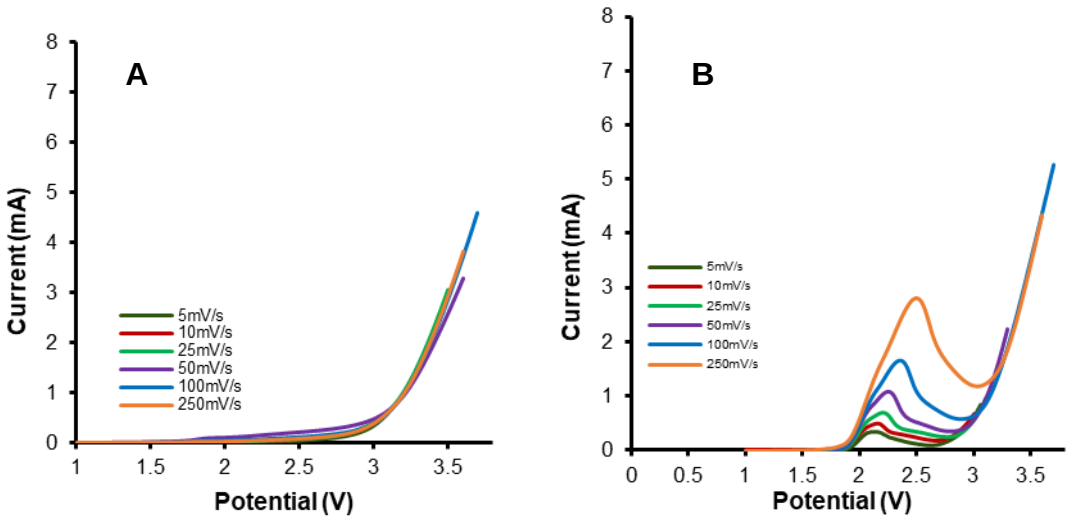

Figure 8: A: Background profile for the solvents, TBAP (0.5 M), MeCN: H_2O (10:1), **B**: scan rate survey for **106** (22.0 mmol). The electrode system consisted of GCE as WE, platinum as CE, and silver wire as RE.

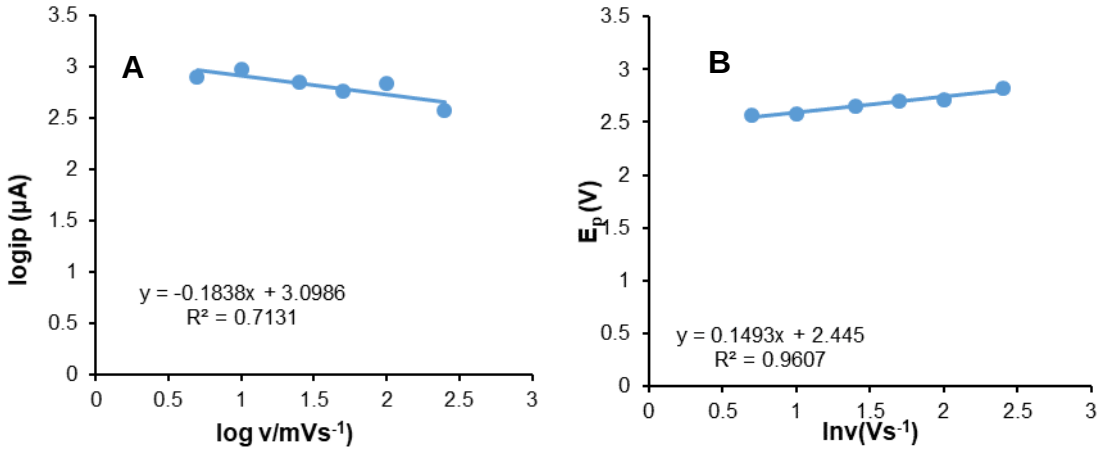

Figure 9: A: Plot of log of peak current (ip) vs log of scan rate (mVs^{-1}). **B**: Plot of peak potential (E_p) vs log of scan rate (mVs^{-1}) for **106** using scan rates 5 mVs^{-1} to 250 mVs^{-} (MeCN/MeOH).

A blank voltammetric profile of the solvents was performed to elucidate possible oxidation peaks arising from the solvents or deduce contamination. The organic solvents used were anhydrous to minimise interference from H_2O.

The reference electrode potential drift when Ag^{+}/Ag was used was regulated by contrasting to Fc^{+}/Fc. Figure 7A is a solvent profile of MeCN/MeOH (10:1) whilst Figure 7B is the profile of **106** that shows two ill-defined oxidation waves occurring at E_p^{ox} +2.20 V and + 2.67 V. When the solvent system is switched to MeCN/H_2O (10:1), Figure 8B shows a single oxidation peak at +2.25 V. Methanol constricts the viable voltammetric window. However, it entails a mild -50 mV reduction at the start of the initial oxidation response.

Figure 9A was plotted when MeCN/MeOH were used as solvents; it shows a non-linear plot, the value determined was closer to 0.5; therefore, a diffusional process is taking place. The non-linear graph is due to the constant change in i_p from 10 mVs^{-1} onwards. Figure 9B slope indicates that the process is quasi-reversible. This is also confirmed by the qualitative approach as the ΔEp values is increasing with each scan rate.

At faster scan rates, there are more chances that vital oxidation peaks may not be detected due to higher background current/broadening of the peaks due to the less interaction time between the electrode and the analyte; hence, 250 mVs^{-1} is used an upper limit for the scan rate. Similarly, a lower limit is also needed for the scan

rate, as a slower scan rate will allow the product to build upon the electrode and block the electrode.

2.3. Calculating the Charge

Bulk electrolysis is the set charge required for a reaction to proceed; this is carried out by holding the reaction at the chosen current; a chronocoulometry method is generally used.[63] The equation below is used to calculate the amount of charge required for a reaction to reach completion:

$$Q = (m_A/RMM)nF \qquad (2.3.1)$$

Integrating the current during the applied potential step is required to calculate *Q* (total charge), *Q* drives the reaction to completion, m_A is the mass (g) of the electroactive analyte, *RMM* is the relative molecular mass ($gmol^{-1}$), *F* is the Faraday's constant and *n* is the total number of electrons passed in the electrochemical reaction. The total time required to reach completion can be calculated by monitoring the charge. To decrease the time taken to complete a reaction, a large surface area electrode and the mechanical stirring of the solution are usually used.

2.4. Optimising electrochemical and purification methods

Optimisation of electrochemical methods such as the concentration, current, electrolyte and purification methods to maximise product yield is reported in the sections below.

2.4.1. Electrolyte

Súarez *et al.*[63] also investigated other electrolytes and concluded that tetrabutylammonium perchlorate (TBAP) is suitable. Building on Súarez *et al.'s* [63] electrolyte work, TBAP and lithium perchlorate ($LiClO_4$) were further examined in the current. Except for the electrolyte, the electrosynthesis of **106** was performed in

an undivided cell, solvents Acetonitrile: Methanol (10:1) and electron input was changed from controlled voltage to a control current 20 mAs^{-1}.

Lithium perchlorate was examined first (Scheme *22*); after the electrosynthesis, ^{1}H-NMR characterisation indicated the product had degraded. None of the proposed products (Shono oxidation, *N*-dealkylation and the starting material) was observed after the electrosynthesis. To improve the selectivity of one of the proposed outcomes, parameters such as electrosynthesis in a divided cell, subjecting the reaction to over and under oxidation, were explored. Starting material was recovered in a divided cell using under oxidation (-50 C). Other parameters did not yield any relevant results

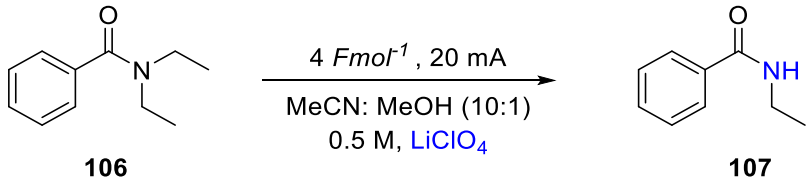

106 **107**

Scheme 22: Electrosynthesis of **106** using lithium perchlorate.

When TBAP is used as an electrolyte *N*-dealkylation of **106** is observed, **107** was isolated at 25% (**Scheme *23***). Over-reaction to primary amide and by-products (99% b.r.s.m) were not detected.

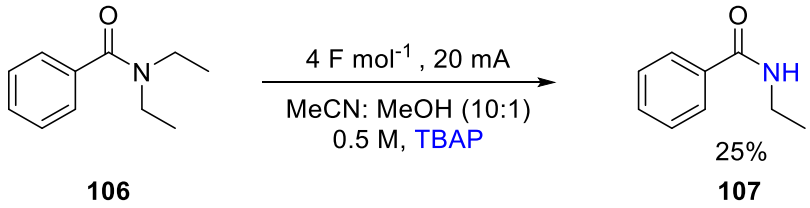

106 **107**

Scheme 23: *N*-dealkylation of **106** is observed when TBAP is used as an electrolyte.

Becker and co-workers. [92] reported different products when using electrochemical oxidation and applying controlled potential vs controlled current. Becker *et al*.[92] synthesised various mono- and disubstituted 1,4-dimethoxybenzene derivatives using both constant current and constant potential methods. An example using one of the compounds reported by Becker *et al.*[92] is shown in Scheme 24. **108** was

synthesised in $LiClO_4$ and was less selective when compared to electrosynthesis performed using basic conditions and generated complex mixtures.

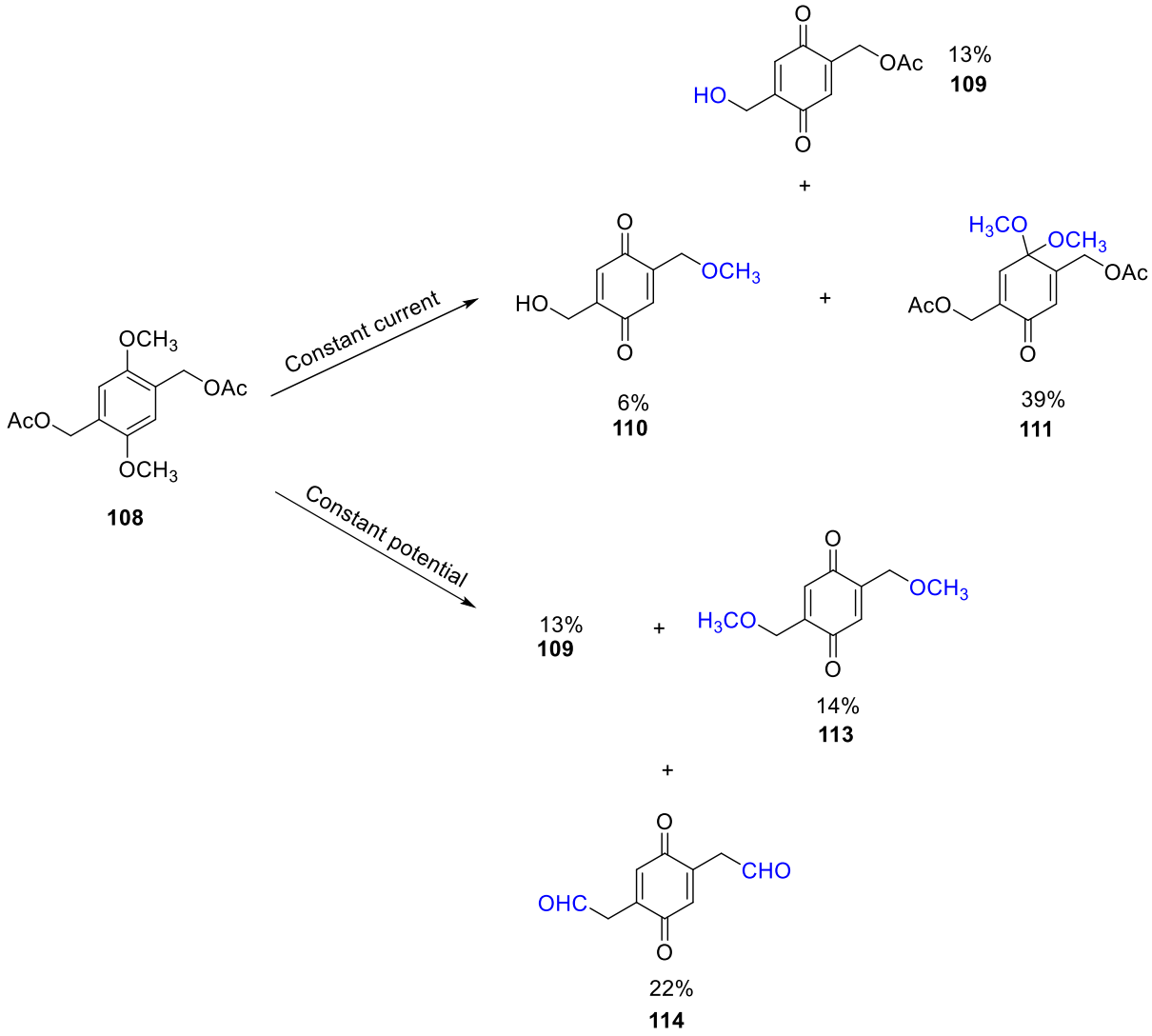

Scheme 24: Products isolated when Becker *et al.*[92] subjected **108** to constant current and constant potential method.

Further optimisation is required to isolate **107** to improve the yields. Therefore a second optimisation with the purification method was performed.

2.4.2. Optimisation purification using column chromatography on silica

Flash column chromatography (FCC) on silica was optimised to improve the isolated yield of **107**. 2D TLC of the product was conducted to observe if the product was stable on silica. In an unoptimised column, **107** was isolated at 24% reported in section 2.4.1.

Several specimens of **106** were subjected to electrochemical conditions (Scheme 23) to be tested for purification. Petroleum ether and ethyl acetate were selected as the solvents because they gave a good separation between **106** and **107**. The ratios of the solvent, Petroleum ether: EtOAc (70:30, 75:25, 80:20, 90:10, 95:5) and the flow rate ranging from 0.5 mL/min to 3 mL/min were examined to obtain the optimal conditions.

The concentration of the electrolyte is x 22, more significant than the analyte. Therefore, column diameters varying from 3.5 to 4.5 cm onwards were tested to observe if a larger surface area and faster flow would aid in isolating a higher yield. However, these were unsuccessful as most gave an isolated yield of < 25%, and the ^{1}H-NMR of **107** indicated the presence of the electrolyte.

A slow flow rate of 0.5 mL/min and increasing the solvent polarity incrementally (95:5 to 75:25, Petroleum ether: EtOAc) whilst using a column with a diameter of 3.5 cm resulted in a yield of 78% for **107**. A slow flow rate is more favourable as the electrolyte takes longer to elute when compared to faster flow rates.

When a faster flow rate of 3 mL/min (95:5 to 75:25, Petroleum ether: EtOAc) is used, the isolated yield for **107** decreased by 63%. This is because increased flow rate increased the sample dispersion (larger load) and band broadening, leading to the electrolyte eluting simultaneously as the product, leading to a less purified product. Although the isolated yields were low, no starting material was observed, with **106** converting > 99% to **107**.

As TBAP forms crystals, recrystallisation was tested for purification. Several non-polar solvents (xylene, toluene, diethyl ether, cyclohexane and hexane) were used to wash the crystals to obtain the products. Once TBAP crystals were formed, the product was isolated and characterised using ^{1}H-NMR. The spectrum indicated a considerable amount of TBAP present. Therefore, further purification of the product was required, which lead to yields between 10- 15 %.

2.4.3. Potential reaction mechanism and optimising electrochemistry method.

The last step to improve the yield was optimising the electrochemical methods by changing the factors listed in Table 1. These factors also helped to comprehend the mechanism for the reaction. The Experiments were performed at 0 °C temperature, and a ratio of 10:1 (MeCN: Additive) was used.

Table 1: Parameters and conditions for the synthesis of **107** from **106** using electrochemistry.

Entry	Electrical input	j (mA/cm^2)	Q (F mol^{-1})	Additive (1)	Atmos	TBAP [M]	Isolated yield of 107 (%)
1	5.0 mA	0.71	4.0	MeOH	air	0.10	0
2	5.0 mA	0.71	4.0	MeOH	air	0.20	22
3	5.0 mA	0.71	4.0	MeOH	air	0.30	31
4	5.0 mA	0.71	4.0	MeOH	air	0.40	85
5	5.0 mA	0.71	4.0	MeOH	air	0.50	86
6	1.0 mA	0.14	4.0	MeOH	air	0.50	11
7	3.0 mA	0.43	4.0	MeOH	air	0.50	32
8	10 mA	1.42	4.0	MeOH	air	0.50	15
9	20 mA	2.84	4.0	MeOH	air	0.50	24
10	30 mA	4.26	4.0	MeOH	air	0.50	22
11	40 mA	5.68	4.0	MeOH	air	0.50	20
12	50 mA	7.10	4.0	MeOH	air	0.50	16
13	-	-	-	MeOH	air	0.50	0
14	+1800 mV	0.0073	4.0	MeOH	air	0.47	0[a]
15	+1500 -+2200 mV	-	2.0-4.0	MeOH	air	0.47	0[b]
16	5.0 mA	0.71	4.0	H_2O	air	0.50	0
17	5.0 mA	0.71	4.0	MeOH NaOH	air	0.50	9
18	5.0 mA	0.71	4.0	MeOH	N_2	0.50	<5[c]
19	5.0 mA	0.71	4.0	MeOH H_2O	N_2	0.50	42

[a] 95% conversion to **117**. [b] n.r to 99% conversion to **117**. [c] Absence of moisture.

The concentration (Table 1, entries 1-5) of TBAP was investigated first. An excess amount of TBAP (0.5 M) is needed to decrease cell resistance in the solvent medium and achieve an effective conversion of **107**. Similar results regarding electrolyte loading were observed by Suarez *et al.*[63] Entries **5-12** show the results obtained when diverse current (*I*) and current density (*j*) were investigated. An upper limit for the generation of **107** was observed in Entry **5** (j = 0.71 mA/cm^2), where I = 5.0 mA when correlated to lower and higher currents (and current densities) Scheme 25. Nematollahi *et al.*[93] observed a similar trend where the product yields increased as the current density decreased.

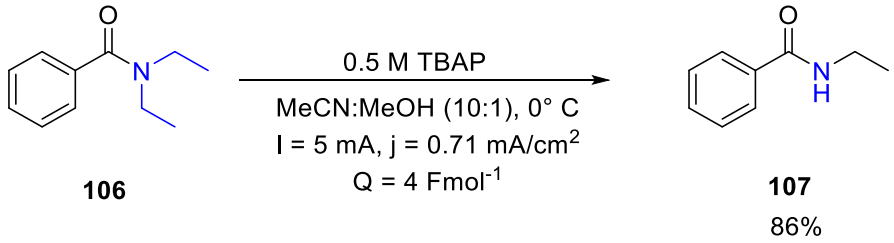

106 **107** 86%

Scheme 25: Formation of **107** using conditions listed in entry 5.

For the reaction to occur selectively, a lower *j* is favoured (entries **6-7**). This is due to the longer charge period/time as the compounds are spending a long time interacting with the surface of the electrode. Selectivity increases with a greater mass of the substrate. Therefore, running the cell with $I_{opt} > I_{cell}$ (optimal current (I_{opt}) from Faraday's laws) will not negatively influence the selectivity; instead will decrease in conversion.

Current efficiency is reduced with higher current density; when equilibrium forms during the reaction, it does so with higher potential, which leads to electromotive forces driving the equilibrium and breaking down products. These cause oxidation/reduction of the solvent/electrolyte, leading to possible side reactions and, at high currents, inefficient *Joule* heating.

The cell potential changes throughout the transfer time when the constant current method is used (as the resistance of the cell changes, $V=I * R$). The perceived average cell potential is typically lower, with lower applied currents opposite to higher currents. This correlates with higher conversion (and isolated yield of **107**

detected, in entry **5** *vs* entries **6-12**). This can be demonstrated by the cell potential being closer to the oxidation of **106** compared to that detected at higher applied currents. Other systems using controlled current experiments reported the fluctuations of cell potential.[94]

Electricity is necessary to convert **106** to **107**, as demonstrated by entry **13**, as no accompanying background reaction occurs with the perchlorate electrolyte. Long reaction times were observed when minimal current densities (entry **14**) were selected for the experiment.

Entry 15 uses the controlled voltage method, which requires a three-electrode set-up and the potential of the compound undergoing the electrosynthesis is milder and more selective than the controlled current method. Various charges were explored. Conversion to Shono-oxidised compound (**117**) was observed in entries **14** and **15.**

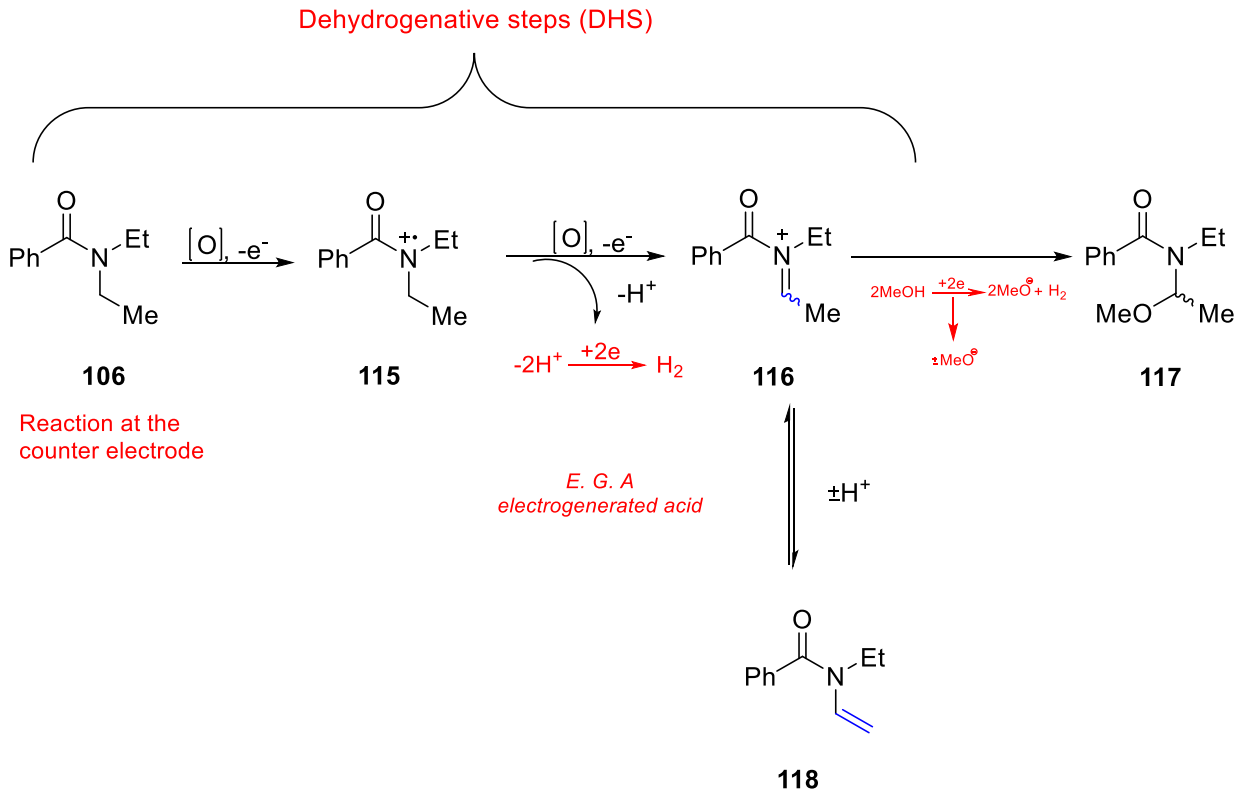

Scheme 26: Reaction of **106** at the counter electrode and the conversion to **117** observed when controlled voltage is used.

Scheme 26 shows the reaction that occurs at the counter electrode. Radical cation (**115**) is formed via a single electron transfer when **106** undergoes a Shono-type dehydrogenative step (DHS). A combination of a single electron transfer (SET) and hydrogen atom transfer (HAT) leads **115** to the formation of *N*-acyliminium (**116**). The reaction of **116** with methoxide generates **117.** The formation of gas bubbles (H_2) at the cathode was observed. This is in accordance with the initial steps for the Shono mechanism. Intermediate **116** is known to equilibrate under the electrogenerated acidic (EGA) conditions of enamide **119**.

Methanol, NaOH, and water were analysed as additives to observe if they would affect the conversion of **106** to **107** (Table 1, entries 16-19). In entry 16, H_2O replaced MeOH as an additive. This did not lead to the expected *N*-dealkylation, indicating that methanol is crucial for reactivity. An introduction of an external base (entry 17) gave a decreased conversion to **107**.

In entry 18, MeOH was used as an additive under stringent inert conditions; **106** was observed in trace amounts, demonstrating that MeOH alone is not responsible for the *N*-dealkylation. In similar inert conditions but with H_2O (1.0 mL), Entry 19, **107** was isolated with a yield of 42%. This entry indicates that H_2O and MeOH are imperative to the reaction, as observed in other entries where the addition or removal of H_2O/MeOH (Entry 16) significantly affects the reaction. The results in Table 1 indicate that MeOH and H_2O are imperative for *N*-dealkylation to occur.

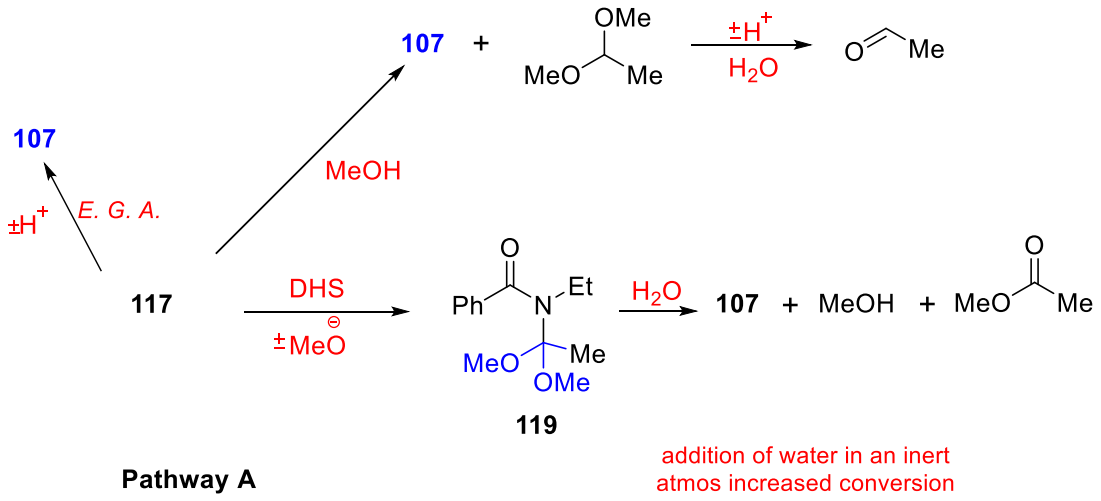

Scheme 27: Pathway A reaction mechanism when MeOH is used as an additive.

Both water and methanol are appropriate nucleophilic traps for **116**. MeOH can be reduced to methoxide and H_2O to hydroxide respectively at the counter electrode. Pathway A starts when a Shono-oxidised product (**117**) is formed. Here onwards, there are three possible sub-pathways. i) Decomposition of electrogenerated acid-meditated hemiaminal to **107** ii) direct attack of **117** where methanol or methoxide would supply **107** and an aldehyde oxidation state-level by-product. The final pathway iii) consequently DHS step for the preparation of acetal, **119** in an identical route to pathway A (ii) collapse or water-mediated cleavage would give **107**. Pathway A (route ii and iii) is supported by Mitzlaff and co-workers[95], where they detected a trace amount of dealkylation in cyclic tertiary amides *via* α-methoxy or α α-dimethoxy intermediates involving methanol-mediated ring-opening and water hydrolysis.

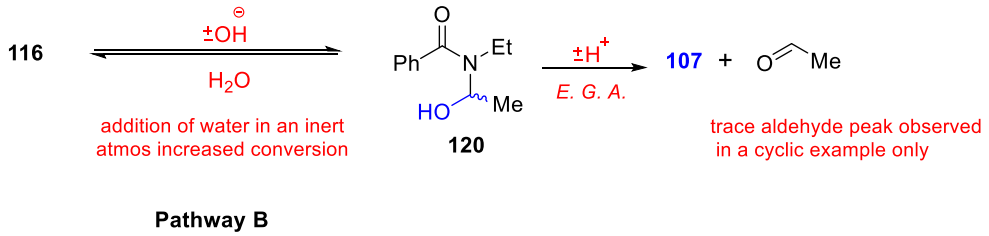

Scheme 28: Mechanistic pathways taken by **116** when water is used as an additive.

Pathway B generates **120** directly when **116** is intercepted by water. The studies of Mori *et al.*[96] are among the few that reported the direct α-hydroxylation of (cyclic) tertiary amides using a MeCN/H_2O (20:1) system. However, the product was not characterised, as only a minimal amount of it was recovered but presented evidence for dehydrogenative coupling without methanol.

Direct replicate of α-hydroxylation of **106** using the parameters listed in Table 1, entry 16 were not accomplished. If **117** were to be formed, hemiaminal collapse would supply **107** and an aldehyde oxidation state by-product.

Pathway A dominates via the typical Shono α-methoxylation initiation. The key observations included: methanol is needed for the reaction with trace quantity of water to assist the reaction, through electro-generation of acid and react with the acetal by-products *via* hydrolysis.

Additional experiment to probe the feasibility of double dealkylation was conducted. An authentic sample of **107** was separately synthesised using the existing method. This was then subjected to the reaction conditions reported in (Table 1, entry 5). The reaction indicated that a primary amide was not formed, and **107** was recovered unreacted.

So why does the reaction stop at mono dealkylation and is preferred over double dealkylation? This can be explained by analysing the LSV (Figure 10) of the compounds. Low potential for **106** is observed due to less electron density on the nitrogen in **107** than in **106**. Hence higher applied voltage is needed to adjust the Fermi level of the electrode to match the energy level of **107**. Until higher overpotentials are applied, (e.g. after consumption of the lower E_p^{ox} substrate, **106**), the reaction of **107** becomes unfavourable. Inefficient routes may be in process when the cell adjusts to the potential of **107** as it is in competition with methanol for redox processes on the electrode surfaces because of the higher E_p^{ox} for **107** than **106**. A similar observation has been reported previously, where secondary amides had higher potential compared to tertiary amides.[97]

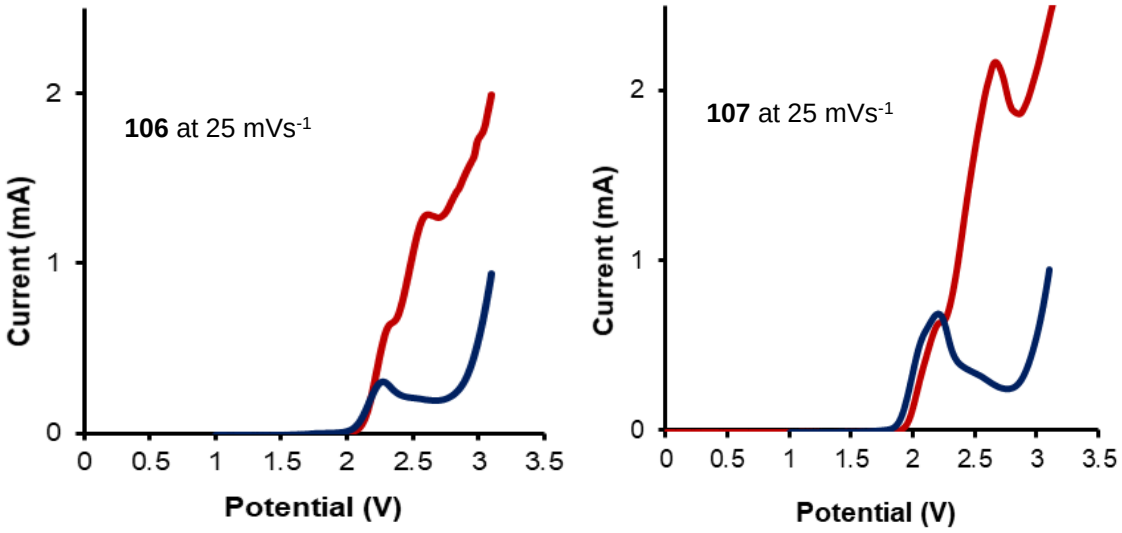

Figure 10: LSV oxidative potential from the scan rate of **106** and **107**. Conditions: MeCN/MeOH or MeCN: H2O (10:1), 5.0 M TBAP, 22.0 mmol of analyte, W.E. = GC, C.E. = Pt wire, R.E. = Ag+/Ag (0.057 V versus Fc+/Fc), v= 5-250 mVs^{-1}. Data for v = 25 mVs^{-1} shown for clarity. † Solvent system: **Red**=MeCN/MeOH, **Blue**=MeCN/H_2O.

Changing the solvent system to MeCN/H_2O led to a single broad oxidation wave for **106** (E_p^{ox} = +2.25 V) and **107** (E_p^{ox} = +2.37 V), respectively. Figure 10 shows two ill-defined oxidation waves for **106** occur at Epox +2.20 V and 2.67 V versus Epox +2.32 and 2.61 V for **107** in MeCN/MeOH. The *E*p^{ox} +2.67 V observed in MeCN/MeOH is dependent on MeOH, as this disappears when H_2O is used. This second oxidation is needed for *N*-dealkylated. Entry 5, entry 16 and entry 19 prove that H_2O and MeCN are both necessary for the reaction, although the presence of H_2O needs to be minimum.

2.6 Summary

LSV for **106** indicated that when MeCN/MeOH were used as solvents, a non-linear plot forms; therefore, a diffusional process occurs. The non-linear graph was due to the constant change in i_p from 10 mVs^{-1} onwards. A single oxidation peak is observed when the solvent system is switched to MeCN/H_2O (10:1). Methanol constricts the viable voltammetric window. However, it entails a mild -50 mV reduction at the start of the initial oxidation response.

When TBAP is used as an electrolyte *N*-dealkylation of **106** is observed, **107** was isolated at 24%. Over-reaction to primary amide and by-products (99% b.r.s.m) were not detected. None of the proposed products (Shono oxidation, *N*-dealkylation and the starting material) were observed $LiClO_4$ was used as an electrolyte.

Flash column chromatography (FCC) on silica was optimised to improve the isolated yield of **107**. A slow flow rate of 0.5 mL/min and increasing the solvent polarity incrementally (95:5 to 75:25, Petroleum ether: EtOAc) whilst using a column with a diameter of 3.5 cm resulted in a yield of 78% for **107**. A slow flow rate is more favourable as the electrolyte takes longer to elute when compared to faster flow rates. Other methods did not give adequate results.

Optimisation of the electrochemical methods by changing the factors listed in Table 1 resulted in an upper limit for the generation of **107** (86%) observed in Entry **5** (*j* = 0.71 mA/cm^2), where I = 5.0 mA when correlated to lower and higher currents (and current densities). The product yields increased as the current density decreased

due to fewer back reactions and side reactions. Current efficiency is reduced when a higher current density is used.

Both water and methanol are appropriate nucleophilic traps for **116**. MeOH can be reduced to methoxide and H_2O to hydroxide respectively at the counter electrode. Pathway A dominates via the typical Shono α-methoxylation initiation. The key observations included: methanol is needed for the reaction with trace quantity of water to assist the hydrolysis, through electro-generation of acid and react with the acetal by-products *via* hydrolysis.

Additional experiments to probe the feasibility of double dealkylation were conducted. Low potential for **106** is observed due to less electron density on the nitrogen in **107** than in **106**. Hence higher applied voltage is needed to adjust the Fermi level of the electrode to match the energy level of **107**. Until higher overpotentials are applied, (e.g. after consumption of the lower E_p^{ox} substrate, **106**), the reaction of **107** becomes unfavourable.

Chapter 3: Reaction Scope

3.1. Introduction

The results reported in this chapter were published in *ChemElectroChem* 2019 (Metabolism Mimicry: An electrosynthetic method for the selective deethylation of tertiary benzamides)[88]. To examine the scope of novel dealkylation of tertiary amides, an array of benzamide and alkyl amide analogues were selected to investigate the scope of this novel dealkylation of tertiary amides. Investigation of electron-donating, withdrawing groups and steric effects near the reacting centre and changes to the *R*-group next to the carbonyl on the reaction outcome were examined. To isolate the dealkylated product, a slow flow rate of 0.5 mL/min and increasing the solvent polarity incrementally (95:5 to 75:25, Petroleum ether: EtOAc) whilst using a column with a diameter of 3.5 were implemented. Except small modifications to increase the polarity of the solvent ratios were changed depending on the compound. The optimised electrochemistry conditions reported in Table 1, entry 5 were applied.

The data reported in the previous chapter indicated that a Shono-type reaction occurs during the *N*-dealkylation reaction, concluding that an *N*-acyliminium ion is formed. Amides can be oxidised to *N*-acyliminium ion, which makes them easier to be captured by various nucleophiles and formation of new C-X bonds (C-O, C-C, C-N etc.).[54, 98-100] A known amide oxidation is the Shono-oxidation (Scheme 7), reported by Prof. Tatsuya Shono (University of Kyoto) who combined organic and electroorganic steps for a C-C bond formation.[58]

3.2. Synthesised and purchased amides

A library of compounds structurally similar to **106** were synthesised. The benzene ring of some compounds were substituted at the *ortho*, *para* or *meta* position. Benzylic amides varying in electronic properties and were selected on their tendency to donate or withdraw electron density to and from the amide bond.

Methyl (**121-123**), chlorine (**124-126**) and methoxy (**127-129**) were selected to observe the effects of the substituents regioisomers at the *ortho*, *meta* and *para*

positions and will facilitate the analysis of how such properties affect the *N*-dealkylation. The methyl and methoxy groups fall into a strict category of EDGs. Methyl activates the ring due to hyperconjugation, positive inductive effect and is considered a weaker EDG group. The methoxy is stronger EDG; due to a stronger mesomeric effect because of the lone pair of electrons on the oxygen; although due to the electronegativity of oxygen itself, it also exerts a negative inductive effect. Both these contribute towards the electron-donating ability of the group because of electron delocalisation. The chlorine group is unique in that the electronegativity of chlorine allows it to serve as an electron-withdrawing (inductive properties) and donating (by conjugation) substituent.

The methyl-substituted group has an inductively electron-rich aryl system. The methyl group at *ortho* and *meta* position might be difficult to electrosynthesised due to the steric hindrance, which can create constraints and cause conformation that may be energetically unfavourable.

Methoxy is a larger group than methyl and chlorine and would cause more steric hindrance for the reaction at *ortho* and *meta* position because of the large electron density.

130 was previously reported by Lorenc *et al.*[62] to undergo *N*-dealkylation using acid. Hence it remains to be observed if *N*-dealkylation using electrosynthesis is possible for this compound. **131** an aromatic and a 5-membered ring with two possible α-carbon sites that can be electrosynthesised. The selectivity regarding this could be used in future work to study and possibly synthesise drugs and small molecules from a parent 5 membered ring system. **132** is selected due to the steric hindrance caused by the two aromatics. The α-carbon sites available would be difficult to access due to the electron density of the aromatic.

The amides were synthesised using acyl chloride and a secondary amine method described in Chapter 4 (section 4.2.1).[54] The yields recorded for the compounds are shown in the Figure below.

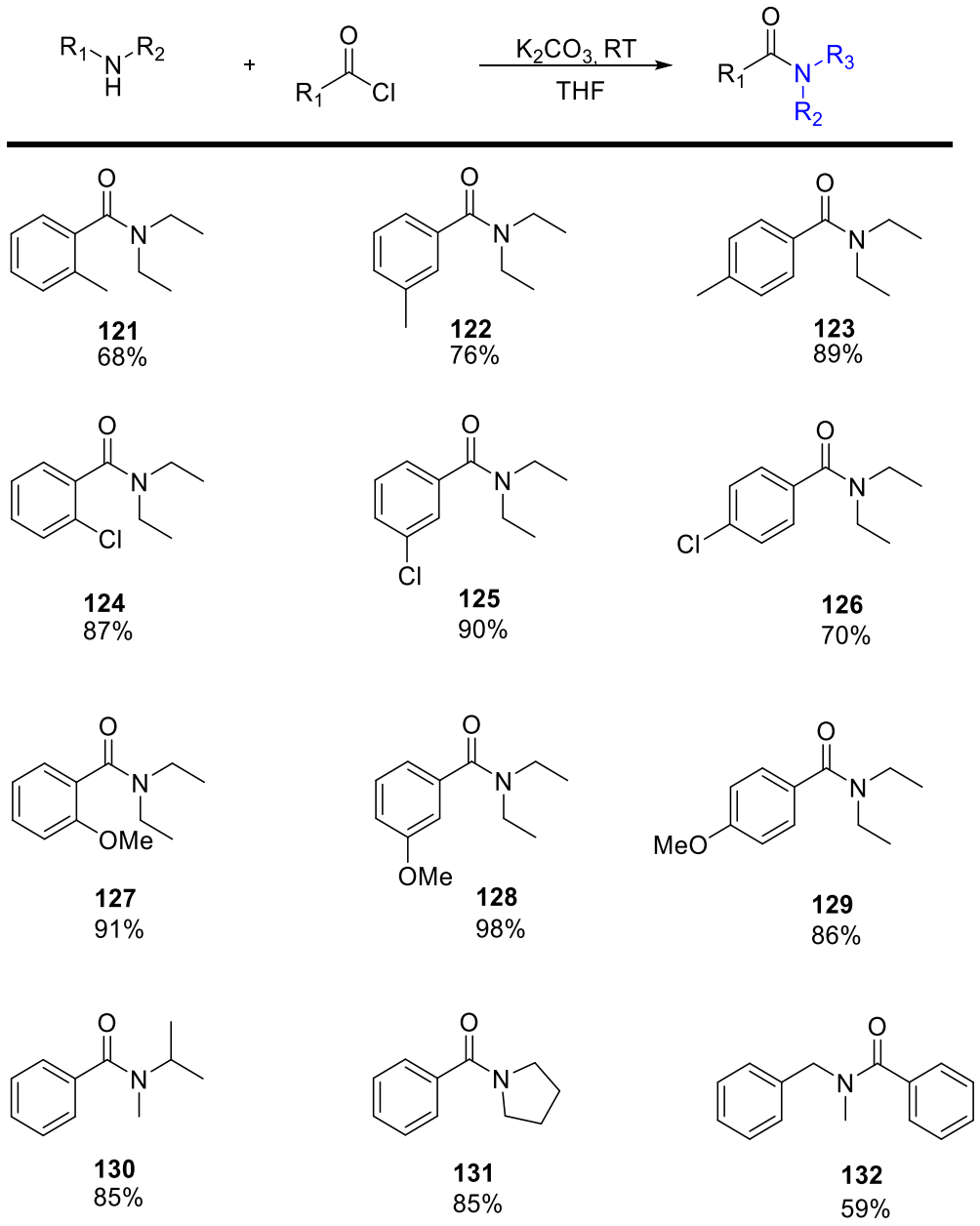

Figure 11: Tertiary amides synthesised and the yields isolated.

The methyl-substituted benzene (**121-123**) rings are *ortho*/*para* directors because they are inductive activators due to resonance, and although this trend is not observed in the isolated yields, the conversion of *ortho*/*para* to the final product was observed in the crude ^{1}H-NMR of the product.

Similar to methyl, the methoxy group (**127-129**) is another *ortho*/*para* director. As with the methyl substitution, the methoxy groups isolated yields do not reflect what has been observed. This is because the compounds (**121-132**) were isolated using the extraction method. Hence the solubility of the compound affected the outcome of the isolated yield.

Aromatics with chlorine substituted are resonance deactivators and *meta* director. The isolated and conversion yields for these compounds align with what has been reported previously in the literature. The higher yields for the *meta* product are because it does not produce a destabilising arenium cation resonance structure during the reaction compared to the *ortho*, *para* positions.

From the library of compounds, the lowest yield was recorded for **132** at 59%. The synthesis of amides is conducted using acyl chloride and secondary amine, an addition-elimination reaction. Hence, when the amine attacks the acyl chloride, it is a slow reaction as the proton can only access one position that would produce the least sterically hinder compound.

N,*N*-Diethyl-*meta*-toluamide (DEET, **122**) is an active ingredient in most insect repellents and is metabolised by CYP-450 to two major metabolites **133** and **134** (Scheme 29).[101] To the best of our knowledge, electrochemical replication for the metabolite of **122** has not been reported. Currently, DEET's metabolites are studied using traditional biological methods.[101, 102]

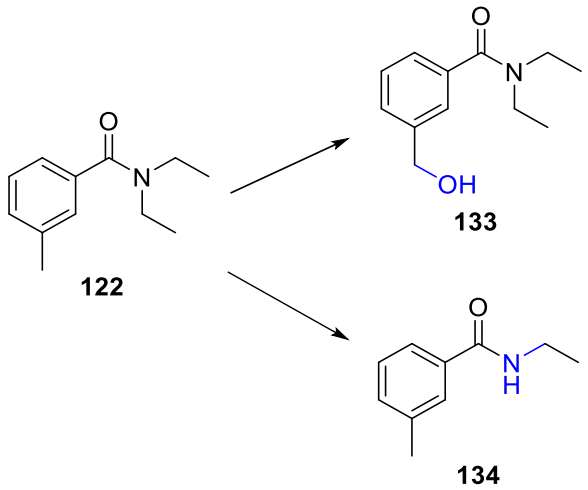

Scheme 29: Metabolites of *N,N-Diethyl-meta-toluamide*.

Furthermore, three more amides were purchased for probing the electrosynthesis method. *N*-Methyl-2-pyrrolidone (NMP) **135** (Scheme 30) is a simple form of γ-lactam, selected as a model for expanding the research into investigating complex derivatives of γ-lactam. Dimethylacetamide **136** (DMA) is a rudimentary form of a tertiary amide and does not have steric hindrance or strong EDG/EWG. Theoretically, it should easily be able to transform to either Shono oxidation or the proposed *N*-dealkylated amide.

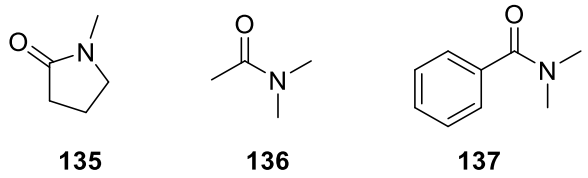

Scheme 30: *N*-Methyl-2-pyrrolidone (NMP) **135**, Dimethylacetamide **136** (DMA) and *N*,*N*-Dimethylbenzamide (**137**) purchased amides for the experiment.

106, 136, and **137** are a framework for building a more complex amide structure, including multiple functional groups, substituting the benzene ring, and expanding the carbon chains attached to the nitrogen atom. If successful, electrosynthesis of these will further aid understanding the reaction mechanism and application of the method to more substantial and intricate structures.

3.3. LSV

LSV of compounds (**106-107**, **121-132**) using RVC as electrodes was attempted; however, no useable data was produced due to the large non-uniform surface area of the electrode. RVC has variable surface area hence, different diffusional rates inside and on the surface. The electrochemical method used in this project does not require the potential of the compounds. However, LSV of the selected compounds (**106-107, 121, 124, 127**) was conducted using a glassy carbon electrode to observe how the oxidation potential differs when various groups are attached to the aromatic group.

Tertiary amides (**121**, **124**, **and 127**) were selected for LSV to observe whether the difference in applied potential will significantly impact the compound when the substituted group is changed, yet the substitution position is kept the same.

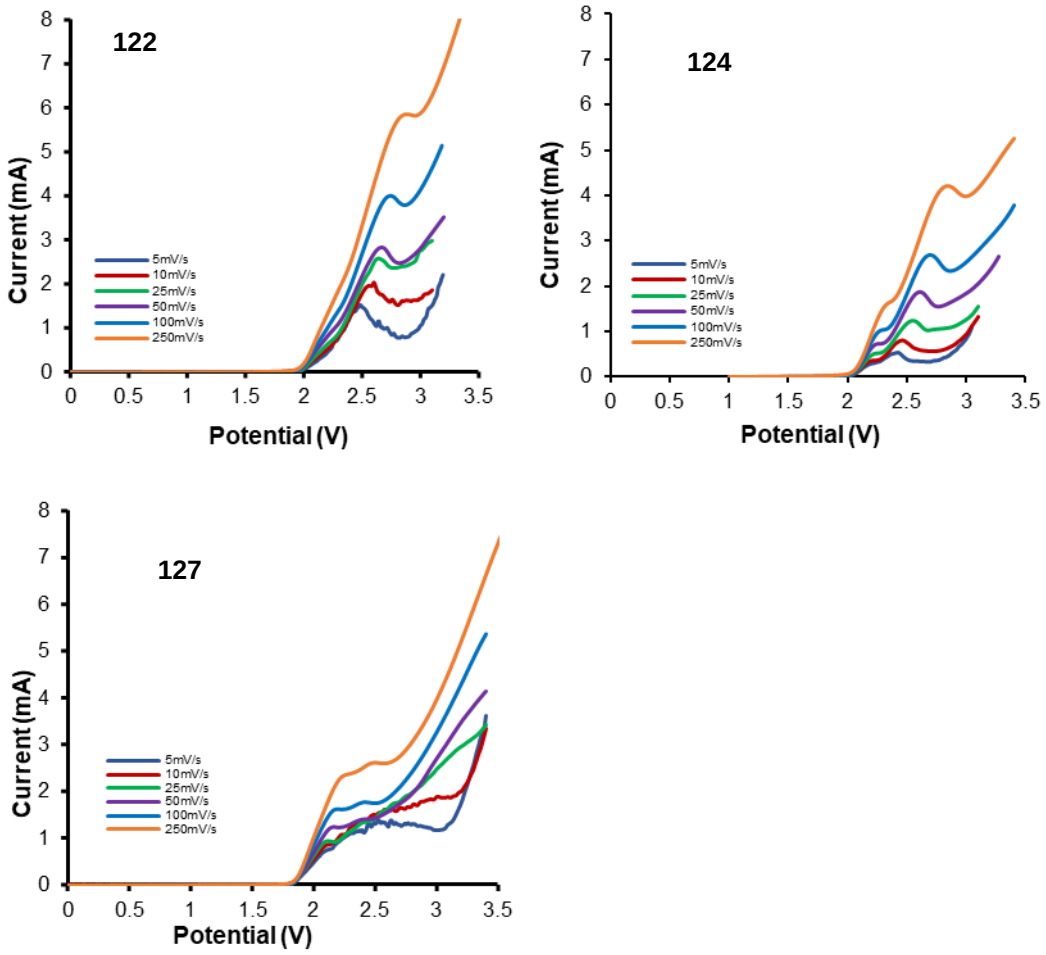

Figure 12: LSV scan rate survey of **122, 124** and **127** (22.0 mmol), using GCE as WE, platinum as CE and silver as RE. TBAP (0.5 M), MeCN: MeOH (10:1).

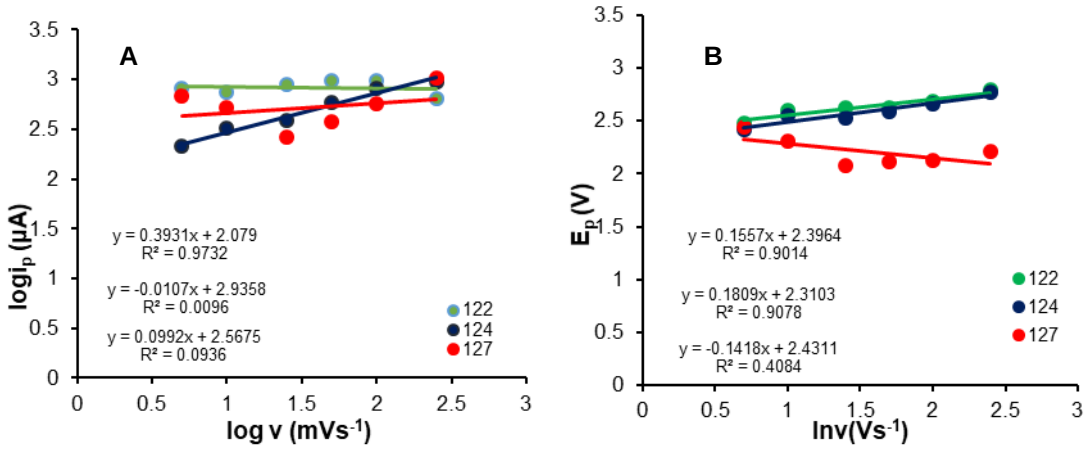

Figure 13: A: Plot of log of peak current (ip) vs log of scan rate (mVs^{-1}). **B**: Plot of peak potential vs (Ep) vs log of scan rate (mVs^{-1}) for **122**, **124** and **127**.

Table 2: Slope and correlation coefficient for a log of peak current vs log of scan for Figure 18A.

Compound	Slope value	R^2
122	Ip (µA) = -0.010 log v(mVs-1) + 2.936	0.009
124	Ip (µA) = 0.393 log v(mVs-1) + 2.079	0.973
127	Ip (µA) = 0.099 log v(mVs-1) + 2.568	0.094

Table 3: Slope and correlation coefficient for peak potential vs log of scan for Figure 18B.

Compound	Slope value	R^2
122	Ep (V) = 0.156 log v(mVs-1) + 2.396	0.901
124	Ep (V) = 0.180 log v(mVs-1) + 2.310	0.907
127	Ep (V) = -0.14 log v(mVs-1) + 2.431	0.408

The LSV for **122** and **124** indicate that an ECE reaction is taking place. The two oxidation peaks for **122** are +2.87, respectively. For **124,** the oxidation peaks are +2.22 V + 2.54 V. These values were taken from 25 mVs^{-1}. The LSV of compound **127** also indicates that a two-electron process is taking place. However, peaks above 50 mVs^{-1} are not well defined and are broad due to the oxidation of the compounds occurring consecutively and a slow electron transfer. The second electron transfer step depends on how much the first intermediate is chemically converted during this ECE reaction. This could lead to no product as the second electron transfer step can efficiently convert back to the starting material.

Table 2 shows the gradient and correlation coefficient found for $\log_{10ip}$ vs $\log_{10v}$ for all the compounds. The slope values calculated indicate that it is a diffusional process. Table 3 shows the gradient and correlation coefficient found for the $\log_{10ip}$ peak potential vs $\log_{10v}$ graph, as the slope value is not near 0, and thus these reactions are quasi-reversible.

3.4. Dealkylation of amides and the reaction mechanism

The LSVs indicated that the compounds selected were electroactive and therefore could be oxidised. Electrochemical oxidations of the amides using the optimised conditions reported in Chapter 2 were applied. Table 4 reports the results obtained and the isolated yields of the *N*-dealkylated products.

Table 4: The scope of electrochemical dealkylation of amides.

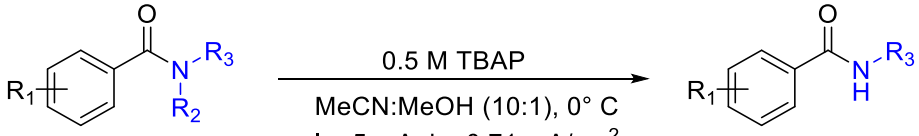

Entry	Substrate		Product		Isolated yield (%)
1	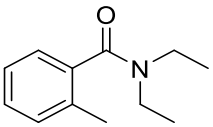	**121**	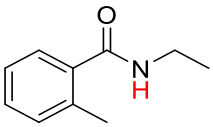	**138**	54
2	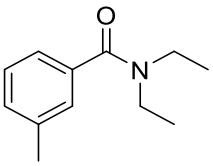	**122**	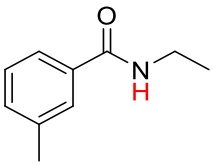	**134**	52
3	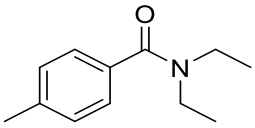	**123**	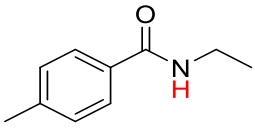	**139**	0[a]
4	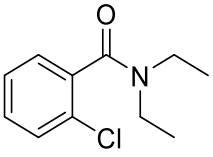	**124**	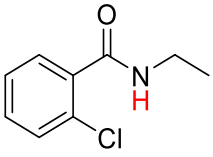	**140**	15[b]
5	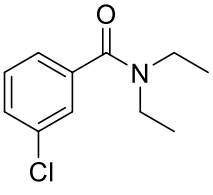	**125**	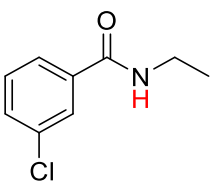	**141**	60[b]

6	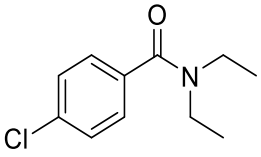	**126**	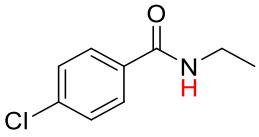	**142**	70
7	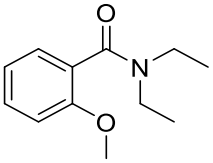	**127**	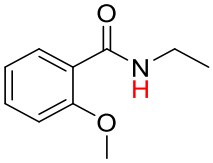	**143**	0 (rsm)
8	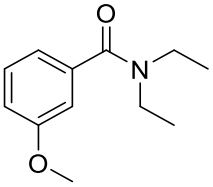	**128**	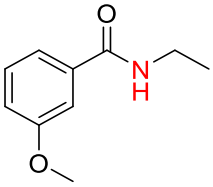	**144**	0(rsm)[c]
9	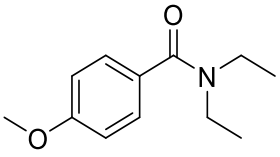	**129**	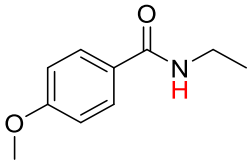	**145**	0 (rsm)
10	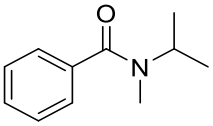	**130**	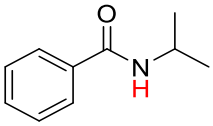	**146**	0 (rsm)
11	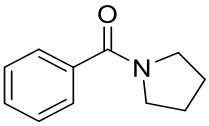	**131**	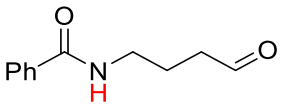	**147**	<5
12	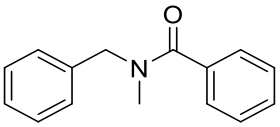	**122**	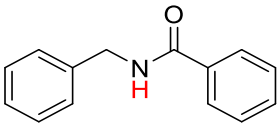	**148**	0 (rsm)
13	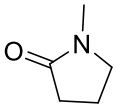	**135**	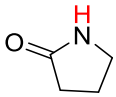	**149**	0 (rsm)
14	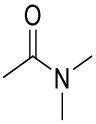	**136**	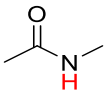	**150**	0 (rsm)
15	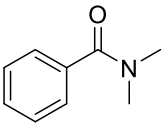	**137**	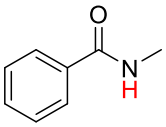	**151**	0 (rsm)

[a] Complex mixture formed (n=3). [b] I=10 mA; [c] under divided conditions the formation of **116** was observed; rsm. =recovered starting material.

Table 4 entries **1-2** were easily controlled and gave an isolated yield with the methodology – as initially thought they would hinder the electrosynthesis due to the inductively electron-rich aryl system in the *ortho* and *meta* positions. A complex mixture is given when the *para*-ethyl system in entry **3** undergoes electrosynthesis. When entry **3** is compared to a similar electronic structure in entry **1**, the *ortho*-ethyl group gives the highest yield observed in the ethyl-substituted benzamide. It is possible that the planar form of the aryl ring significantly hinders the effect of the ethyl group upon the *N*-centred radical, leading to the formation of a complex mixture.[103]

The ethyl group was replaced by chlorine in entries **4-6** to examine a modest electron-withdrawing functionality on the adjacent tertiary amide. Apart from *ortho*-chloro (entry **4**), the isolated yields of entries **5** and **6** are comparable to the ethyl substituted amides. This low yield could be attributed to the superior rotation applied to the adjacent amide carbonyl system.[104] An improvement to the isolated yield for entries **4** and **5** was observed when the current (and density) was slightly increased.

The *N*-deethylation of entries **7-9** in an undivided cell was not observed when the chloride group was replaced with a strong electron-donating methoxy group in the *ortho*, *meta* or *para* position. Starting material was recovered in all cases. This was possibly caused by the production of a methoxy radical (favouring tertiary amide oxidation) which might help redox travel inefficiently at the working and counter electrodes.[105-108] To determine whether methoxy radical was hampering the formation of *N*-dealkylation product of entries **7-9**. Entry **8** was subjected to electrosynthesis using the same method. However, the reaction vessel was changed to a divided H-cell with a sintered glass frit. Surprisingly, the substrate reacted efficiently, producing a mixture of product and **106,** demethoxylation of **128**. A conversion yield of 10% for **106** was determined by ^{1}H NMR spectroscopy.

A complex mixture of products for entry **11** of the cyclic tertiary amide was produced. The crude ^{1}H NMR spectrum of entry **11** indicated an aldehyde peak. This entry gave another mechanistic insight into the reaction. No reaction was observed with the nitrogen radical stabilising phenyl group on the amide entry **12**.

Interestingly, only deethylation is observed; however, *N*-demethylation is not observed once this group is changed to methyl, as per entries **13 -15**. Once these compounds undergo *N*-demethylation, they become unstable and similarly to entries **7-9**, the species shuffles between the two electrodes. This was further investigated in the H-cell. The crude ^{1}H NMR spectrum indicated the presence of starting material, electrolyte, and several other peaks compared to the possible formation of *N*-dealkylation, **106**, and Shono-oxidised compound, but the determination of the product was not possible.

Compound **152** contains two electronegative groups on the aromatic and hence was selected to investigate and observe how disubstituted benzene would affect the outcome of *N*-dealkylation.

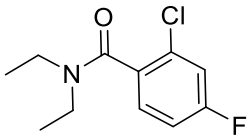

152

Figure 14: 2-Chloro-*N*,*N*-diethyl-4-fluorobenzamide for investigating disubstituted affect.

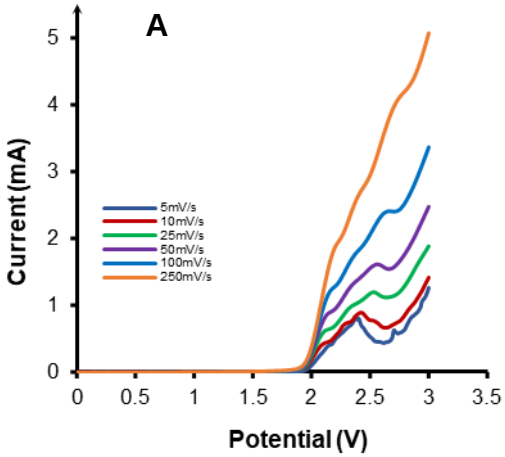

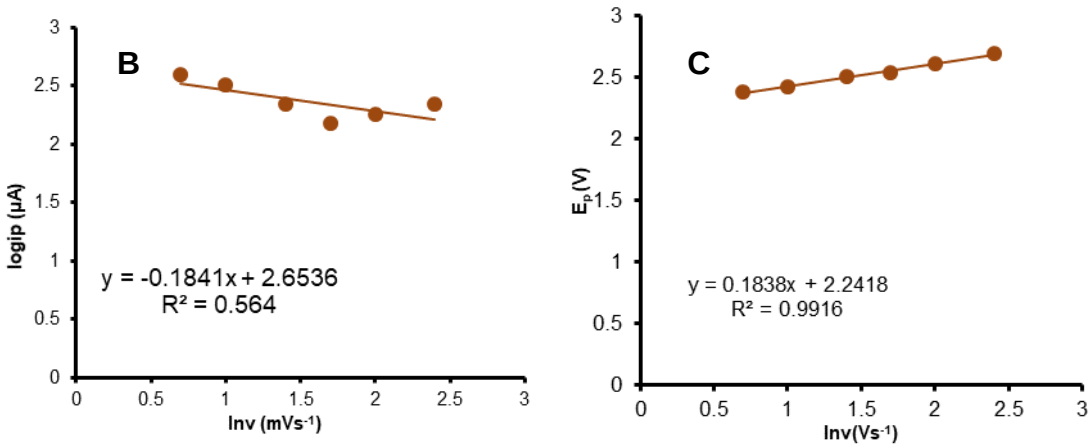

Figure 15: A: LSV of **152** using GCE as WE, platinum as CE and silver as RE. TBAP (0.5 M): MeOH (10:1). B: Plot of log of peak current (ip) vs log of scan rate (mVs^{-1}). C: Plot of peak potential (Ep) vs log of scan rate (mVs^{-1}) for the compound using scan rate 5 mVs^{-1} to 250 mVs^{-1}.

LSV determined how the oxidation potential is affected when two electronegative groups are attached to the aromatic. The LSV helped to determine if the process is diffusional or adsorbed the values. Multiple oxidation peaks are observed at the LSV

The peaks above 10mV are weak and broad due to slow electron transfer. The slope value calculated for the compound is closer to an ideal diffusional controlled process.[91] Hence, the compound is diffusional in process and not precipitating onto the electrode surface. The diffusional behaviour is caused by the poor adherence of products on the electrode surface.[109]

152 was electrosynthesised using TBAP as an electrolyte; it did not lead to the formation of an electrolyte. Hence, $LiClO_4$ was visited in a last attempt to observe if it would be successful. Surprisingly when $LiClO_4$ electrolyte was used, it produced a Shono-oxidised product (Scheme 31). 10% product was recovered, the remaining was starting material.

The effects of electrolytes were studied in CO_2 and oxygen reduction. However, enough data was not collected to conclusively state why the electrolyte change would lead to a dramatic result. However, previous data published suggests that electrolyte ions can impact the reaction environment of electrochemical systems and be a key driver in determining the reaction rate and selectivity. [110] Blanco and co-worker[111] also reported these effects when adiponitrile was synthesised.

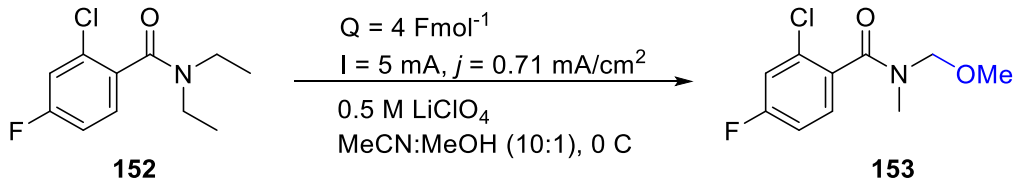

152 **153**

Scheme 31: Shono-oxidation of **152** using lithium perchlorate under galvanostatic conditions in the undivided cell.

3.5. Modification of drug-like compounds

Finally, various compounds, including herbicides and existing drugs (Figure 16), were inspected. These compounds were purchased except for **154** and **161**. To observe if the bulk electrochemical method can be applied to more complex systems, the selected compounds contain more than one substitution on the benzene ring**.**

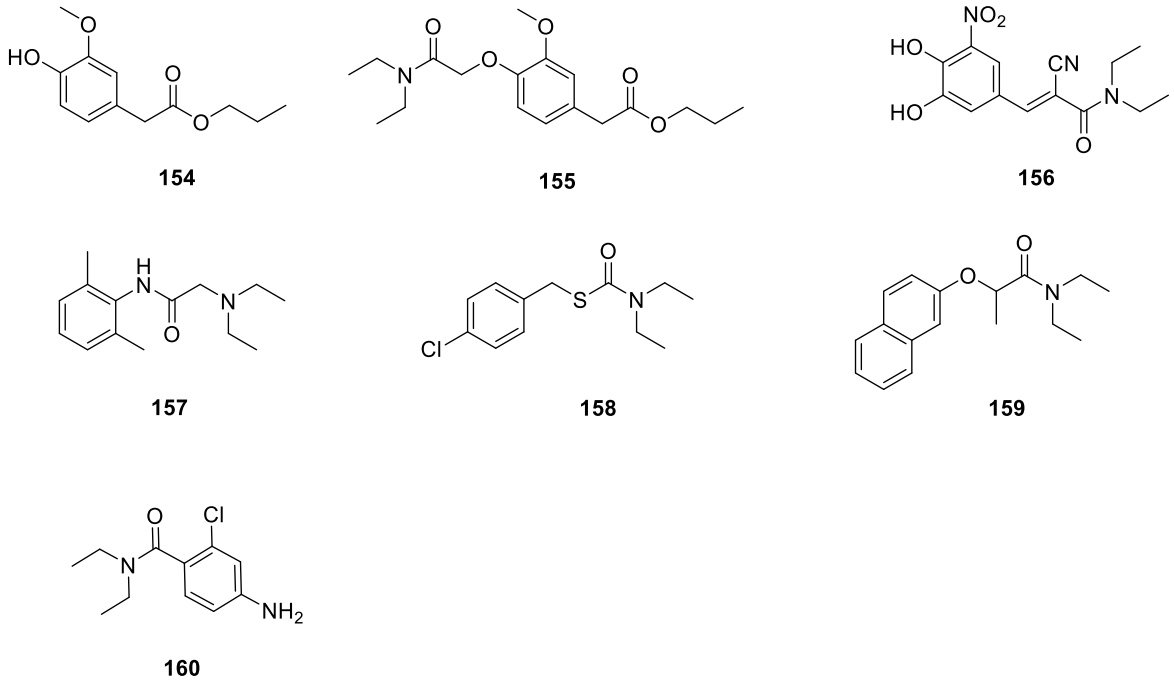

154 **155** **156**

157 **158** **159**

160

Figure 16: Compounds selected for the electrosynthesis.

3.5.1 Synthesis of propanidid

Propanidid (**155**) was synthesised using a method reported in the literature in two stages.[112] The first stage was Fisher's esterification of a carboxylic acid with 1-propanol. At the second step, the chloroacetamide reacted with the OH group to give the final product.

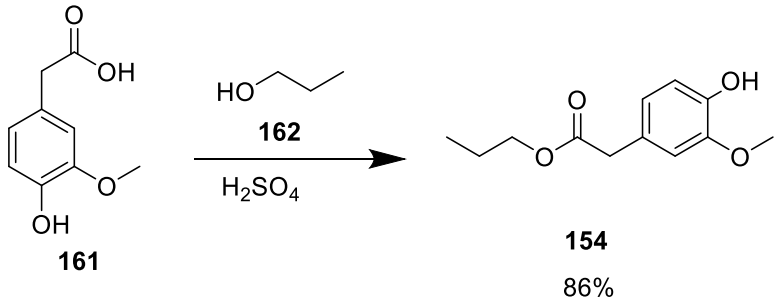

Scheme 32: Reaction mechanism of propyl 4-hydroxy-3-methoxyphenylacetate (**154**).[112]

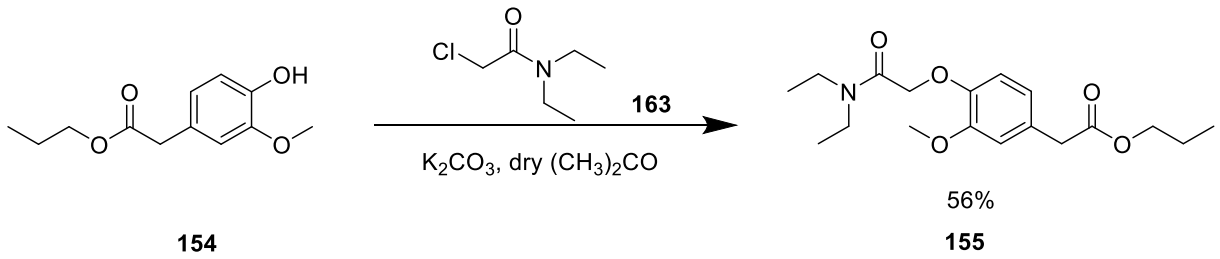

Scheme 33: Reaction mechanism for propanidid **155**.[112]

3.5.1 Linear sweep voltammetry of drugs

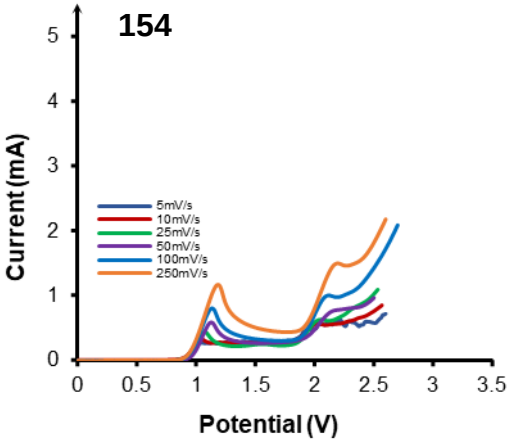

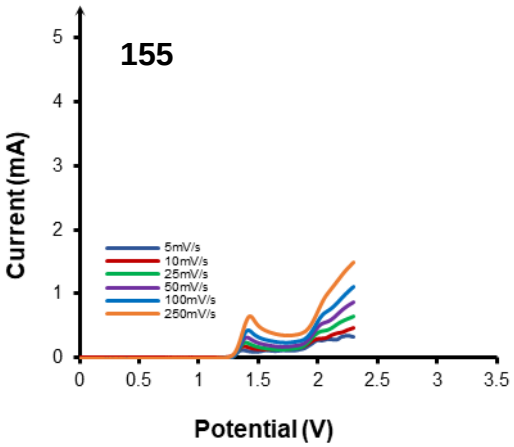

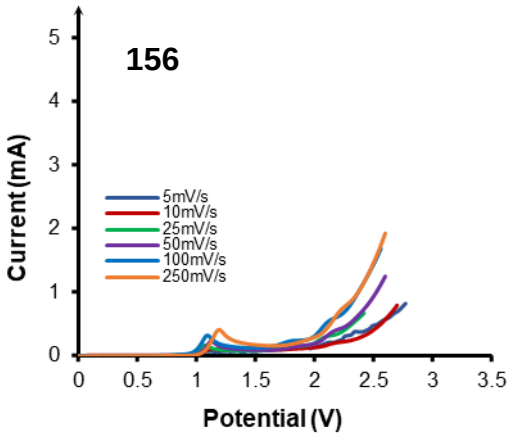

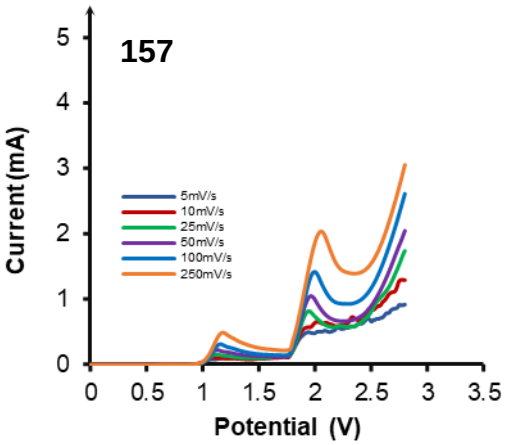

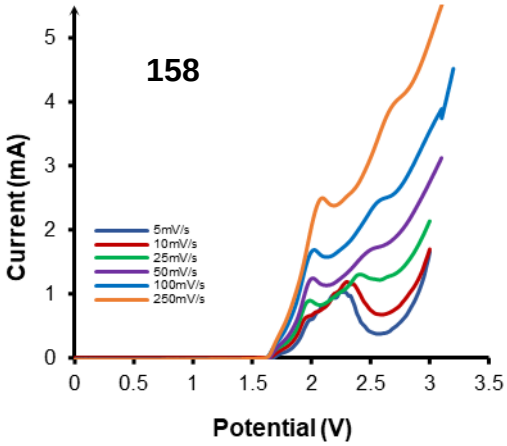

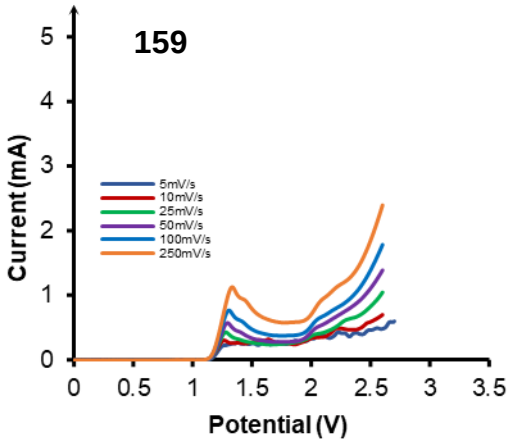

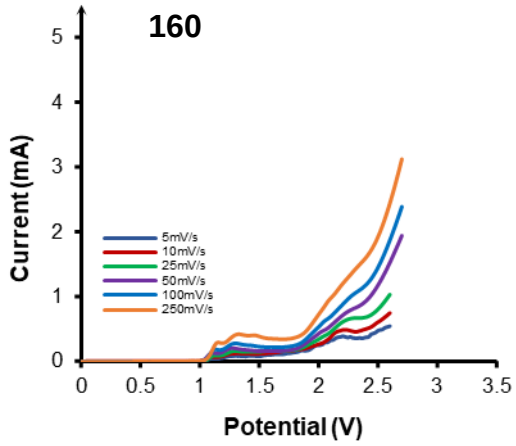

Figure 17*:* LSV of the compounds using GCE as WE, platinum as CE and silver as RE. TBAP (0.5 M), MeCN: MeOH (10:1).

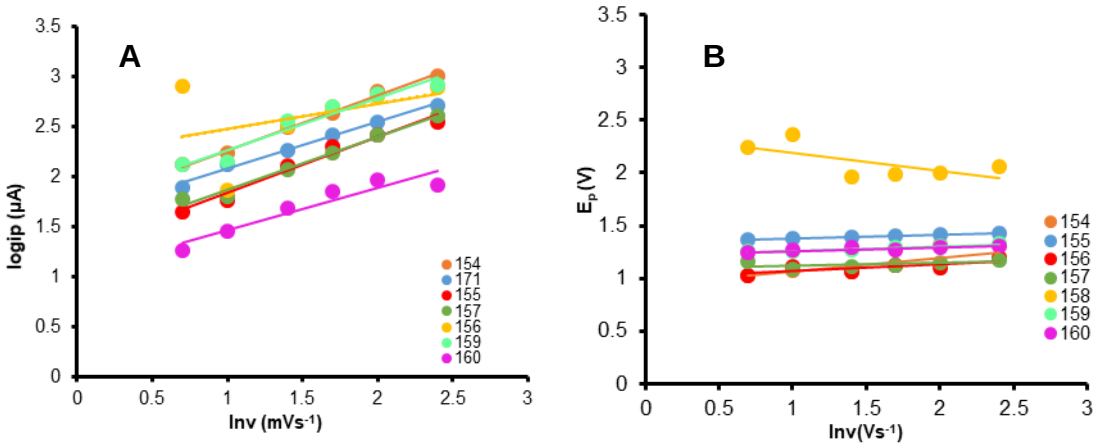

Figure 18: A: Plot of log of peak current (ip) vs log of scan rate (mVs^{-1}). **B**: Plot of peak potential vs (Ep) vs log of scan rate (mVs^{-1}) for the compounds using scan rates 5 mVs^{-1} to 250 mVs^{-1}.

Table 5: Slope and correlation coefficient for Figure 22A.

Compound	Slope value	R^2
154	Ip (µA) = 0.547 log v(mVs^{-1}) + 1.723	0.993
155	Ip (µA) = 0.469 log v(mVs^{-1}) + 1.613	0.989
156	Ip (µA) = 0.561 log v(mVs^{-1}) + 1.277	0.969
157	Ip (µA) = 0.529 log v(mVs^{-1}) + 1.343	0.982
158	Ip (µA) = 0.255 log v(mVs^{-1}) + 2.225	0.169
159	Ip (µA) = 0.524 log v(mVs^{-1}) + 1.745	0.943
160	Ip (µA) = 0.418 log v(mVs^{-1}) + 1.053	0.899

Table 6: Slope correlation coefficient values for Figure 22B

Compound	Slope value	R^2
154	Ep (V) = 0.131 log v(mVs^{-1}) + 0.932	0.596
155	Ep (V) = 0.037 log v(mVs^{-1}) + 1.337	0.998
156	Ep (V) = 0.070 log v(mVs^{-1}) + 0.996	0.603
157	Ep(V) = 0.022 log v(mVs^{-1}) + 1.100	0.175
158	Ep (V) = -0.173 log v(mVs^{-1}) + 2.37	0.453
159	Ep (V) = 0.043 log v(mVs^{-1}) + 1.219	0.948
160	Ep (V) = 0.034 log v(mVs-1) + 1.227	0.823

The oxidation of these drugs occurs through at least two consecutive electron-transfer processes separated by chemical deprotonation, where first oxidation and deprotonation of the selected radical occur and further oxidation to the equivalent cation occurs, leading to the formation of the product. The peaks around 1.0 V indicate that products with low oxidation energy, most likely an electron-rich aryl system, are oxidised as amide would be oxidised at a higher potential. However, apart from the visible first E_p^{ox}, the other oxidation peaks occurring after 2.0 V are broad and undefined. These wide peaks could be caused by slow electron transfer would need to be investigated further to determine the number of electron transfer taking place and what intermediates are being formed to understand the reaction mechanism.

The E_p^{ox} values were determined from 25 mVs^{-1}. The analysis of **154** and **157** indicates two clear E_p^{ox}, +1.08 V and + 2.04 V for **154** +1.15 V and + 1.97 V for **157**, indicating that ECE reaction is taking place. The LSV of **157** indicates that oxidation occurs through two consecutive electron-transfer processes separated by chemical deprotonation, first oxidation and deprotonation to the amidyl radical and then further oxidation to the corresponding cation. Gieshoff *et al.*[113] observed a similar oxidation mechanism when they investigated the oxidation of anilides.

A clear single E_p^{ox} for **160** is observed at +1.04 V when scan rate 25 mVs^{-1} is used. However, there are at least three E_p^{ox} recorded after +1.04 V that are wide and ill-defined. This could be because the same redox-active species undergo sequential electron transfer events, possibly associated with NH_2. Although, a single oxidation peak of oxidation is also observed around +2.20 V, which could be associated with the removal of the second H in the same group and would require considerably larger potential to remove.

Table 5 shows the slope values calculated from Figure 18 to observe if the process was diffusional or adsorbed, the values used for these graphs came from the first oxidation peak of the compounds. The theoretical value of 0.5 is an ideal diffusional controlled process.[91] The slope value calculated for these compounds are closer to this. Hence these compounds are diffusional in process and are not precipitating onto the electrode surface. The diffusional behaviour is caused by the poor adherence of products on the electrode surface.[109]

Table 6 shows the slope value obtained from Figure 18B; peak potential increases with the scan rate except for **158**, where the peak potential fluctuates. **156**, **157**, **159,** and **169** are likely irreversible to some extent as the peak potential shifts to more positive potentials. The remaining compounds **154**, **155** and **158** are likely quasi-reversible as the peak potential difference observed by the slope is not enormous.

3.5.2 Electrochemical reactions of the substrates

The compounds were subjected to the electrochemical methods reported in Table 1 in a divided cell using TBAP as an electrolyte. The crude ^{1}H-NMR spectra of compounds indicated that they had undergone an electrochemical process. However, assigning peaks and working out conversion yield was impossible because the ^{1}H-NMR spectrum showed multiple products and starting material peaks. This is consistent with the LSV results, which indicated that more than one electro-active group was present in many compounds. The Isolation of the primary product proved challenging.

To improve isolating the product, electrosynthesis of the compound was conducted using a divided cell, but the results were comparable to an undivided cells usage. Isolating the products was not possible when FCC was used.

To demonstrate the difficulty in the purification of the electrosynthesised compound, an example of what a typical crude ^{1}H-NMR looks like after removal of the electrolyte is shown in Figure 19. The spectra for **159** is in red; the black spectra is for the electrosynthesis product. The peaks in the spectra include solvent peaks, minor

peaks assigned to the electrolyte, starting material and several other unknown peaks.

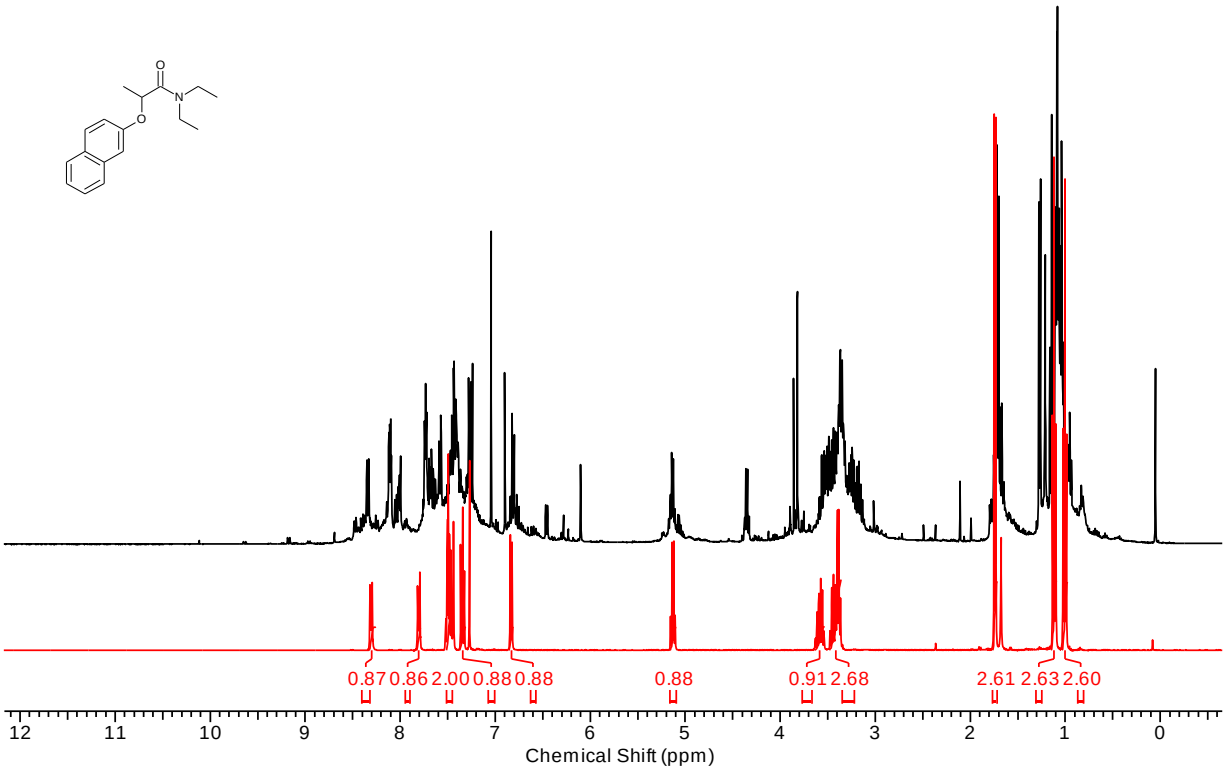

Figure 19: Crude ^{1}H-NMR for **159** after electrosynthesis and removal of electrolyte.

Reverse-phase HPLC (uses a hydrophobic stationary phase) was examined to isolate the product. The HPLC spectrum showed poor peak to peak separation and hence, was challenging to separate, despite changing the flow rate and solvent ratios. Furthermore, each compound required further optimisation for both the starting material and the electrosynthesised product.

3.6 Conclusion and Future Work

LSV for **106** indicated that when MeCN/MeOH were used as solvents, a non-linear plot forms. The non-linear graph was due to the constant change in ip from 10 mVs-1 onwards. A single oxidation peak is observed when the solvent system is switched to MeCN/H2O (10:1). Methanol constricts the viable voltammetric window. Therefore, a diffusional process is taking place. However, it entails a mild -50 mV reduction at the start of the initial oxidation response.

When TBAP is used as an electrolyte *N*-dealkylation of **106** is observed, **107** was isolated at 24%. Over-reaction to primary amide and by-products (99% b.r.s.m) were not detected. None of the proposed products (Shono oxidation, *N*-dealkylation and the starting material) was observed $LiClO_4$ was used as an electrolyte.

Flash column chromatography (FCC) on silica was optimised to improve the isolated yield of **107**. A slow flow rate of 0.5 mL/min and increasing the solvent polarity incrementally (95:5 to 75:25, Petroleum ether: EtOAc) whilst using a column with a diameter of 3.5 cm resulted in a yield of 78% for **107**. A slow flow rate is more favourable as the electrolyte takes longer to elute when compared to faster flow rates. Other methods did not give adequate results.

Optimisation of the electrochemical methods by changing the factors listed in Table 4 resulted in an upper limit for the generation of **107** (86%) observed in Entry **5** (j = 0.71 mA/cm^2), where I = 5.0 mA when correlated to lower and higher currents (and current densities). The product yields increased as the current density decreased due to fewer back reactions and side reactions. Current efficiency is reduced when a higher current density is used.

Both water and methanol are appropriate nucleophilic traps for **116**. MeOH can be reduced to methoxide and H_2O to hydroxide respectively at the counter electrode. Pathway A dominates via the typical Shono α-methoxylation initiation. The key observations included: methanol is needed for the reaction with trace quantity of water to assist the reaction, through electro-generation of acid and react with the acetal by-products *via* hydrolysis.

Additional experiment to probe the feasibility of double dealkylation was conducted. Low potential for **106** is observed due to less electron density on the nitrogen in **107** than in **106**. Hence higher applied voltage is needed to adjust the Fermi level of the electrode to match the energy level of **107**. Until higher overpotentials are used, (e.g. after consumption of the lower E_p^{ox} substrate, **106**), the reaction of **107** becomes unfavourable.

The second part of the project was to investigate the scope of the method. Varieties of benzamide and alkylamide analogues were explored to examine the effects of electron-donating/withdrawing groups, steric effects, and changes to the alkyl group on the reaction. A multi milligram sample of the major human metabolite of the (DEET) **106** was produced. Interestingly, dealkylation is only observed in compounds that contain an ethyl group. Therefore, *N*-demethylation is not observed. However, for **127**, an aldehyde by-product was detected in crude ^{1}H-NMR. Interestingly **152** gave a Shono-oxidised product when an alternative electrolyte $LiClO_4$ was used as an electrolyte.

The project's final phase was the application of the method to complex drug-like structures and herbicides compounds. Crude ^{1}H-NMR spectrum indicated that compounds had changed, although no major products or *N*-dealkylation were detected. Flash column chromatography and Reverse-phase HPLC failed to assist in isolating the product.

Several parameters can be explored to make this method more viable for studying the metabolite of drugs. One of the main challenges for this method was the inability to produce *N*-deethylation of complex compounds. Hence, other types of electrolysis need to be explored. One possible pathway could be to use a flow cell. Flow cell electrochemical reactions have been reported to be successful in the electrosynthesis of various functional groups.[105, 114, 115] Potentiostatic methods effectively produce electrochemical compounds and, as reported by literature, gives more control over the selectivity.[63, 116]

One of the significant downsides to using TBAP as an electrolyte is that removing it is difficult and time-consuming. Hence, other electrolytes need to be investigated, which are less hazardous and simpler to separate. A mechanistic study will need to be conducted into why simply switching the electrolyte from TBAP to $LiClO_4$ lead to the production of Shono-oxidised compound instead of the expected *N*-dealkylation.

LC-MS, in combination with electrochemistry, is successful in detecting *N*-deethylation of drugs. Another method applied within electrochemistry is a computational (computer stimulation) for studying compounds likely to undergo electrosynthesis. The method is already used for drug discovery and could be modified for electrosynthesis. With electrochemistry and electrosynthesis, a combination of LC-MS could lead to more efficient drug discovery and development processes.

The group recently published a paper in Scientia Pharmaceutica 2020 (Voltammetric Behaviour of Drug Molecules as a Predictor of Metabolic Liabilities). The LSV for Compounds **155**, **156** and **157**, respectively, were analysed against the half-life of the drugs. The research concluded that the oxidation potential has an inverse relationship with the drug's stability in the body (half-life), with 1450 mV, 1250 mV and 1150 mV correlating to 5.9 min, 24 min and 87–108 min, for 171, 173 and 175, respectively. This is another exciting area that the research conducted in the thesis can be explored in the future.

Chapter 4: Experimental

4.1. General information

All commercial reagents and solvents were used as received without further purification. All electrosynthesis and cyclic voltammetry experiments were performed using an Autolab (PGSTAT 100N, The Netherlands) potentiostat. Reactions were monitored by TLC and purified using silica flash column chromatography (ethyl acetate: petroleum ether) using high-purity grade, pore size 60 Å, 200- 400 mesh particle size silica gel (Sigma-Aldrich)

^{1}H and ^{13}C-NMR spectra were recorded on a JEOL (ECS 400 MHz NMR spectrometer). ^{1}H and ^{13}C-NMR chemical shifts (δ) are reported in parts per million relative to tetramethylsilane (TMS), with the solvent resonance employed as the internal standard ($CDCl_3$ at 7.26 ppm, $CDCl_3$ at 77.20 ppm). Data is reported as follows: chemical shift, multiplicity (s = singlet, br s = broad singlet, d = doublet, t = triplet, q = quartet, m = multiplet and combinations thereof), coupling constants (Hz) and integration. Low and high-resolution mass spectrometry analysis was obtained using an Agilent 6450 LC-MS/MS system.

4.2. Experimental Procedure

4.2.1. Synthesis of benzamide

All reactions were conducted under a nitrogen atmosphere. The appropriate acyl chloride (10.0 mmol), potassium carbonate (2.07 g, 15.0 mmol) and anhydrous tetrahydrofuran (35.0 mL) were cooled to 0 °C (using an ice-bath). Under stirring, the appropriate amine (10.0 mmol) was added portion-wise at 0 °C. The reaction mixture was allowed to stir at room temperature (25 °C) for an additional 24 h. The reaction was quenched with hydrochloric acid (1.0 M, 4.0 mL) portion-wise and extracted with ethyl acetate (3 × 30 mL), washed with saturated $NaHCO_3$ (30 mL) and brine (30 mL). The combined organic layer was dried (using $MgSO_4$), filtered and concentrated *in vacuo* to afford the title compound.

4.2.2 Synthesis of Propanidid

Step 1

The procedure was adapted from Hiltman *et al.* [117] A 30 mL glass pressure tube was equipped with a magnetic stirrer; 4-hydroxy-3-methoxyphenethyl alcohol (12.0 mmol) was added and dissolved with anhydrous 1-propanol (0.27 M, 21.0 mL). To this solution (1.0 ml) of concentrated sulphuric acid was added, and the solution was heated at 100 °C for 5 hours. The solvent was removed under reduced pressure. The resulting oil was diluted with ethyl acetate (40.0 mL), washed with saturated sodium bicarbonate (20.0 mL), distilled water (20.0 mL) and brine (20.0 mL). The organic layer was dried (MgSO4), filtered and concentrated in vacuo to afford 3-methoxy-4-hydroxyphenylacetic acid propyl ester (86%).

Step 2

In a 50mL round bottom flask equipped with a magnetic stir bar, 3-methoxy-4-hydroxyphenylacetic acid propyl ester (3.4 mmol, 0.8 g) was dissolved in dry acetone (0.27 M, 20 ml). Potassium carbonate (5.1 mmol, 705 mg) was added to the solution, followed by 2-chloro-*N,N*-diethylacetamide (4.0 mmol, 0.55 ml). Under vigorous stirring, the suspension was warmed to reflux (60 °C) for 16 hours. After cooling to room temperature, the reaction mixture was filtered, and the remaining solvent was removed under reduced pressure. The product was purified using silica column chromatography (SiO_2, EtOAc/Hexane (1:1))) to produce the title compound.

4.2.3. Dealkylation of compounds

The appropriate amide (0.22 mM/mL) and the electrolyte (tetrabutylammonium perchlorate (TBAP), 0.5 mol/L are added to an undivided glass cell (28 mL). The cell was equipped with a magnetic stirrer and solvents acetonitrile (9.0 mL) and methanol (0.9 mL). Rectangular reticulated vitreous carbon anode (4.7 cm^2) and cathode (4.7 cm^2) are arranged opposite each other at a distance of 9.8 mm.

Chronocoulometry (bulk electrolysis) was employed to conduct electrosynthetic reactions. The equation, Q = (mA /RMM) nF was used to calculate the charge required for each electrosynthetic reaction (**Section 2.3**).

The electrochemical reaction is monitored by TLC and by total charge (Q) transferred. The RVCs are washed with a minimum amount of MeOH upon reaction completion into the reaction vessel to dislodge the reaction mixture. The solution was concentrated *in vacuo* to afford a solid white coloured powder. The powder was dissolved in a minimum amount of EtOAc for flash column chromatography. The FCC ((SiO_2) was conducted using a flow rate of 0.5 mL/min. The solvents EtOAc: petroleum ether (5:95 to 35:65) were used to isolate the dealkylated product.

4.2.4 Recrystallisation for dealkylated *N,N*-Diethylbenzamide

Upon the completion of electrosynthesis, the solution was concentrated in vacuo to afford a solid white powder. Hot MeOH was added to the beaker containing the compound and left overnight for TBAP crystals. Crystals were collected using a gravity filter and washed with a non-polar solvent. The solution was concentrated in vacuo and prepared for FCC to isolate the product.

4.2.5. Linear sweep voltammetry

LSV experiments were performed using a glassy carbon electrode (GCE, area = 0.071 cm^2) as a working electrode, a platinum wire was used as a counter, and Ag/AgCl wire (standardised to Fc^+/Fc by comparison) was used as a reference electrode, respectively. Prior to each experiment and in-between scan rate studies, the GCE was polished manually. First, with 1µm diamond spray (Kemet) on a smooth polishing pad (BAS velvet polishing pad). Then rinsed with distilled water, and second polishing was done using 0.25 microns diamond spray (Kemet) on a smooth polishing pad (BAS velvet polishing pad). The GCE was finally rinsed with distilled water thoroughly and then dried with medical tissue before the experiment. The linear regression equations were calculated by the least-squares method using Microsoft Excel® software**.**

4.3. Compound Characterisation

106 *N,N*-Diethylbenzamide[63]

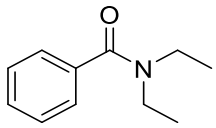

The title compound afforded as a pale yellow oil (1.61 g, 91%) using the general procedure outlined in section 4.2.1.

^{1}H-NMR (400 MHz, $CDCl_3$) δ: 7.33 - 7.25 (m, 5H), 3.48 (s, 2H), 3.17 (s, 2H), 1.18 (br s, 3H), 1.03 (br s, 3H).
^{13}C-NMR (101 MHz, $CDCl_3$) δ: 171.3, 137.3, 129.1, 128.5, 126.3, 43.4, 39.3, 14.3, 13.0.
LC-MS (ESI) *m/z* 178 $[M+H]^+$.
Hi-Res LC-MS (ESI) *m/z* calcd for $C_{11}H_{15}NO$ $[M+H]^+$ 178.1226, found 178.1229.

121 *N,N*-diethyl-2-methylbenzamide[118]

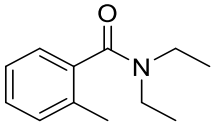

The title compound afforded as a pale yellow oil (1.31 g, 68%) using the general procedure outlined in section 4.2.1.

^{1}H NMR (400 MHz, $CDCl_3$) δ: 7.26 - 7.13 (m, 4H), 3.75 (br s, 1H), 3.40 (br s, 1H), 3.11 (q, *J* = 7.0 Hz, 2H), 2.27 (s, 3H), 1.24 (t, *J* = 7.0 Hz, 3H), 1.01 (t, *J* = 7.0 Hz, 3H).
^{13}C-NMR (101 MHz, $CDCl_3$) δ: 170.9, 137.2, 133.9, 130.3, 128.6, 125.8, 125.5, 42.6, 38.7, 18.9, 14.1, 13.0.
LC-MS (ESI) *m/z* 192 $[M+H]^+$.
Hi-Res LC-MS (ESI) *m/z* calcd for $C_{12}H_{17}NO$ $[M+H]^+$ 192.1383, found 192.1387

122 *N,N*-diethyl-3-methylbenzamide[118]

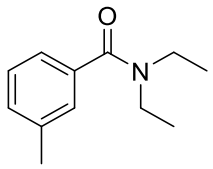

The title compound afforded as a pale yellow oil (1.46 g, 76%) using the general procedure outlined in section 4.2.1.

^{1}H NMR (400 MHz, $CDCl_3$) δ: 7.27 - 7.12 (m, 4 H), 3.53 (s, 2H), 3.23 (s, 2H), 2.35 (s, 3H), 1.23 (br s, 3H), 1.08 (br s, 3H).
^{13}C-NMR (101 MHz, $CDCl_3$) δ: 170.9, 137.2, 133.9, 130.3, 128.6, 125.8, 125.5, 42.6, 38.7, 18.9, 14.1, 13.0.
LC-MS (ESI) *m/z* 192 $[M+H]^+$.
Hi-Res LC-MS (ESI) *m/z* calcd for $C_{12}H_{17}NO$ $[M+H]^+$ 192.1383, found 192.1385.

123 *N,N*-diethyl-4-methylbenzamide[118]

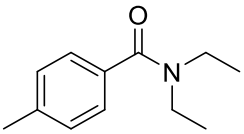

The title compound afforded as a pale yellow oil (1.70 g, 89%) using the general procedure outlined in section 4.2.1.

^{1}H NMR (400 MHz, $CDCl_3$) δ: 7.26 - 7.24 (m, 2H), 7.18 - 7.16 (m, 2H), 3.52 (br s, 2H), 3.25 (br s, 2H), 2.35 (s, 3H), 1.23 (s, 3H), 1.10 (s, 3H).
^{13}C-NMR (101 MHz, $CDCl_3$) δ: 171.6, 139.1, 134.4, 129.1, 126.4, 43.4, 39.3, 21.4, 14.3, 13.0.
LC-MS (ESI) *m/z* 192 $[M+H]^+$.
Hi-Res LC-MS (ESI) *m/z* calcd for $C_{12}H_{17}NO$ $[M+H]^+$ 192.1383, found 192.1387.

124 *N,N*-diethyl-2-chlorobenzamide[119]

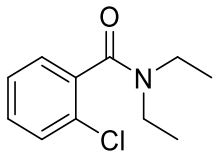

The title compound afforded as a pale yellow oil (1.86 g, 87%) using the general procedure outlined in section 4.2.1.

^{1}H NMR (400 MHz, $CDCl_3$) δ: ppm 7.38 - 7.34 (m, 1H), 7.31 - 7.23 (m, 3H), 3.80 - 3.75 (m, 1H), 3.38 - 3.33 (m, 1H), 3.13 (quint, *J* = 7.1 Hz, 2H), 1.25 (t, *J* = 7.0 Hz, 3H), 1.04 (t, *J* = 7.0 Hz, 3H).
^{13}C-NMR (101 MHz, $CDCl_3$) δ: 167.8, 136.8, 130.4, 129.9, 129.7, 127.5, 127.1, 42.7, 39.0, 14.0, 12.7.
LC-MS (ESI) *m/z* 212 $[M+H]^+$.
Hi-Res LC-MS (ESI) *m/z* calcd for $C_{11}H_{14}ClNO$ $[M+H]^+$ 212.0837, found 212.0833.

125 *N,N*-diethyl-3-chlorobenzamide[120]

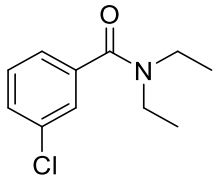

The title compound afforded as a pale yellow oil (1.31 g, 68%) using the general procedure outlined in section 4.2.1.

^{1}H NMR (400 MHz, $CDCl_3$) δ: 7.37 - 7.28 (m, 3H), 7.25 - 7.20 (m, 1H), 3.52 (m, 2 H), 3.22 (m, 2H), 1.22 (br s, 3H), 1.09 (br s, 3H).
^{13}C-NMR (101 MHz, $CDCl_3$): 169.7, 138.9, 134.5, 129.9, 129.3, 126.6, 124.4, 43.4, 39.4, 14.3, 12.9.
LC-MS (ESI) *m/z* 212 $[M+H]^+$.
Hi-Res LC-MS (ESI) *m/z* calcd for $C_{11}H_{14}ClNO$ $[M+H]^+$ 212.0837, found 212.0836.

126 *N,N*-diethyl-4-chlorobenzamide[118]

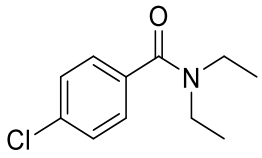

The title compound afforded as a pale yellow oil (1.48 g, 70%) using the general procedure outlined in section 4.2.1.

^{1}H NMR (400 MHz, $CDCl_3$) δ: 7.36 - 7.28 (m, 4H), 3.51 (br s, 2H), 3.22 (br s, 2H), 1.22 (br s, 3H), 1.09 (br s, 3H).
^{13}C-NMR (101 MHz, $CDCl_3$) δ: 170.3, 135.7, 135.2, 128.8, 127.9, 43.4, 39.5, 14.3, 12.9.
LC-MS (ESI) *m/z* 212 $[M+H]^+$.
Hi-Res LC-MS (ESI) *m/z* calcd for $C_{11}H_{14}ClNO$ $[M+H]^+$ 212.0837, found 212.0836.

127 *N,N*-diethyl-2-methoxybenzamide[121]

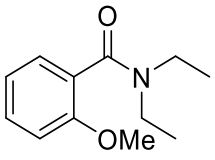

The title compound afforded as a pale yellow oil (1.88 g, 91%) using the general procedure outlined in section 4.2.1.

^{1}H NMR (400 MHz, $CDCl_3$) δ: 7.34 - 7.30 (m, 1H), 7.17 (dd, *J* = 7.0, 1.0 Hz, 1H), 6.98 - 6.95 (m, 1H), 6.91 – 6.89 (d, *J* = 7.0 Hz, 1H), 3.82 (s, 3H), 3.60 - 3.55 (m, , 2H), 3.17 – 3.12 (q, *J* = 7.0 Hz, 2H), 1.24 (t, *J* = 7.0 Hz, 3H), 1.03 (t, *J* = 7.0 Hz, 3H).
^{13}C-NMR (101 MHz, $CDCl_3$) δ: 168.9, 155.2, 129.9, 127.5, 127.0, 120.8, 111.0, 55.6, 42.8, 38.9, 14.0, 13.0.
LC-MS (ESI) *m/z* 208 $[M+H]^+$.
Hi-Res LC-MS (ESI) *m/z* calcd for $C_{12}H_{17}NO_2$ $[M+H]^+$ 208.1332, found 208.1339.

128 *N,N*-diethyl-3-methoxybenzamide[122]

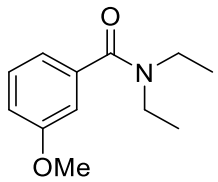

The title compound afforded as a pale yellow oil (1.31 g, 68%) using the general procedure outlined in section 4.2.1.

^{1}H NMR (400 MHz, $CDCl_3$) δ: 7.30 - 7.25 (m, 1H), 6.92 - 6.87 (m, 3H), 3.80 (s, 3H), 3.52 (d, *J* = 6.4 Hz, 2H), 3.24 (d, *J* = 5.5 Hz, 2H), 1.23 (br s, 3H), 1.09 (br s, 3H).
^{13}C-NMR (101 MHz, $CDCl_3$) δ: 171.1, 159.6, 138.6, 129.6, 118.5, 115.1, 111.7, 55.4, 43.3, 39.3, 14.4, 13.0.
LC-MS (ESI) *m/z* 208 $[M+H]^+$.
Hi-Res LC-MS (ESI) *m/z* calcd for $C_{12}H_{17}NO_2$ $[M+H]^+$ 208.1332, found 208.1331.

129 *N,N*-diethyl-4-methoxybenzamide [118]

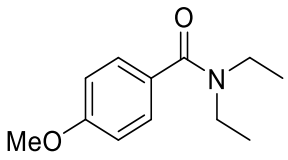

The title compound afforded as a pale yellow oil (1.78 g, 86%) using the general procedure outlined in section 4.2.1.

^{1}H NMR (400 MHz, $CDCl_3$) δ: 7.37 - 7.33 (m, 2H), 6.92 - 6.89 (m, 2H), 3.83 (s, 3H), 3.48 - 3.35 (m, 4H), 1.18 (br s, 6H).
^{13}C-NMR (101 MHz, $CDCl_3$) δ: 171.3, 160.3, 129.6, 128.3, 113.7, 55.4, 42.9, 39.8, 14.3, 12.9.
LC-MS (ESI) *m/z* 208 $[M+H]^+$.
Hi-Res LC-MS (ESI) *m/z* calcd for $C_{12}H_{17}NO_2$ $[M+H]^+$ 208.1332, found 208.1337.

130 *N*-Isopropyl-*N*-methylbenzamide[123]

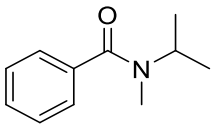

The title compound afforded as a pale yellow oil (1.80 g, 85%) using the general procedure outlined in section 4.2.1.

^{1}H NMR (400 MHz, $CDCl_3$) δ ppm 7.39 - 7.32(m, 5 H), 3.94 (br. s., 1 H), 3.40 (br. s., 2 H) 3.20 (br. s., 1 H) 1.2 - 1.4 (m, 3 H) 1.1 (br. s., 3 H)
^{13}C NMR (101 MHz, $CDCl_3$) δ ppm 171.2, 137.8, 129.0, 128.5, 126.1, 50.3, 35.4, 21.2, 14.9.
Hi-Res LC-MS (ESI) *m/z* calcd for $C_{12}H_{17}NO_2$ $[M+H]^+$ 178.1226, found 178.1222

131 *N*-Benzoylpyrrolidine[118]

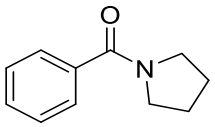

The title compound afforded as a pale yellow oil (1.80 g, 85%) using the general procedure outlined in section 4.2.1.

^{1}H NMR (400 MHz, $CDCl_3$) δ: 7.42 - 7.37 (m, 2H), 7.30 - 7.24 (m, 3H), 3.52 (t, *J* = 6.8 Hz, 2H), 3.30 (t, *J* = 6.6 Hz, 2H), 1.83 (quin, *J* = 7.0 Hz, 2H), 1.73 (quin, *J* = 6 Hz, 2H).
^{13}C NMR (101 MHz, $CDCl_3$) δ: 169.8, 137.3, 129.5, 128.6, 127.9, 49.4, 46.2, 26.8, 24.3.
LC-MS (ESI) *m/z* 176 $[M+H]^+$.
Hi-Res LC-MS (ESI) *m/z* calcd for $C_{11}H_{13}NO$ $[M+H]^+$ 176.1070, found 176.1069.

132 *N*-Benzyl-*N*-methylbenzamide[124]

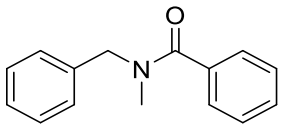

The title compound afforded as a brown-yellow oil (1.34 g, 59 %) using the general procedure outlined in section 4.2.1.

^{1}H NMR (400 MHz, $CDCl_3$) δ: 7.46 - 7.25 (m, 9H), 7.15 (d, *J*=6.2 Hz, 1H), 4.75 (br.s, 1H), 4.50 (br.s, 1H), 3.02 - 2.84 (m, 3H),

^{13}C-NMR (101 MHz, $CDCl_3$) δ: 172.4, 137.1, 136.7, 129.7, 128.9, 128.5, 128.3, 127.7, 127.6, 127.1, 126.9, 55.3, 50.9, 37.1, 33.3.

LC-MS (ESI) *m/z* 226 $[M+H]^+$.

Hi-Res LC-MS (ESI) *m/z* calcd for $C_{15}H_{15}NO$ $[M+H]^+$ 226.1226, found 226.1221.

154 3-methoxy-4-hydroxyphenylacetic acid propyl ester

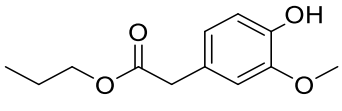

The title compound afforded as a red oil (2.45 g, 86 %) using procedure 4.2.2, step 1.

^{1}H-NMR (400 MHz, $CDCl_3$) δ: ppm 6.85 - 6.89 (m, 1H), 6.82 (d, *J*=1.4 Hz, 1H), 6.75 - 6.80 (m, 1H), 5.63 (s, 1H), 4.06 (t, *J*=6.6 Hz, 2H), 3.89 (s, 3H), 3.55 (s, 2H), 1.65 (sxt, *J*=7.1 Hz, 2H), 0.92 (t, *J*=7.3 Hz, 3H).

^{13}C-NMR (101 MHz, $CDCl_3$) δ: ppm 172.5, 146.9, 145.0, 125.8, 122.0, 114.8, 112.2, 66.5, 55.6, 40.9, 21.9, 10.3.

LC-MS (ESI) *m/z* 225 $[M+H]^+$.

Hi-Res LC-MS (ESI) *m/z* calcd for $C_{12}H_{16}O_4$ $[M+H]^+$ 225.1121, found 225.1120.

155 [4-[(diethylcarbamoyl) methoxy]-3-methoxyphenyl] acetic acid propyl ester

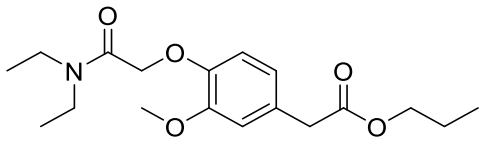

The title compound afforded as a pale yellow oil (0.64 g, 56 %) using the procedure in 4.2.2 step 2.

^{1}H-NMR (400 MHz, $CDCl_3$) δ: ppm 6.88 (d, *J*=8.2 Hz, 1H), 6.82 (d, *J*=1.4 Hz 1H), 6.77 (d, *J*=8.2 Hz, 1H), 4.7 (s, 2H), 4.0 - 4.04 (m, 2H), 3.84 (s, 3H), 3.52 (s, 2H), 3.32 - 3.42 (m, 4H), 1.57 - 1.64 (m, 2H), 1.18 - 1.14 (m, 3H), 1.12 - 1.08 (m, 3H), 0.89 (t, *J*=7.3 Hz, 3H)
^{13}C-NMR (101 MHz, $CDCl_3$) δ: ppm 170.7, 166.0, 148.4, 145.7, 127.0, 120.4, 113.2, 112.1, 67.4, 65.3, 54.7, 40.5, 39.8, 39.2, 21.0, 13.2, 11.8, 9.4.
LC-MS (ESI) *m/z* 338 $[M+H]^+$.
Hi-Res LC-MS (ESI) *m/z* calcd for $C_{18}H_{27}NO_5$ $[M+H]^+$ 338.1962, found 338.1967.

107 *N*-Ethylbenzamide[125]

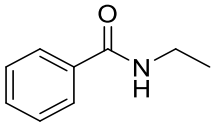

The title compound afforded as a pale yellow oil (1.07 mg, 72%) using the general procedure outlined in section 4.2.3.

^{1}H NMR (400 MHz, $CDCl_3$) δ: 7.77 - 7.71 (m, 2H), 7.49 - 7.37 (m, 3H), 6.22 (br. s, 1H), 3.51 - 3.44 (m, 2H), 1.23 (t, *J* = 7.3 Hz, 3H).
^{13}C-NMR (101 MHz, $CDCl_3$) δ: 167.6, 134.9, 131.4, 128.6, 126.9, 35.0, 15.0.
LC-MS (ESI) *m/z* 150 $[M+H]^+$.
Hi-Res LC-MS (ESI) *m/z* calcd for $C_9H_{11}NO$ $[M+H]^+$ 150.0913, found 150.0909.

138 *N*-Ethyl-2-methylbenzamide[126]

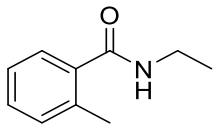

The title compound afforded as a pale yellow oil (20 mg, 54%) using the general procedure outlined in section 4.2.3.

^{1}H NMR (400 MHz, $CDCl_3$) δ: 7.33 - 7.08 (m, 4H), 5.87 (br. s, 1H), 3.52 - 3.28 (m, 2H), 2.40 (s, 3H), 1.20 (t, *J* = 7.3 Hz, 3H).
LCMS *m/z* calcd for $C_{10}H_{13}NO$ $[M+H]^+$ 164.1070, found 164.1057

134 *N*-Ethyl-3-methylbenzamide[127]

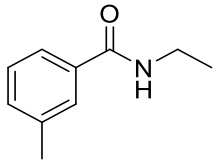

The title compound afforded as a pale yellow oil (19 mg, 52%) using the general procedure outlined in section 4.2.3.

^{1}H NMR (400 MHz, $CDCl_3$) δ: 7.60 - 7.21 (m, 4H), 6.21 (br s, 1H), 3.37 - 3.52 (m, 2H), 2.36 (s, 3H), 1.22 (t, *J* = 7.1 Hz, 3H).
^{13}C-NMR (101 MHz, $CDCl_3$) δ: 167.8, 138.4, 134.8, 132.1, 128.5, 127.7, 123.9, 35.0, 21.4, 15.0.
LC-MS (ESI) *m/z* 164$[M+H]^+$.
Hi-Res LC-MS (ESI) *m/z* calcd for $C_{10}H_{13}NO$ $[M+H]^+$ 164.1070, found 164.1067.

140 *N*-Ethyl-2-chlorobenzamide[125]

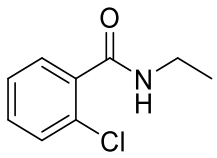

The title compound afforded as a pale yellow oil (6.2 mg, 15%) using the general procedure outlined in section 4.2.3.

^{1}H NMR (400 MHz, $CDCl_3$) δ: 7.65 - 7.59 (m, 1H), 7.40 - 7.23 (m, 3H), 6.17 (br.s, 1H), 3.56 - 3.30 (m, 2H), 1.24 (t, *J* = 7.5 Hz, 3H).
^{13}C-NMR (101 MHz, $CDCl_3$) δ: 166.5, 135.4, 131.3, 130.6, 130.3, 130.2, 127.2, 35.1, 14.8.
LC-MS (ESI) *m/z* 184 $[M+H]^+$.
Hi-Res LC-MS (ESI) *m/z* calcd for $C_9H_{10}ClNO$ $[M+H]^+$ 184.0524, found 184.0521.

141 *N*-ethyl-3-chlorobenzamide[128]

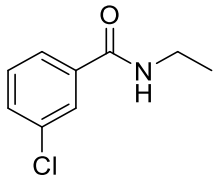

The title compound afforded as a pale yellow oil (24 mg, 60%) using the general procedure outlined in section 4.2.3.

^{1}H NMR (400 MHz, $CDCl_3$) δ: 7.76 - 7.27 (m, 4 H), 6.36 (br s, 1H), 3.50 - 3.41 (m, 2H), 1.34 - 1.13 (m, 3H).
^{13}C-NMR (101 MHz, $CDCl_3$) δ: 166.3, 136.6, 134.7, 131.4, 129.9, 127.3, 125.1, 35.2, 14.9.
LC-MS (ESI) *m/z* 184 $[M+H]^+$
Hi-Res LC-MS (ESI) *m/z* calcd for $C_9H_{10}ClNO$ $[M+H]^+$ 184.0524, found 184.0546.

142 *N*-ethyl-4-chlorobenzamide[126]

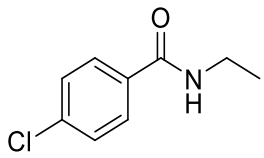

The title compound afforded as a pale yellow oil (28 mg, 70%) using the general procedure outlined in section 4.2.3.

^{1}H NMR (400 MHz, $CDCl_3$) δ: 7.77 - 7.59 (m, 2H), 7.53 - 7.24 (m, 2H), 6.15(br.s, 1H), 3.52 - 3.42 (m, 2H), 1.23 (t, *J* = 7.3 Hz, 3H).
LC-MS (ESI) *m/z* 184 $[M+H]^+$.
Hi-Res LC-MS (ESI) *m/z* calcd for $C_9H_{10}ClNO$ $[M+H]^+$ 184.0524, found 184.0523.

153 2-chloro-4-fluoro-*N*-(methoxymethyl)-*N*-methylbenzamide

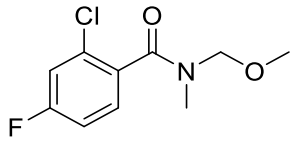

The title compound afforded as a pale yellow oil (5 mg, 10%) using the general procedure outlined in section 4.2.3.

^{1}H NMR (400 MHz, $CDCl_3$) δ ppm 7.31 - 7.24 (m, 1H), 7.16 - 7.11 (m, 1H), 7.03 – 6.98(m, 1H), 5.05 - 4.86 (m, 0.75 H), 4.45 - 4.43 (d, *J*=6.0 Hz, 2H), 3.40 (s, 1H), 3.11 (s, 3H), 2.81 (s, 3H)
^{13}C-NMR (101 MHz, $CDCl_3$) δ ppm 169.9(m), 168.2 (M), 163.9 (m), 161.5 (M), 132.4, 132.1, 131.7, 129.8, 129.7, 129.1, 129.0, 117.4, 117.1, 115.0, 114.7, 114.6, 114.4, 81.9, 56.4 (m), 55.4 (M), 34.3 (m), 32.0 (M)
LC-MS (ESI) *m/z* 232 $[M+H]^+$.
Hi-Res LC-MS (ESI) *m/z* calcd for $C_{10}H_{11}ClFNO_2$ $[M+H]^+$ 232.0535, found 232.0535.

Chapter 5: Reference

1. A. G. A. Volta, *Nat. Philos. Chem. Arts*, 1800, **4**, 179 - 187.
2. H. Lund, *J. Electrochem. Soc.*, 2002, **149**, S21 - S33.
3. M. Faraday, *Ann. Phys. Leipzig*, 1834, **47**, 438.
4. H. Kolbe, *J. Prakt, Chem.*, 1847, **41**, 138.
5. C. F. Schoenbein, *Liebigs Ann. Chem.*, 1845, **54**.
6. L. Jia and X. Liu, *Curr. Drug Metab.*, 2007, **8**, 822-829.
7. A. Álvarez-Lueje, M. Pérez and C. Zapata, *Journal*, 2012, DOI: 10.5772/28647, 221-246.
8. J. Vrbanac and R. Slauter, in *A Comprehensive Guide to Toxicology in Preclinical Drug Development*, ed. A. S. Faqi, Academic Press, 2013, DOI: https://doi.org/10.1016/B978-0-12-387815-1.00002-2, pp. 3-30.
9. A. Baumann and U. Karst, *Expert Opin. Drug Metab. Toxicol.*, 2010, **6**, 715-731.
10. E. F. A. Brandon, C. D. Raap, I. Meijerman, J. H. Beijnen and J. H. M. Schellens, *Toxicol. Appl. Pharmacol.*, 2003, **189**, 233-246.
11. W. Lohmann and U. Karst, *Anal. Chem.*, 2007, **79**, 6831-6839.
12. M. Yan, Y. Kawamata and P. S. Baran, *Chem. Rev.*, 2017, **117**, 13230-13319.
13. M. Pumera, *Curr. Opin. Electrochem.*, 2019, **14**, 133-137.
14. A. Fernández-la-Villa, D. F. Pozo-Ayuso and M. Castaño-Álvarez, *Curr. Opin. Electrochem.*, 2019, **15**, 175-185.
15. A. Florea, M. de Jong and K. De Wael, *Curr. Opin. Electrochem.*, 2018, **11**, 34-40.
16. A. J. Fry, *J. Am. Chem. Soc.*, 2001, **123**, 8880-8880.
17. R. D. Little and K. D. Moeller, *Electrochem. Soc. Interface*, 2002, **11**, 36-42.
18. D. E. Collin, A. A. Folgueiras-Amador, D. Pletcher, M. E. Light, B. Linclau and R. C. D. Brown, *Chem. Eur. J.*, 2019, **26**.
19. D. Alejandro Alvarez-Lueje and Soledad Bollo, *Comb. Chem. High Throughput Screening*, 2010, **13**, 712-727.
20. U. Jurva, H. V. Wikström, L. Weidolf and A. P. Bruins, *Rapid Commun. Mass Spectrom.*, 2003, **17**, 800-810.
21. U. Karst, *Angew. Chem., Int. Ed.*, 2004, **43**, 2476-2478.
22. H. Faber, M. Vogel and U. Karst, *Anal. Chim. Acta*, 2014, **834**, 9-21.
23. W. Lohmann, H. Hayen and U. Karst, *Anal. Chem.*, 2008, **80**, 9714-9719.
24. E. Tareke, J. F. Bowyer and D. R. Doerge, *Rapid Commun. Mass Spectrom.*, 2007, **21**, 3898-3904.
25. L. Tang, J. H. Matuska, Y.-H. Huang, Y.-H. He and Z. Guan, *ChemSusChem*, 2019, **12**, 2570-2575.
26. R. M. Lanigan, P. Starkov and T. D. Sheppard, *J. Org. Chem.*, 2013, **78**, 4512-4523.
27. T. Cupido, J. Tulla-Puche, J. Spengler and F. Albericio, *Curr. Opin. Drug Discovery Dev.*, 2007, **10**, 768-783.
28. J. M. Humphrey and A. R. Chamberlin, *Chem. Rev.*, 1997, **97**, 2243-2266.
29. J. W. Bode, *Curr. Opin. Drug Discovery Dev.*, 2006, **9**, 765-775.
30. R. Fu, Y. Yang, Z. Chen, W. Lai, Y. Ma, Q. Wang and R. Yuan, *Tetrahedron*, 2014, **70**, 9492-9499.
31. X. Zhang, W. T. Teo and P. W. H. Chan, *J. Organomet. Chem.*, 2011, **696**, 331-337.
32. K. S. Pang, J. A. Terrell, S. D. Nelson, K. F. Feuer, M.-J. Clements and L. Endrenyi, *J. Pharmacokinet. Biopharm.*, 1986, **14**, 107-130.
33. G. T. Tucker, N. D. Bax, M. S. Lennard, S. Al-Asady, H. S. Bharaj and H. F. Woods, *Br. J. Clin. Pharmacol.*, 1984, **17**, 21S-28S.
34. J. Iley, R. Tolando and i. p. L. Constantino, *J. Chem. Soc., Perkin Trans. 2*, 2001, DOI: 10.1039/B102731J, 1299-1305.
35. M. Katohgi and H. Togo, *Tetrahedron*, 2001, **57**, 7481-7486.

36. Y. Wang, D. Li, K. Han and S. Shaik, *J. Phys. Chem. B*, 2010, **114**, 2964-2970.
37. M. H. Rahman, M. K. Bal and A. M. Jones, *ChemElectroChem*, 2019, **6**, 4093-4104.
38. D. A. Smith, K. Beaumont, T. S. Maurer and L. Di, *J. Med. Chem.*, 2019, **62**, 2245-2255.
39. N.-N. Eslam, B. Rainer and P. B. a. H. P. P. Andries, *Curr. Drug Metab.*, 2011, **12**, 359-371.
40. B. Testa and S. D. Krämer, *Chem. Biodiv.*, **4**, 2031-2122.
41. J. Belcher, K. McLean, S. Matthews, L. Woodward, K. Fisher, S. Rigby, D. Nelson, D. Potts, M. Baynham, D. Parker, D. Leys and A. Munro, *J. Biol. Chem.*, 2014, **289**.
42. J. T. Groves and G. A. McClusky, *J. Am. Chem. Soc.*, 1976, **98**, 859-861.
43. J. Rittle and M. T. Green, *Science*, 2010, **330**, 933.
44. B. K. Yap, C.-Y. Lee, S. B. Choi, E. E. Kamarulzaman, M. Hariono and H. A. Wahab, in *Encyclopedia of Bioinformatics and Computational Biology*, eds. S. Ranganathan, M. Gribskov, K. Nakai and C. Schönbach, Academic Press, Oxford, 2019, DOI: https://doi.org/10.1016/B978-0-12-809633-8.20158-1, pp. 761-779.
45. A. Paci, T. Martens and J. Royer, *Bioorg. Med. Chem. Lett.*, 2001, **11**, 1347-1349.
46. E. Nouri-Nigjeh, H. P. Permentier, R. Bischoff and A. P. Bruins, *Anal. Chem.*, 2010, **82**, 7625-7633.
47. S. Torres, R. Brown, T. Zelesky, G. Scrivens, R. Szucs, J. M. Hawkins and M. R. Taylor, *J. Pharm. Biomed. Anal.*, 2016, **131**, 71-79.
48. R. Stalder and G. P. Roth, *ACS Med. Chem. Lett.*, 2013, **4**, 1119-1123.
49. H. Mayr, A. R. Ofial, E.-U. Würthwein and N. C. Aust, *J. Am. Chem. Soc.*, 1997, **119**, 12727-12733.
50. Y. Yamamoto, T. Nakada and H. Nemoto, *J. Am. Chem. Soc.*, 1992, **114**, 121-125.
51. W. N. Speckamp and H. Hiemstra, *Tetrahedron*, 1985, **41**, 4367-4416.
52. J. Royer, M. Bonin and L. Micouin, *Chem. Rev.*, 2004, **104**, 2311-2352.
53. J.-i. Yoshida, K. Kataoka, R. Horcajada and A. Nagaki, *Chem. Rev.*, 2008, **108**, 2265-2299.
54. A. M. Jones and C. E. Banks, *Beilstein J. Org. Chem.*, 2014, **10**, 3056-3072.
55. S. D. Ross, M. Finkelstein and R. C. Petersen, *J. Am. Chem. Soc.*, 1966, **88**, 4657-4660.
56. T. Shono, H. Hamaguchi and Y. Matsumura, *J. Am. Chem. Soc.*, 1975, **97**, 4264-4268.
57. T. Shono, T. Toda and N. Oshino, *J. Am. Chem. Soc.*, 1982, **104**, 2639-2641.
58. T. Shono, Y. Matsumura and K. Tsubata, *J. Am. Chem. Soc.*, 1981, **103**, 1172-1176.
59. L. Hall and R. Hanzlik, *J. Biol. Chem.*, 1990, **265**, 12349-12355.
60. L. R. Hall and R. P. Hanzlik, *Xenobiotica*, 1991, **21**, 1127-1138.
61. L. R. Hall, R. T. Iwamoto and R. P. Hanzlik, *J. Org. Chem.*, 1989, **54**, 2446-2451.
62. C. Lorenc, J. T. Reeves, C. A. Busacca and C. H. Senanayake, *Tetrahedron Lett.*, 2015, **56**, 1280-1282.
63. P. Alfonso-Súarez, A. V. Kolliopoulos, J. P. Smith, C. E. Banks and A. M. Jones, *Tetrahedron Lett.*, 2015, **56**, 6863-6867.
64. B. A. Frontana-Uribe, R. D. Little, J. G. Ibanez, A. Palma and R. Vasquez-Medrano, *Green Chem.*, 2010, **12**, 2099-2119.
65. R. D. Little and K. D. Moeller, *Electrochem. Soc. Interface*, 2002, **11**, 36-42.
66. D. S. P. Cardoso, B. Šljukić, D. M. F. Santos and C. A. C. Sequeira, *Org. Process Res. Dev.*, 2017, **21**, 1213-1226.
67. A. J. Bard, M. Stratmann, E. Gileadi, M. Urbakh, E. J. Calvo, P. R. Unwin, G. S. Frankel, D. Macdonald, S. Licht and H. J. Schäfer, *Encyclopedia of Electrochemistry, 10 Volume Set + Index*, Wiley, 2007.
68. J.-i. Yoshida and K. Nishiwaki, *J. Chem. Soc., Dalton Trans.*, 1998, DOI: 10.1039/A803343I, 2589-2596.
69. J. C. Lewis, B. Redfern and F. C. Cowlard, *Solid-State Electron.*, 1963, **6**, 251-254.
70. F. C. Cowlard and J. C. Lewis, *Am. J. Mater. Sci. Eng.*, 1976, **2**, 507 – 510.
71. J. M. Friedrich, C. Ponce-de-León, G. W. Reade and F. C. Walsh, *J. Electroanal. Chem.*, 2004, **561**, 203-217.
72. J. Friedl and U. Stimming, *Electrochim. Acta*, 2017, **227**, 235-245.
73. D. Szanto, P. Trinidad and F. Walsh, *J. Appl. Electrochem.*, 1998, **28**, 251–258.

74. W. J. Blaedel and J. Wang, *Anal. Chem.*, 1980, **52**, 1697-1700.
75. Q. Li, C. Batchelor-McAuley, N. S. Lawrence, R. S. Hartshorne, C. J. V. Jones and R. G. Compton, *J. Solid State Electrochem.*, 2014, **18**, 1215-1221.
76. G. W. Reade, University of Portsmouth, 1996.
77. J. Wang and H. D. Dewald, *Anal. Chim. Acta*, 1982, **136**, 77-84.
78. P. A. Flowers, M. A. Maynor and D. E. Owens, *Anal. Chem.*, 2002, **74**, 720-723.
79. R. Ciriminna, M. Ghahremani, B. Karimi and M. Pagliaro, *ChemistryOpen*, 2017, **6**, 5-10.
80. C. Gütz, A. Stenglein and S. R. Waldvogel, *Org. Process Res. Dev.*, 2017, **21**, 771-778.
81. A. J. Bard and L. R. Faulkner, *Electrochemical Methods: Fundamentals and Applications, 2nd Edition*, Wiley Textbooks, 2000.
82. J. Wang, *Analytical Electrochemistry*, Wiley, 2004.
83. R. G. Compton and C. E. Banks, *Understanding Voltammetry*, Imperial College Press, 2011.
84. F. Scholz, in *Electroanalytical Methods: Guide to Experiments and Applications*, eds. F. Scholz, A. M. Bond, R. G. Compton, D. A. Fiedler, G. Inzelt, H. Kahlert, Š. Komorsky-Lovrić, H. Lohse, M. Lovrić, F. Marken, A. Neudeck, U. Retter, F. Scholz and Z. Stojek, Springer Berlin Heidelberg, Berlin, Heidelberg, 2010, DOI: 10.1007/978-3-642-02915-8_2, pp. 11-31.
85. G. Wilson, A. Bard and M. Stratmann, *Encyclopedia of Electrochemistry, Vol. 8*, 2004.
86. A. C. Fisher, *Electrode Dynamics*, Oxford University Press, 1996.
87. A. Hickling, *Trans. Faraday Soc.*, 1942, **38**, 27-33.
88. M. K. Bal, C. E. Banks and A. M. Jones, *ChemElectroChem*, 2019, **6**, 4284-4291.
89. J. Clayden, N. Greeves and S. Warren, *Organic Chemistry*, OUP Oxford, 2012.
90. Y. Jean, I. Demachy, A. Lledos and F. Maseras, *J. Mol. Struct.: THEOCHEM*, 2003, **632**, 131-144.
91. E. Laviron, L. Roullier and C. Degrand, *J. Electroanal. Chem. Interfacial Electrochem.*, 1980, **112**, 11-23.
92. C.-C. Zeng and J. Y. Becker, *J. Org. Chem.*, 2004, **69**, 1053-1059.
93. D. Nematollahi, D. Habibi, M. Rahmati and M. Rafiee, *J. Org. Chem.*, 2004, **69**, 2637-2640.
94. J. T. Hill-Cousins, J. Kuleshova, R. A. Green, P. R. Birkin, D. Pletcher, T. J. Underwood, S. G. Leach and R. C. D. Brown, *ChemSusChem*, 2012, **5**, 326-331.
95. M. Mitzlaff, K. Warning and H. Jensen, *Liebigs Ann. Chem.*, 1978, **1978**, 1713-1733.
96. M. Mori, Y. Washioka, T. Urayama, K. Yoshiura, K. Chiba and Y. Ban, *J. Org. Chem*, 1983, **48**, 4058-4067.
97. J. F. O'Donnell and C. K. Mann, *J. Electroanal. Chem. Interfacial Electrochem.*, 1967, **13**, 157-162.
98. P. Wu and T. E. Nielsen, *Chem. Rev.*, 2017, **117**, 7811-7856.
99. M. G. Vinogradov, O. V. Turova and S. G. Zlotin, *Russ. Chem. Rev.*, 2017, **86**, 1-17.
100. B. E. Maryanoff, H.-C. Zhang, J. H. Cohen, I. J. Turchi and C. A. Maryanoff, *Chem. Rev.*, 2004, **104**, 1431-1628.
101. K. A. Usmani, R. L. Rose, J. A. Goldstein, W. G. Taylor, A. A. Brimfield and E. Hodgson, *Drug Metab. Dispos.*, 2002, **30**, 289.
102. L. Constantino and J. I. M. Iley, *Xenobiotica*, 1999, **29**, 409-416.
103. J. Hioe, D. Šakić, V. Vrček and H. Zipse, *Org. Biomol. Chem.*, 2015, **13**, 157-169.
104. A. M. Jones, T. Lebl, S. Patterson, T. van Mourik, H. A. Früchtl, D. Philp, A. M. Z. Slawin and N. J. Westwood, *Tetrahedron*, 2009, **65**, 563-578.
105. R. A. Green, K. E. Jolley, A. A. M. Al-Hadedi, D. Pletcher, D. C. Harrowven, O. De Frutos, C. Mateos, D. J. Klauber, J. A. Rincón and R. C. D. Brown, *Org. Lett.*, 2017, **19**, 2050-2053.
106. A. Zweig, W. G. Hodgson and W. H. Jura, *J. Am. Chem. Soc.*, 1964, **86**, 4124-4129.
107. M. R. Barone and A. M. Jones, *Org. Biomol. Chem.*, 2017, **15**, 10010-10015.
108. U. Azzena, T. Denurra, G. Melloni, E. Fenude and G. Rassu, *J. Org. Chem.*, 1992, **57**, 1444-1448.
109. B. Yilmaz, S. Kaban and B. K. Akcay, *Indian J Pharm Sci*, 2015, **77**, 413-421.

110. C. Stoffelsma, P. Rodriguez, G. Garcia, N. Garcia-Araez, D. Strmcnik, N. M. Marković and M. T. M. Koper, *Journal of the American Chemical Society*, 2010, **132**, 16127-16133.
111. D. E. Blanco, R. Atwi, S. Sethuraman, A. Lasri, J. Morales, N. N. Rajput and M. A. Modestino, *Journal of The Electrochemical Society*, 2020, **167**, 155526.
112. *United States Pat.,* 2003.
113. T. Gieshoff, A. Kehl, D. Schollmeyer, K. D. Moeller and S. R. Waldvogel, *J. Am. Chem. Soc.*, 2017, **139**, 12317-12324.
114. H. Huang, G. Yuan, X. Li and H. Jiang, *Tetrahedron Lett.*, 2013, **54**, 7156-7159.
115. A. A. Folgueiras-Amador, A. E. Teuten, D. Pletcher and R. C. D. Brown, *Reaction Chemistry & Engineering*, 2020, **5**, 712-718.
116. B. R. Rosen, E. W. Werner, A. G. O'Brien and P. S. Baran, *J. Am. Chem. Soc.*, 2014, **136**, 5571-5574.
117. *German Pat.,* 1963.
118. H. Mei, J. Hu, S. Xiao, Y. Lei and G. Li, *Appl. Catal., A*, 2014, **475**, 40-47.
119. Z. Zhao and V. Snieckus, *Org. Lett*, 2005, **7**, 2523-2526.
120. M.-T. Zeng, W. Xu, M. Liu, X. Liu, C.-Z. Chang, H. Zhu and Z.-B. Dong, *Synth. Commun.*, 2017, **47**, 1434-1440.
121. B. J. Naysmith and M. A. Brimble, *Org. Lett.*, 2013, **15**, 2006-2009.
122. Y. Zhao and V. Snieckus, *Org. Lett.*, 2018, **20**, 2826-2830.
123. H. Suezawa, T. Hashimoto, K. Tsuchinaga, T. Yoshida, T. Yuzuri, K. Sakakibara, M. Hirota and M. Nishio, *J. Chem. Soc., Perkin Trans. 2 ,*, 2000, DOI: 10.1039/A909450D, 1243-1249.
124. K.-i. Shimizu, K. Ohshima and A. Satsuma, *Chem.: Eur. J*, 2009, **15**, 9977-9980.
125. Y. Du, T. K. Hyster and T. Rovis, *Chem. Commun. ,*, 2011, **47**, 12074-12076.
126. R. Sakamoto, S. Sakurai and K. Maruoka, *Chem. Commun.*, 2017, **53**, 6484-6487.
127. T. H. Ali, T. Heidelberg and R. S. D. Hussen, *Synlett*, 2015, **26**, 1361-1364.
128. *China Pat.,* 2017.

^{1}H and ^{13}C NMR spectra

^{1}H NMR spectrum of **106** (400 MHz, $CDCl_3$)

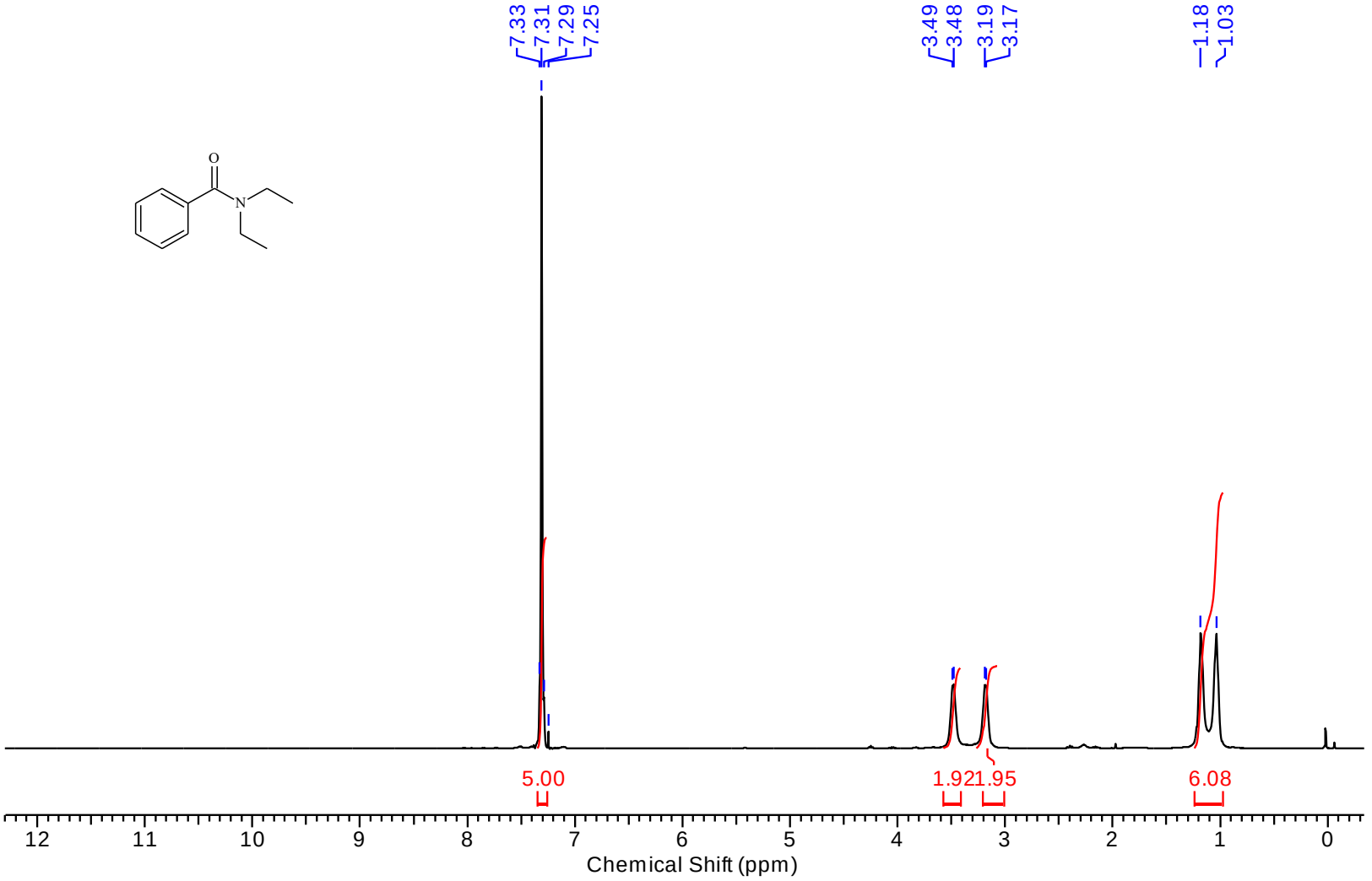

^{13}C NMR spectrum of **106** (101 MHz, $CDCl_3$

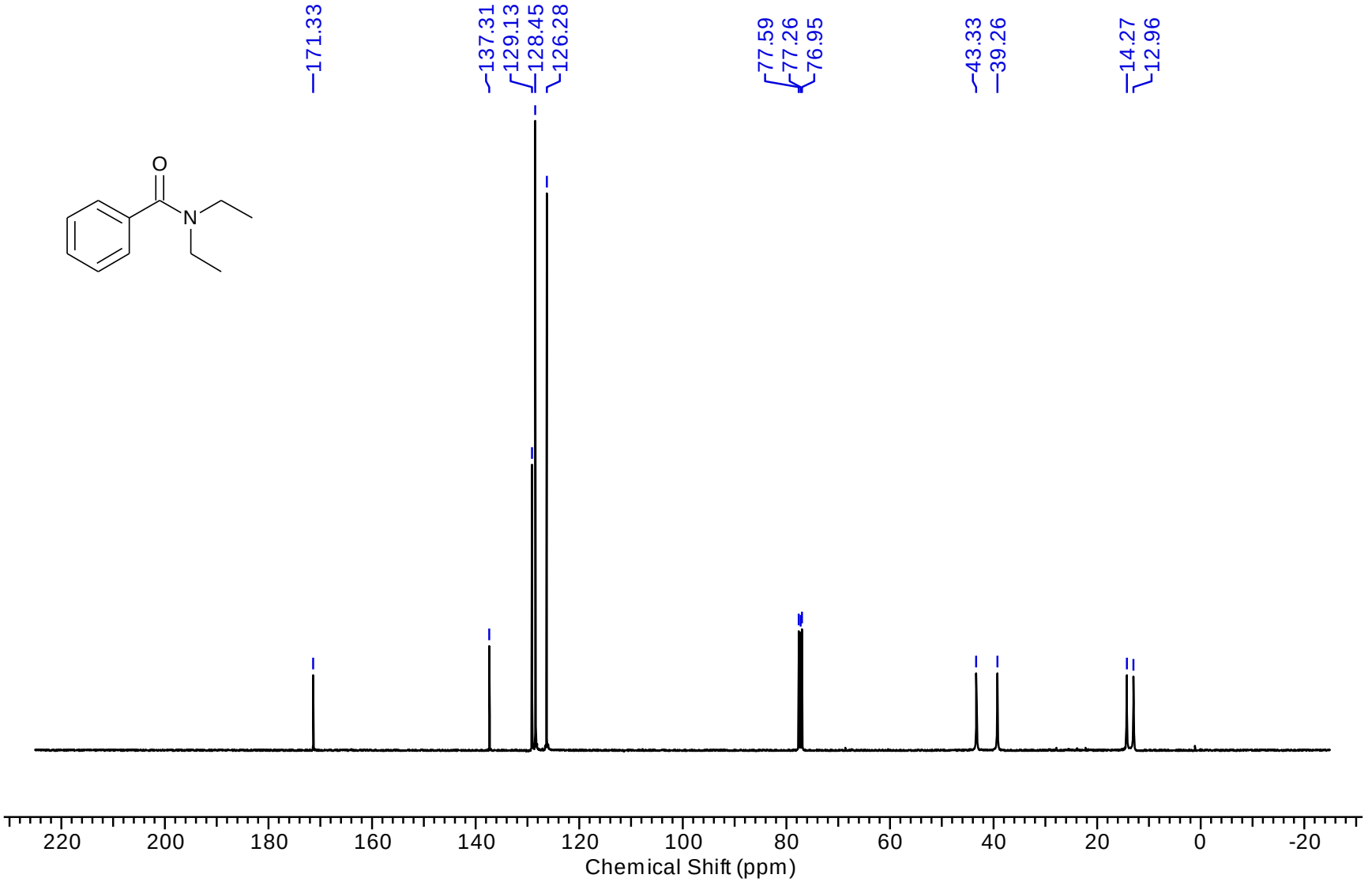

^{1}H NMR spectrum of **121** (400 MHz, $CDCl_3$

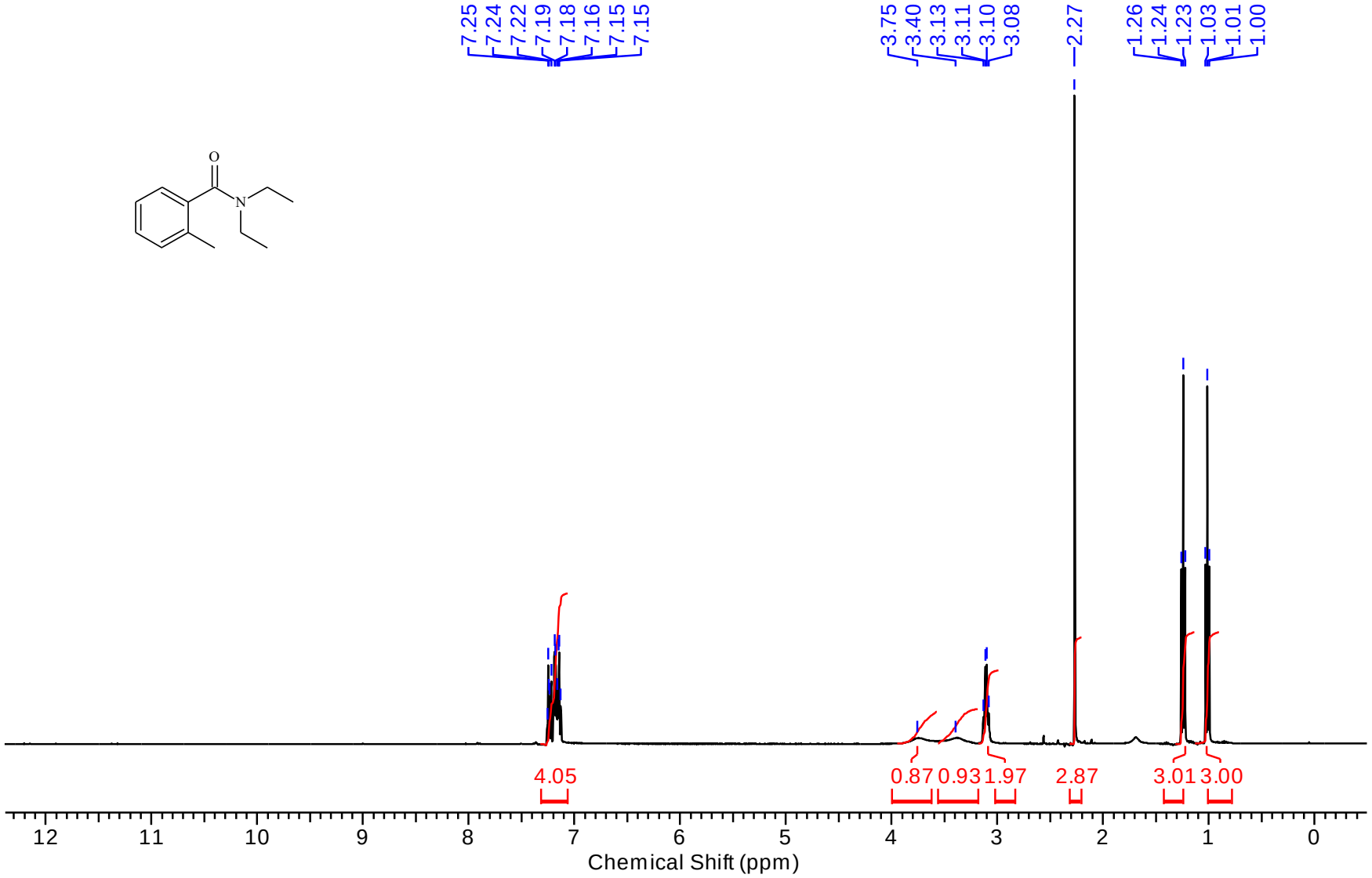

^{13}C NMR spectrum of **121** (101 MHz, $CDCl_3$)

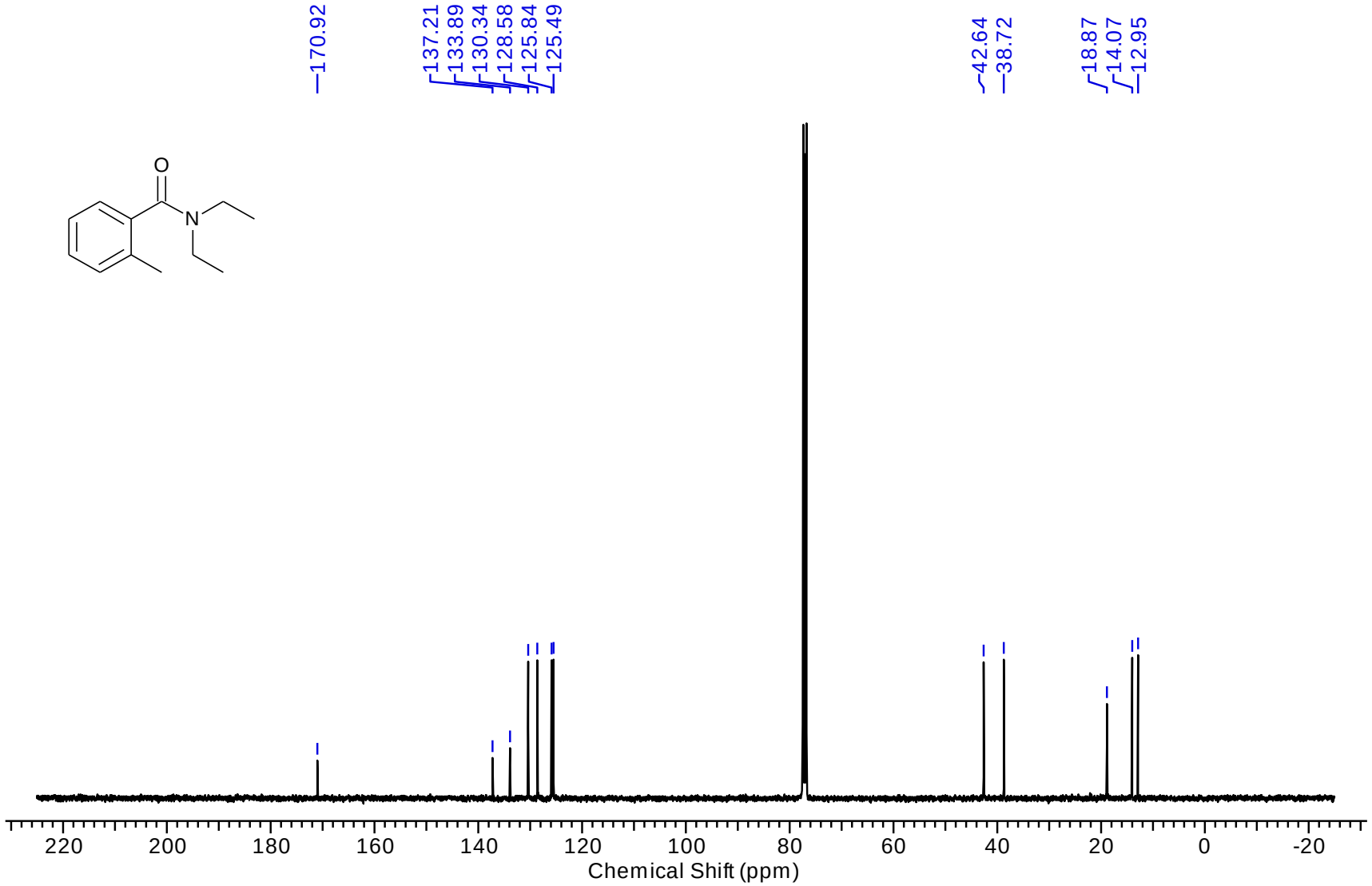

^{1}H NMR spectrum of **122** (400 MHz, $CDCl_3$)

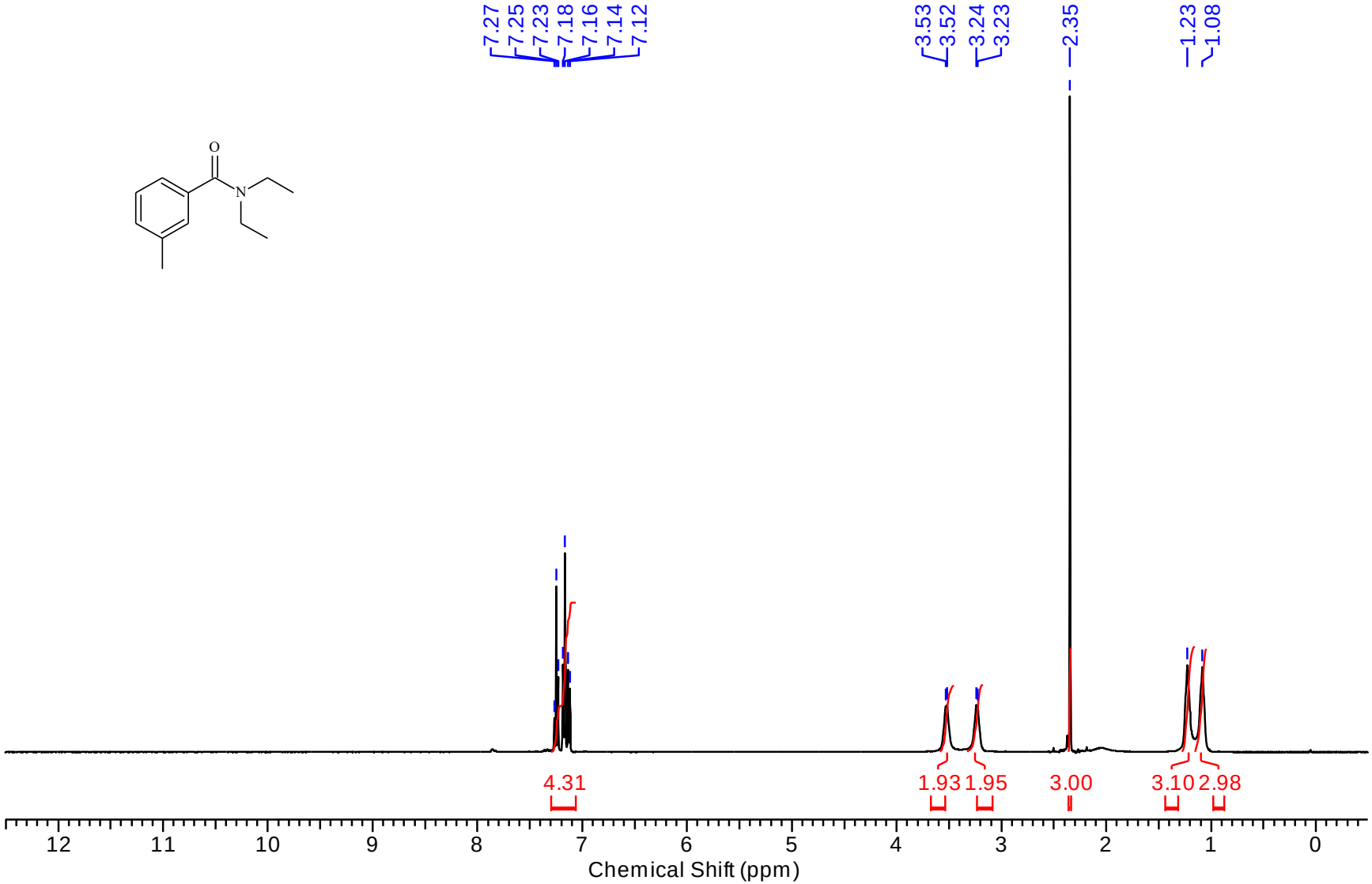

^{13}C NMR spectrum of **122** (101MHz,

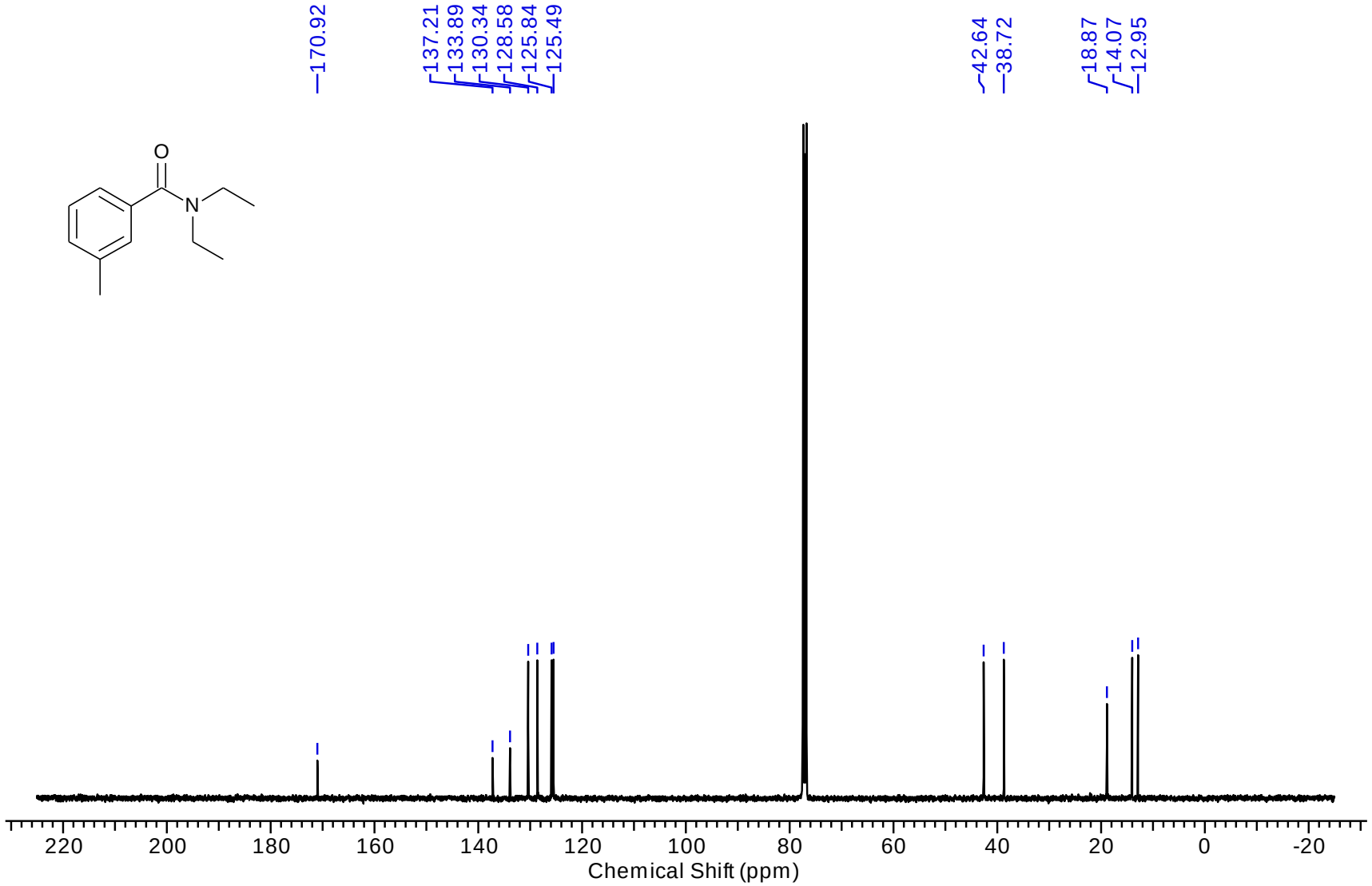

^{1}H NMR spectrum of **123** (400 MHz, $CDCl_3$)

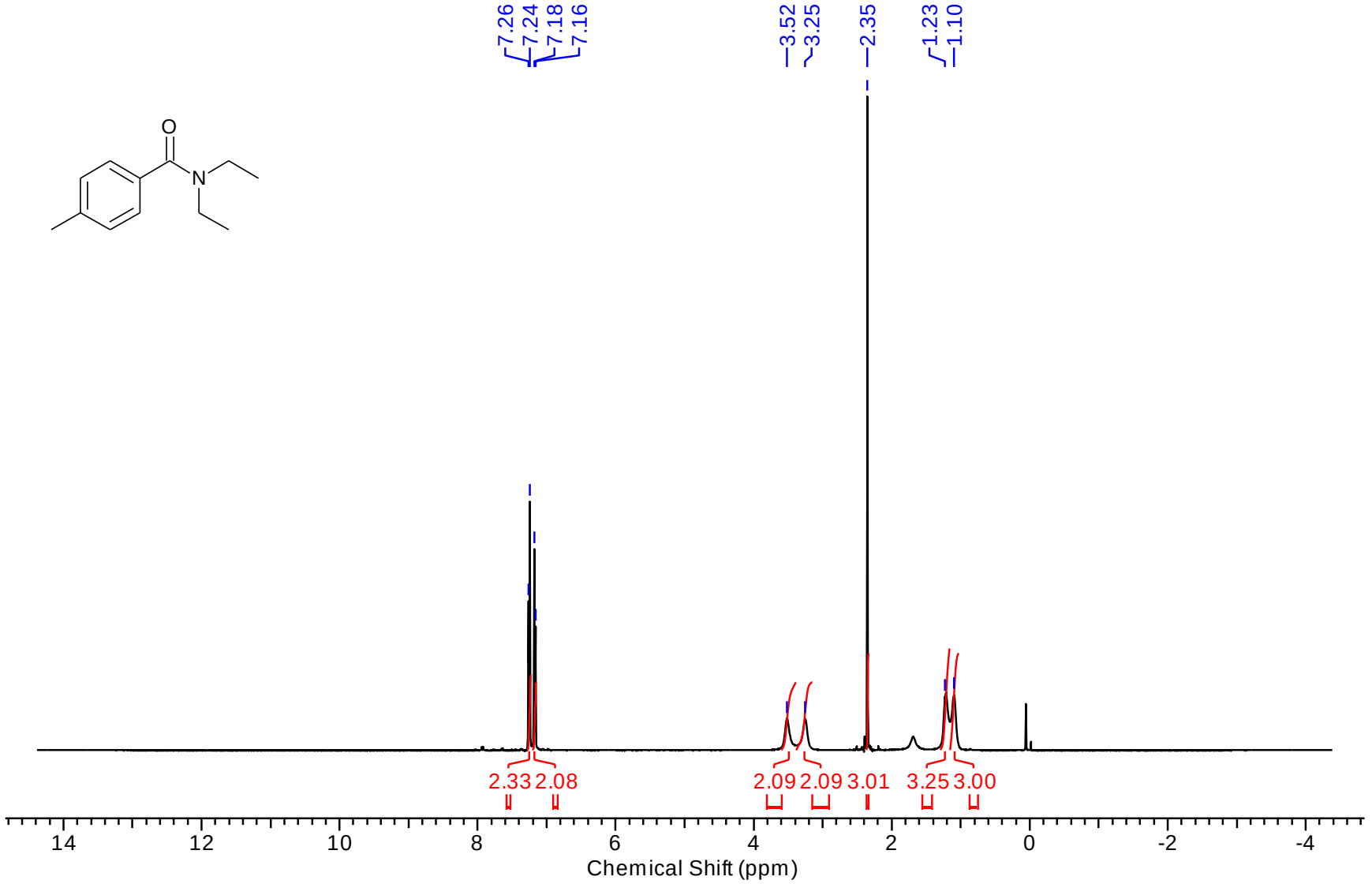

^{13}C NMR spectrum of **123** (101 MHz, $CDCl_3$)

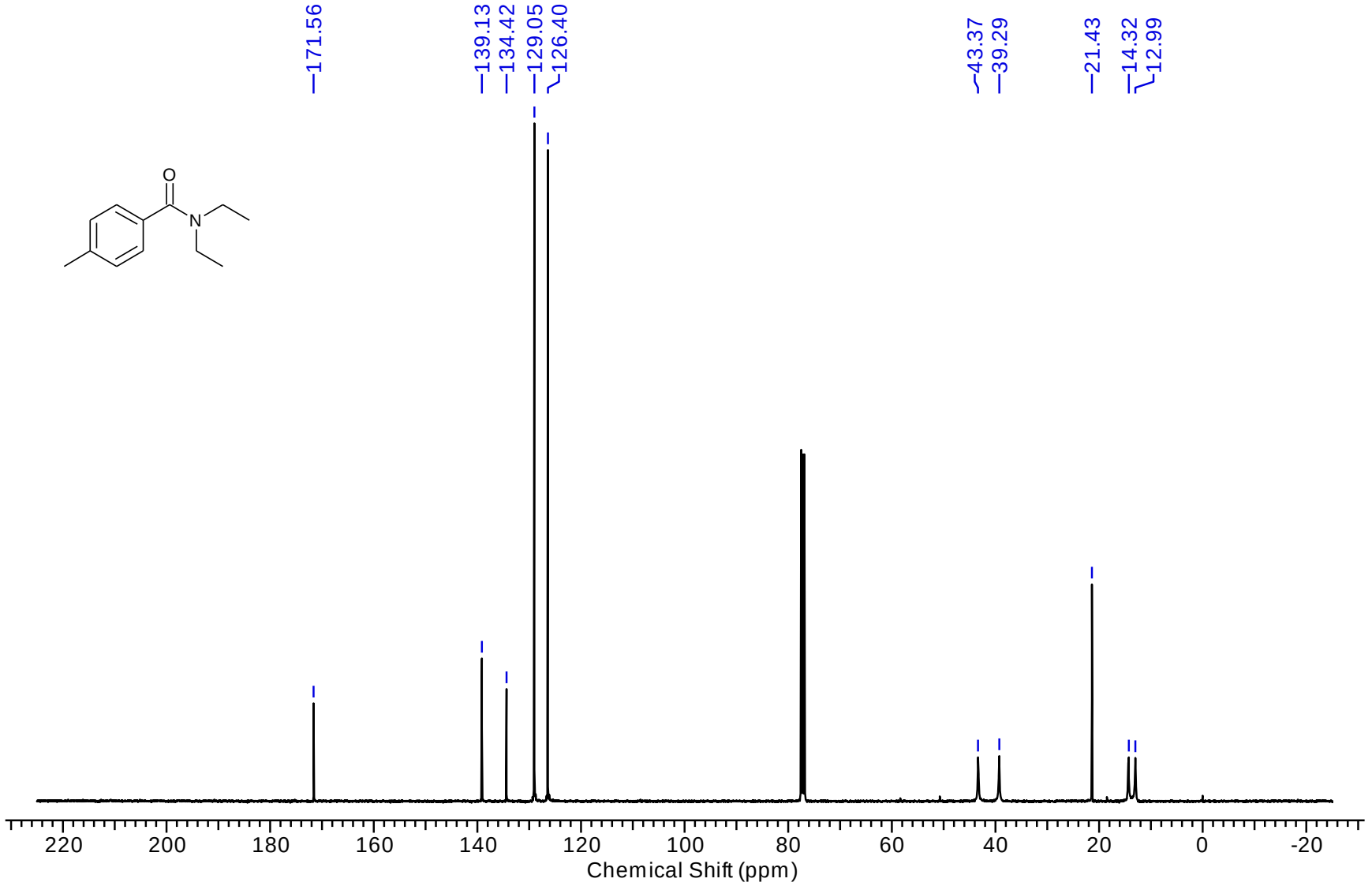

^{1}H NMR spectrum of **124** (400 MHz, $CDCl_3$)

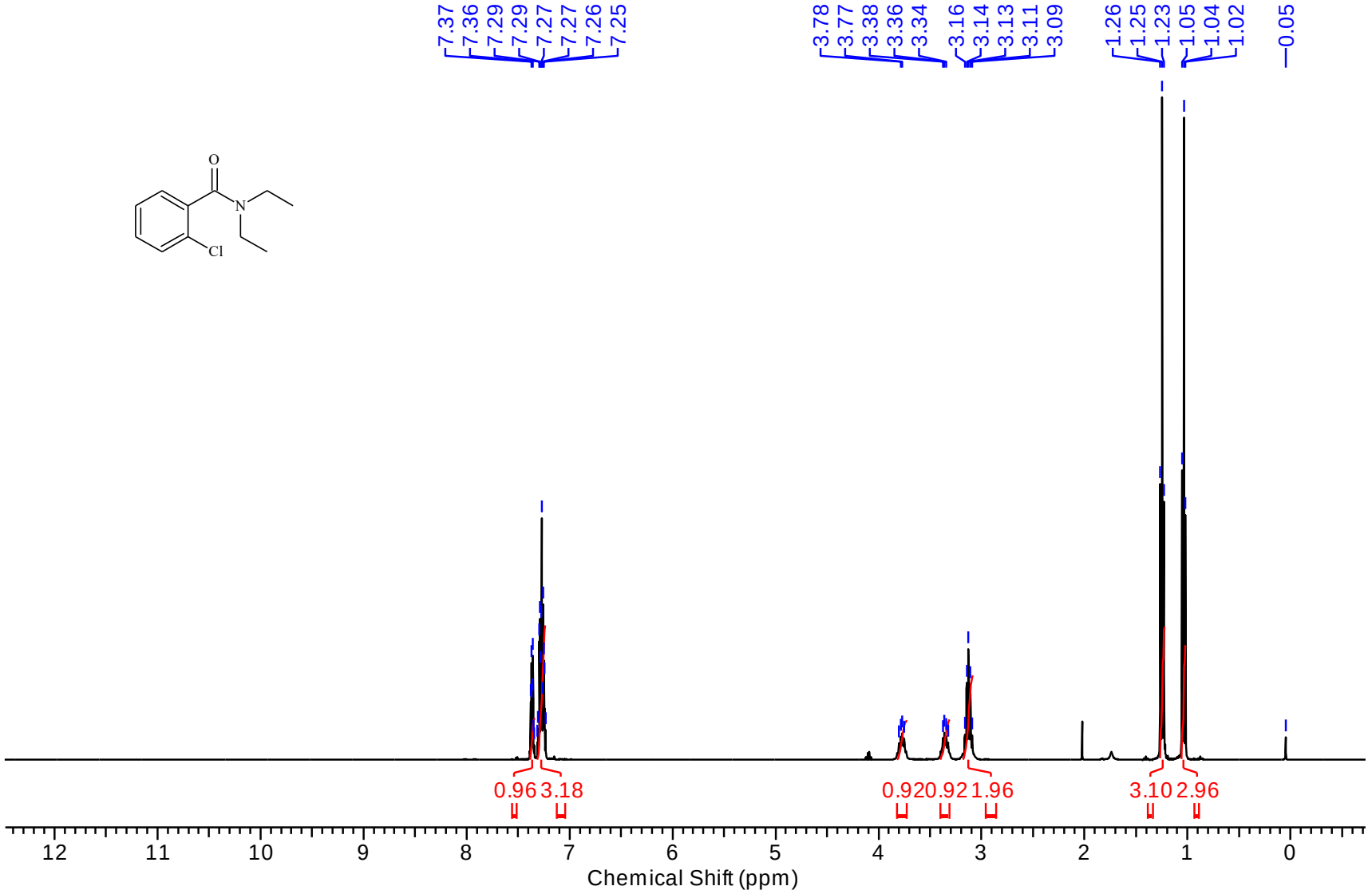

^{13}C NMR spectrum of **124** (101 MHz, $CDCl_3$)

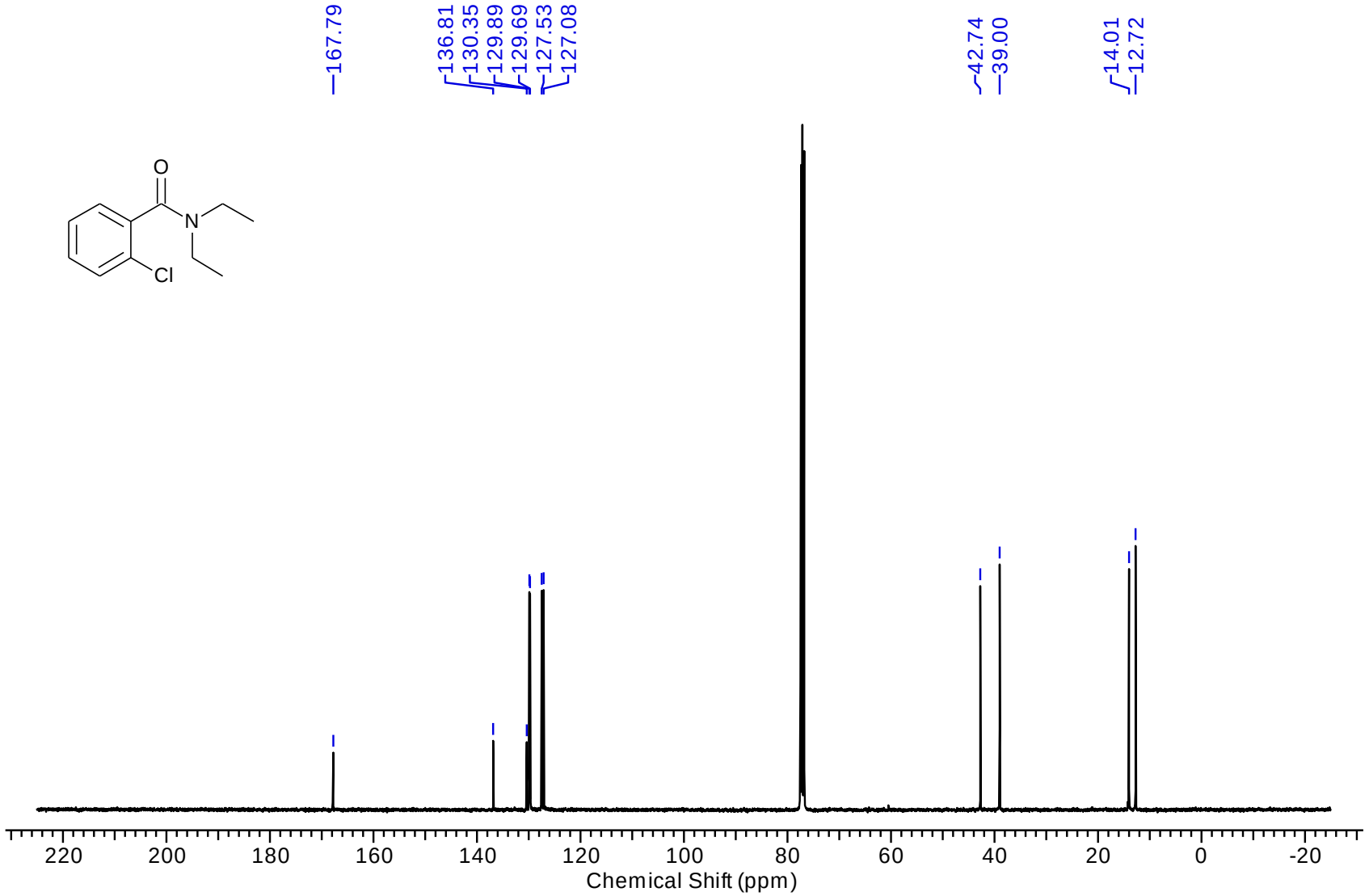

^{1}H NMR spectrum of **125** (400 MHz, $CDCl_3$)

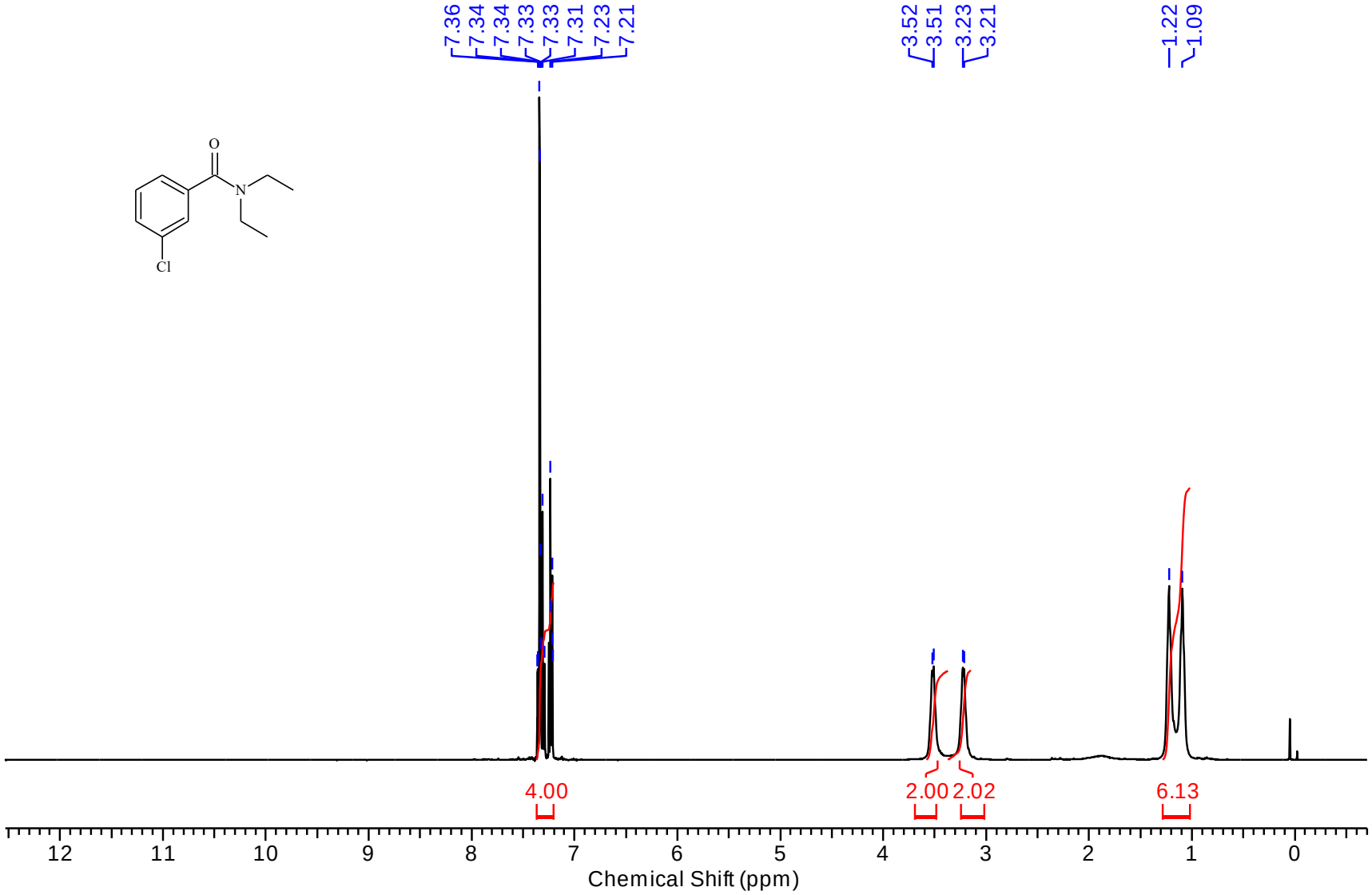

^{13}C NMR spectrum of **125** (101 MHz, $CDCl_3$)

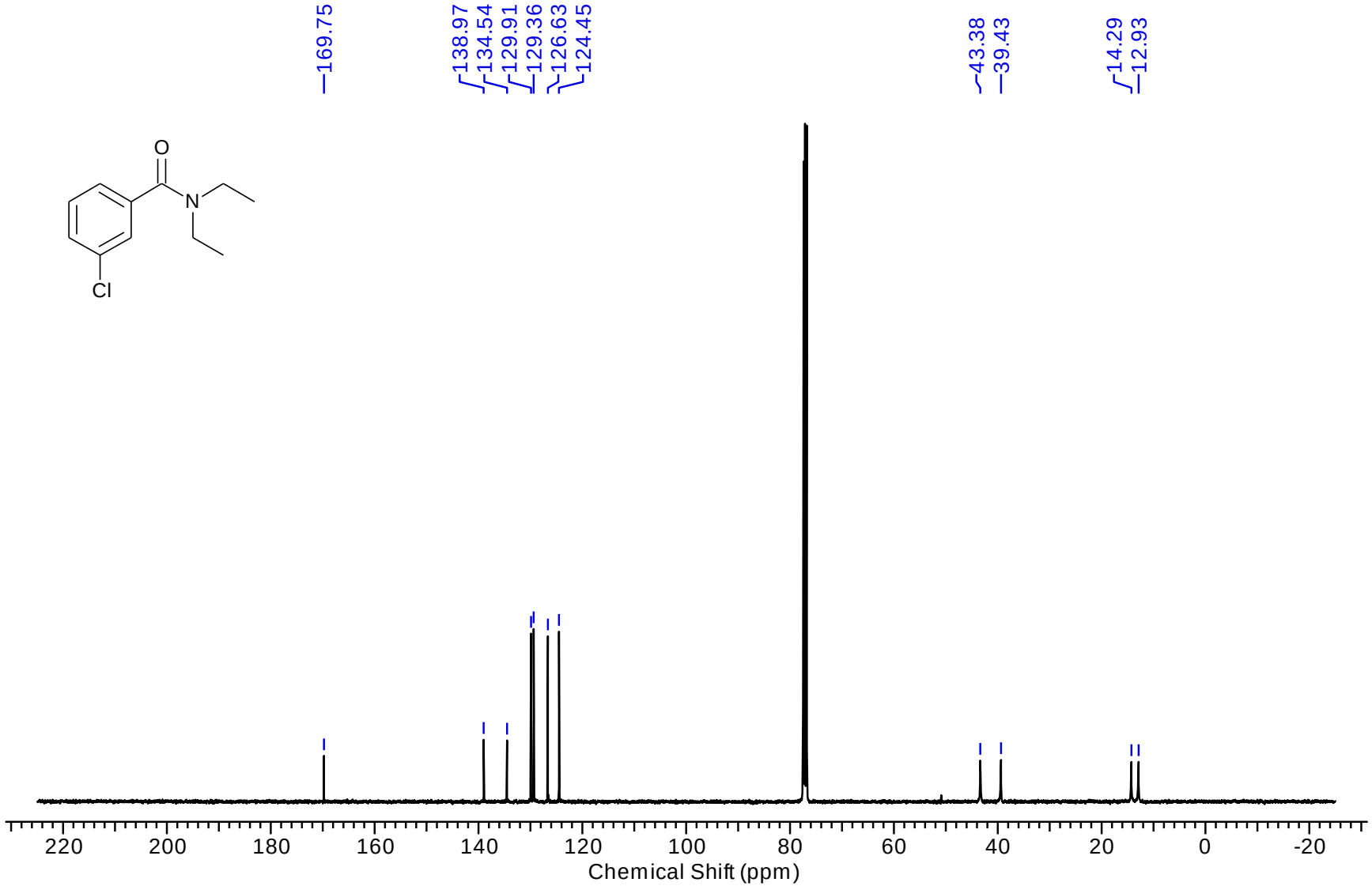

^{1}H NMR spectrum of **126** (400 MHz, CDC

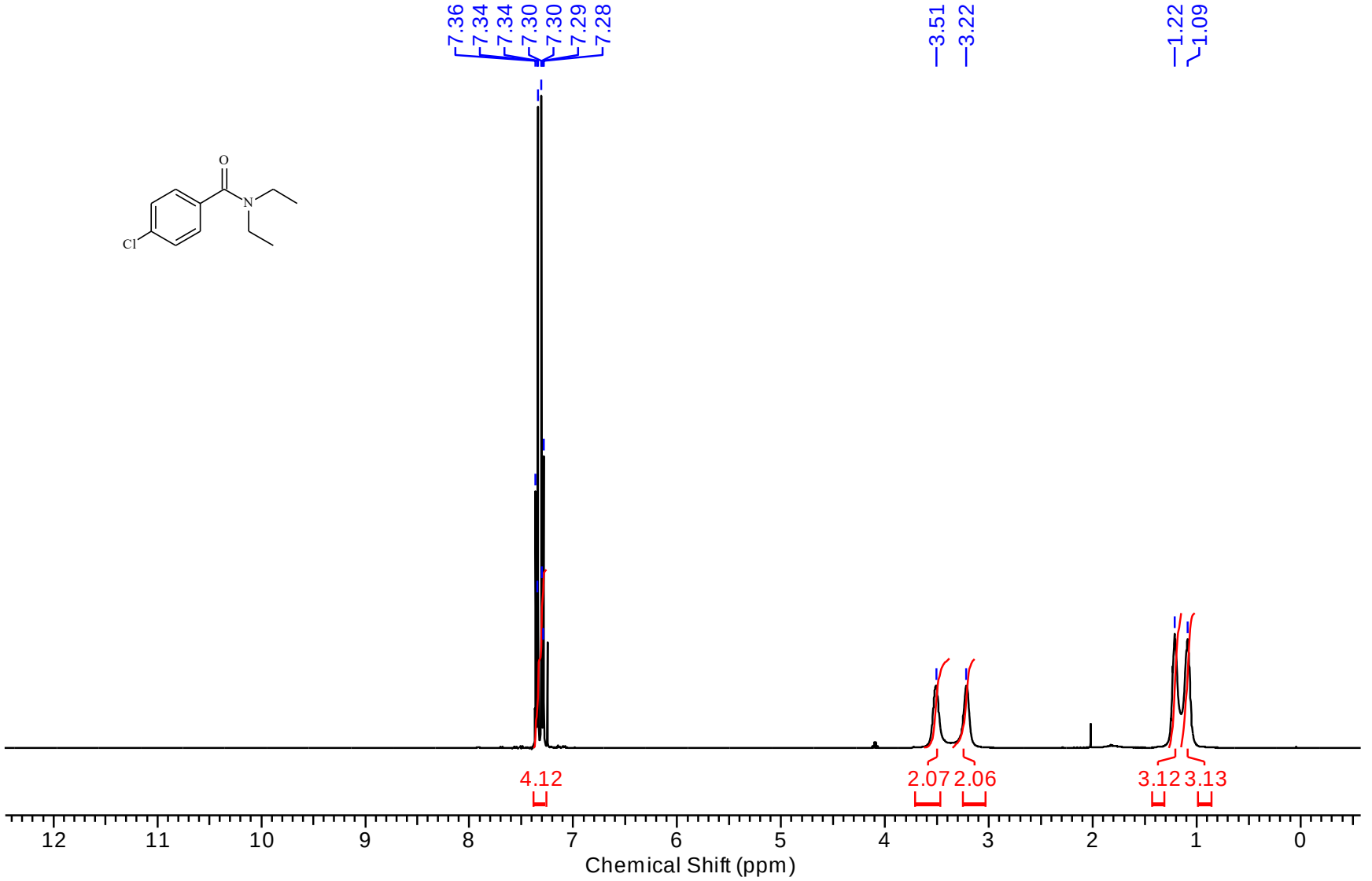

^{13}C NMR spectrum of **126** (101 MHz, $CDCl_3$)

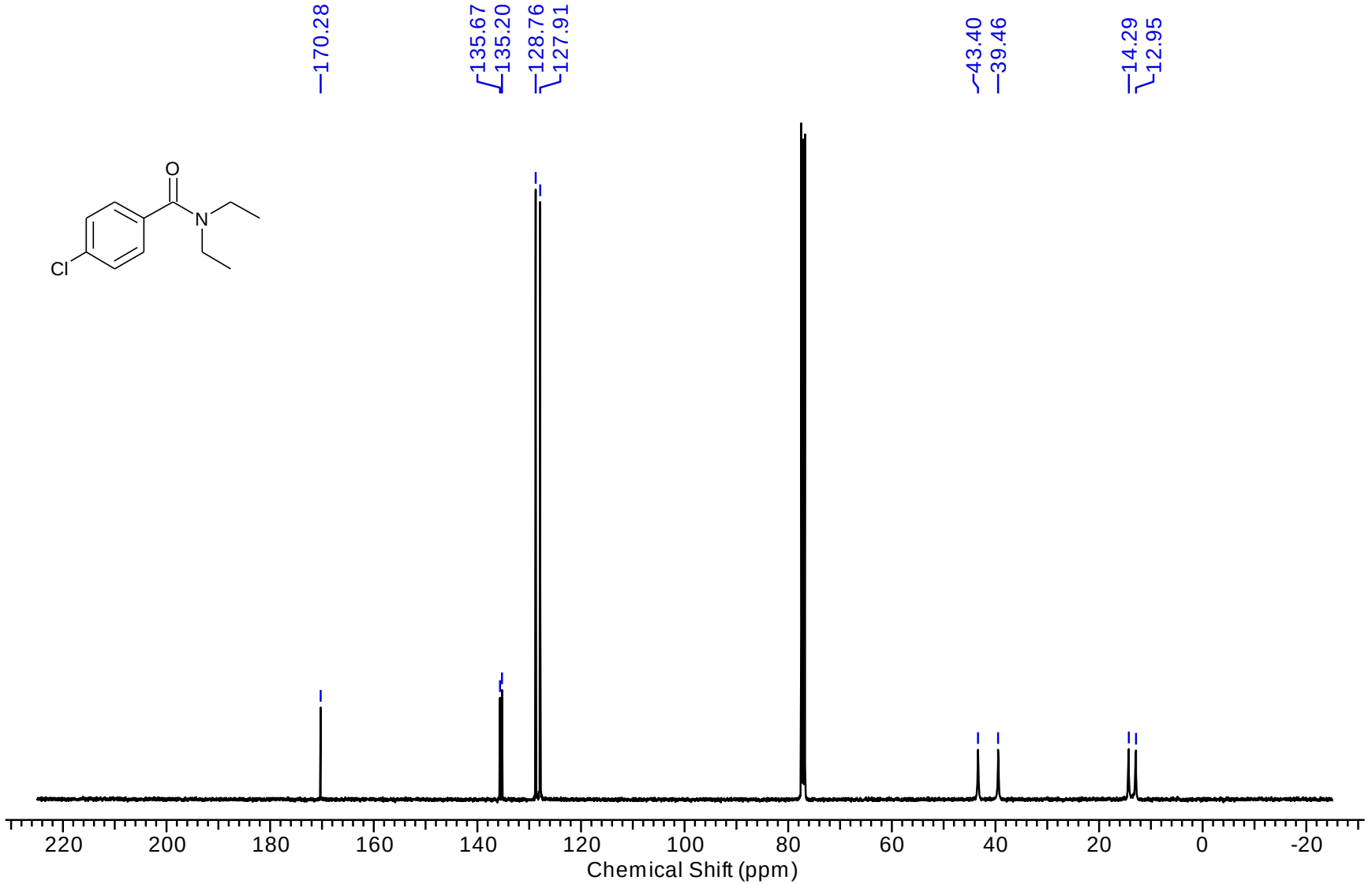

^{1}H NMR spectrum of **127** (400 MHz, $CDCl_3$)

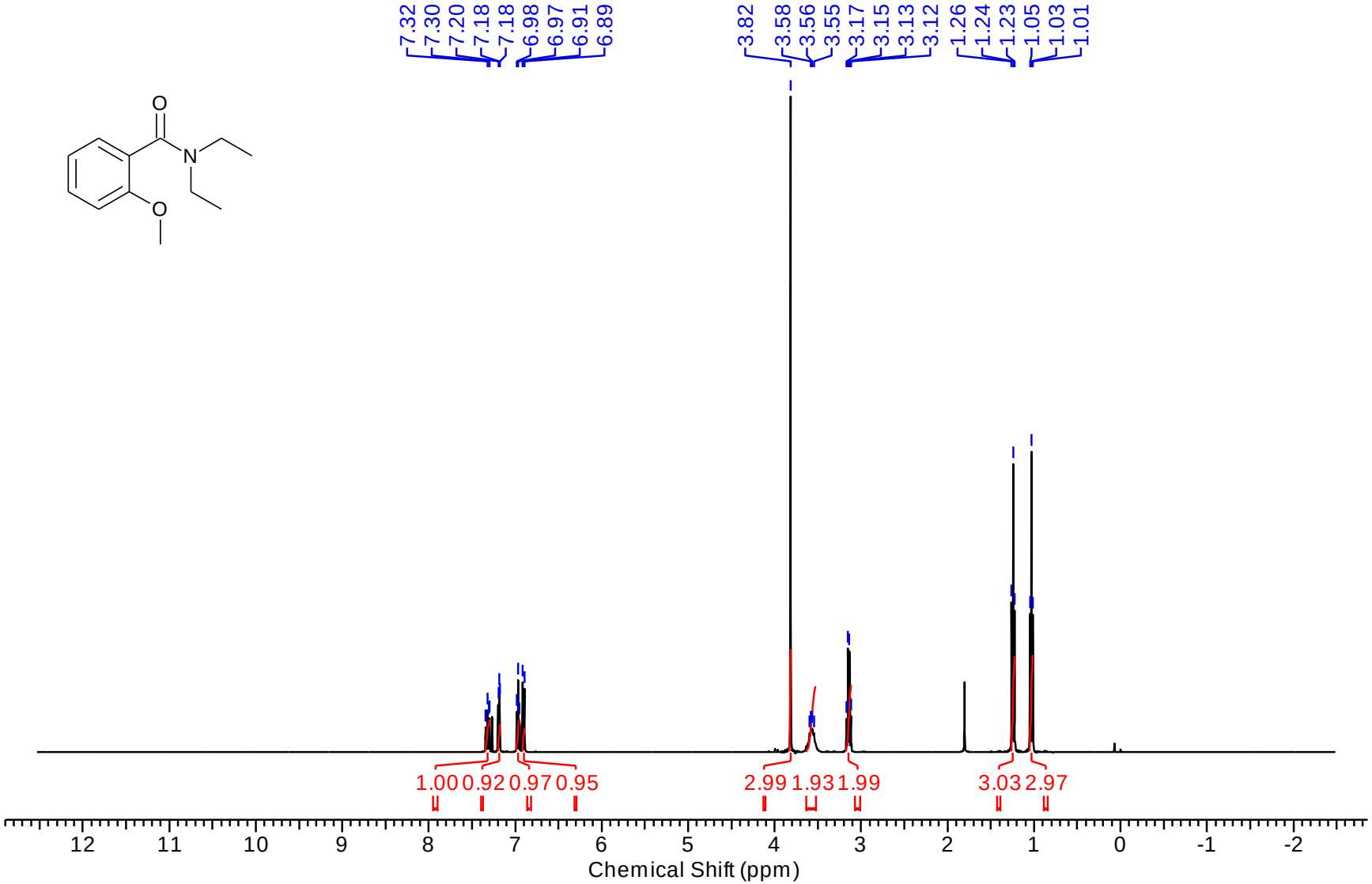

^{13}C NMR spectrum of **127** (101 MHz, $CDCl_3$)

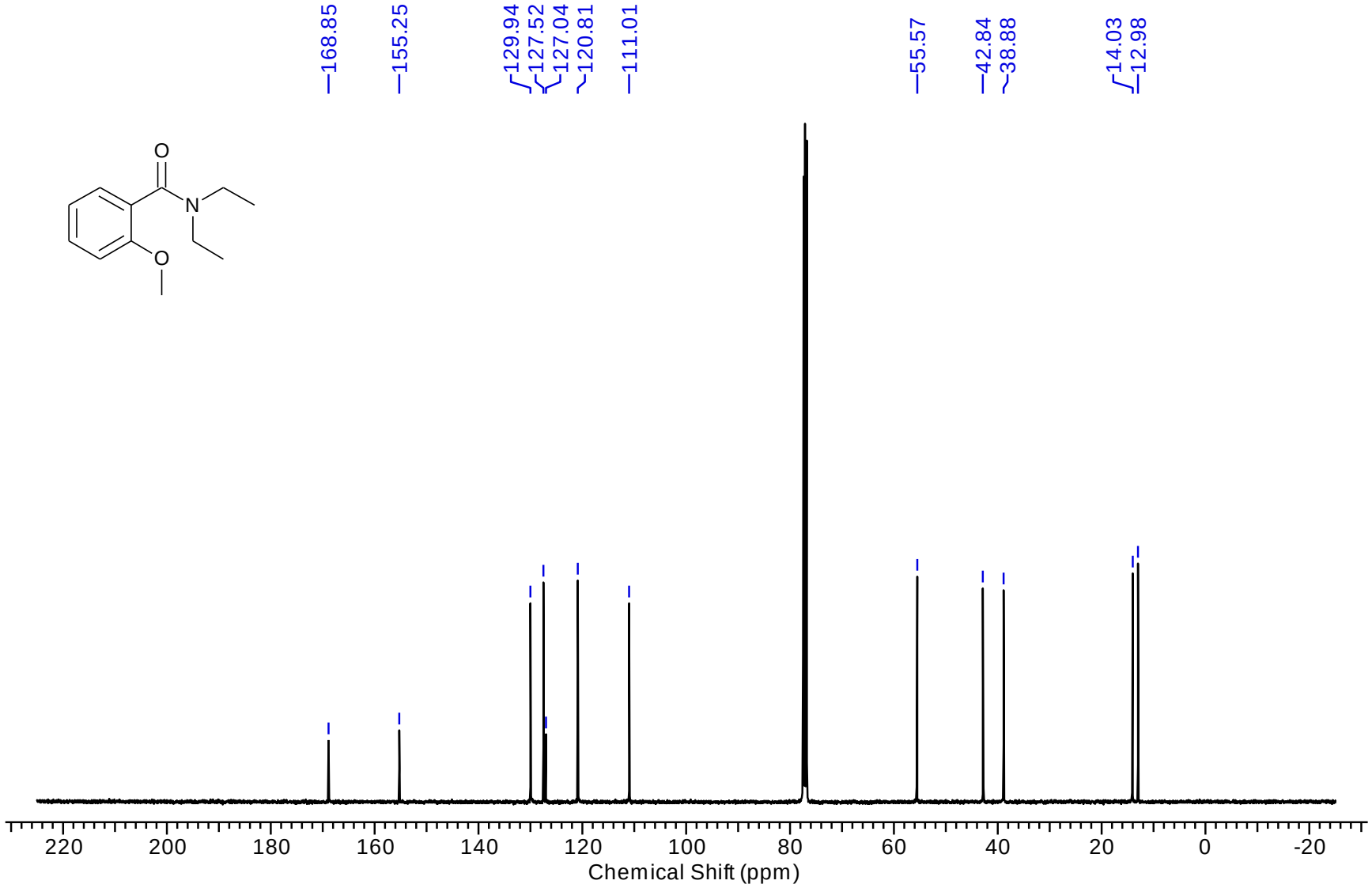

^{1}H NMR spectrum of **128** (400 MHz, $CDCl_3$)

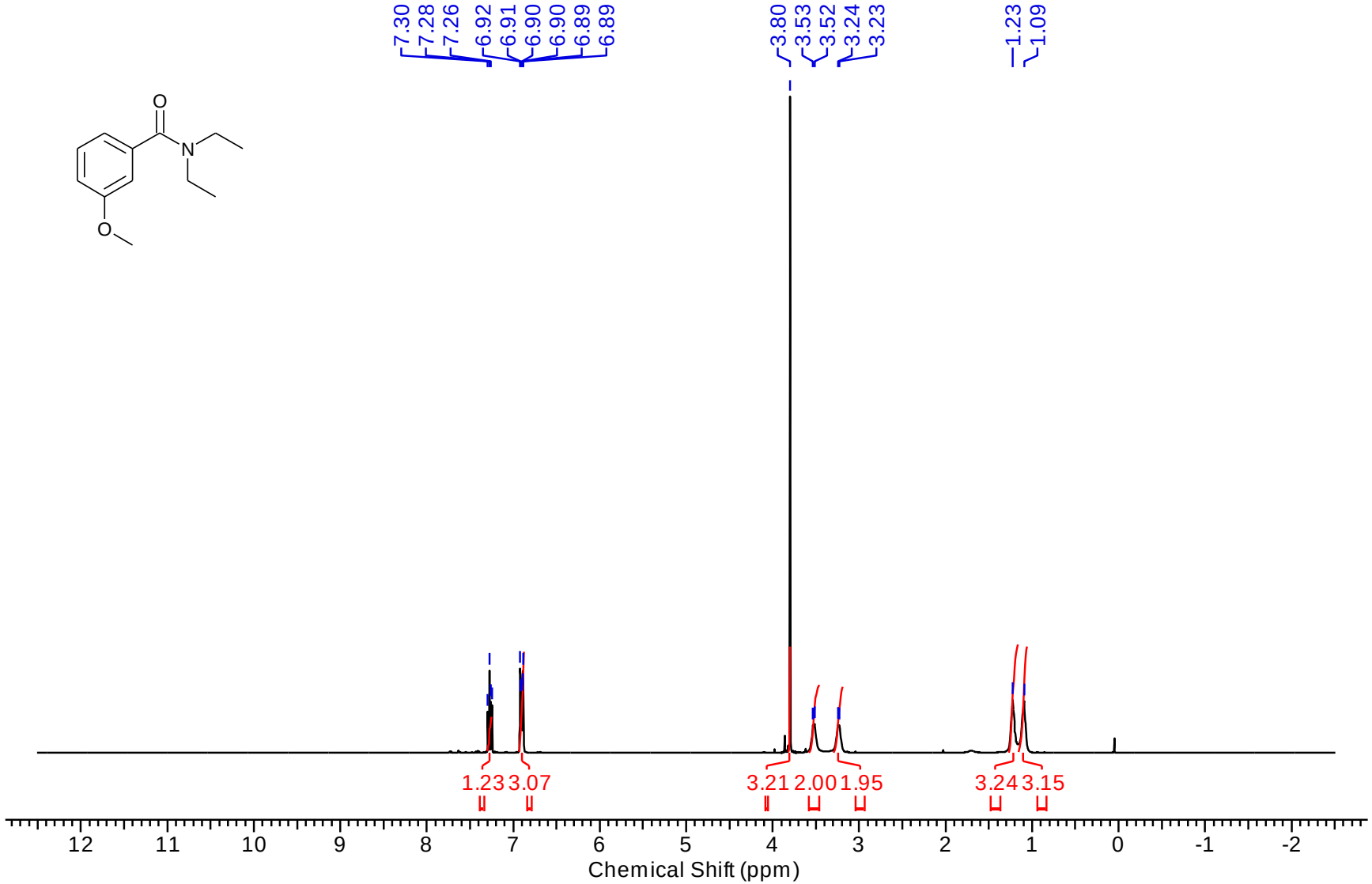

^{13}C NMR spectrum of **128** (101 MHz, $CDCl_3$)

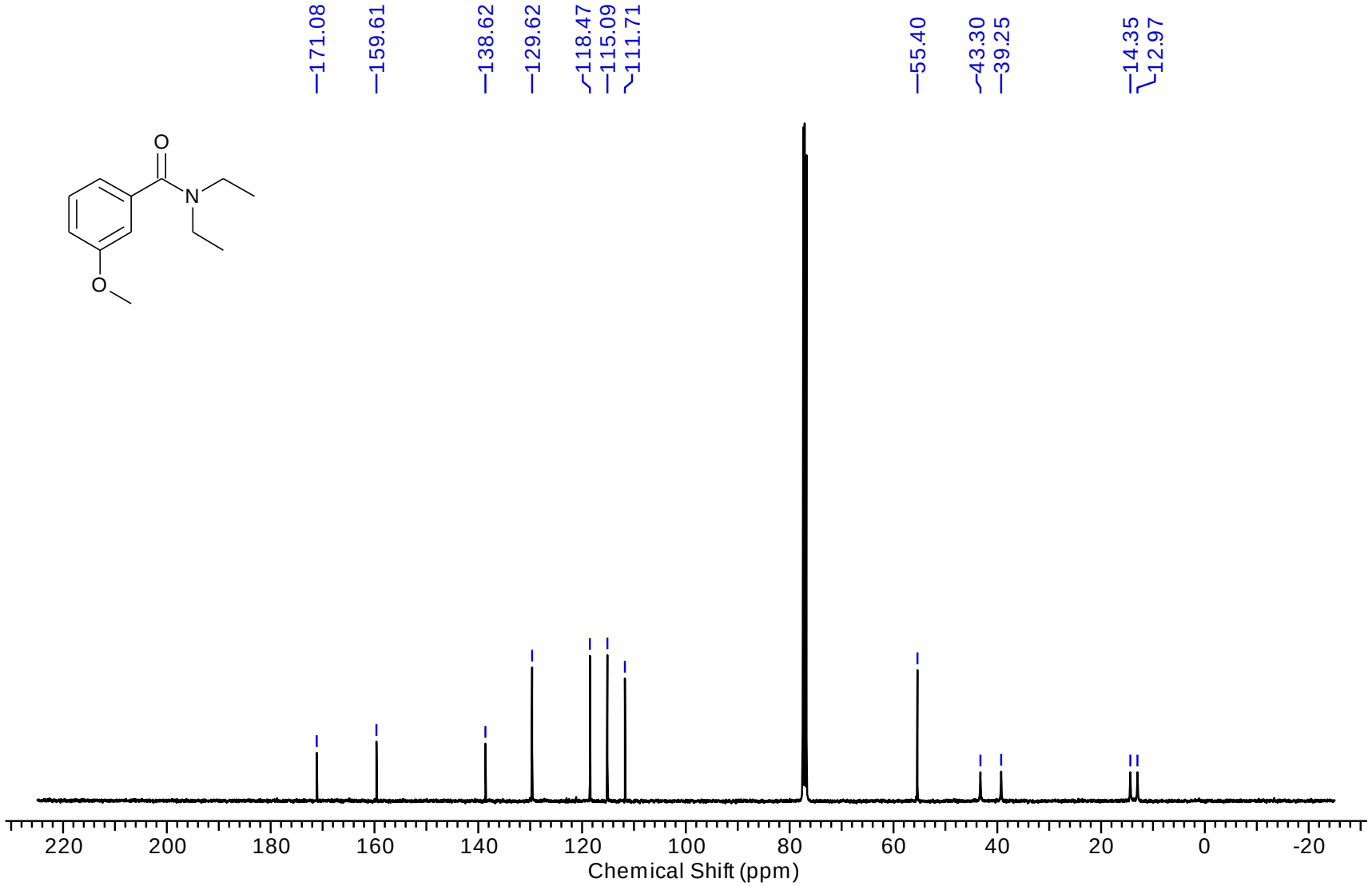

^{1}H NMR spectrum of **129** (400 MHz, $CDCl_3$)

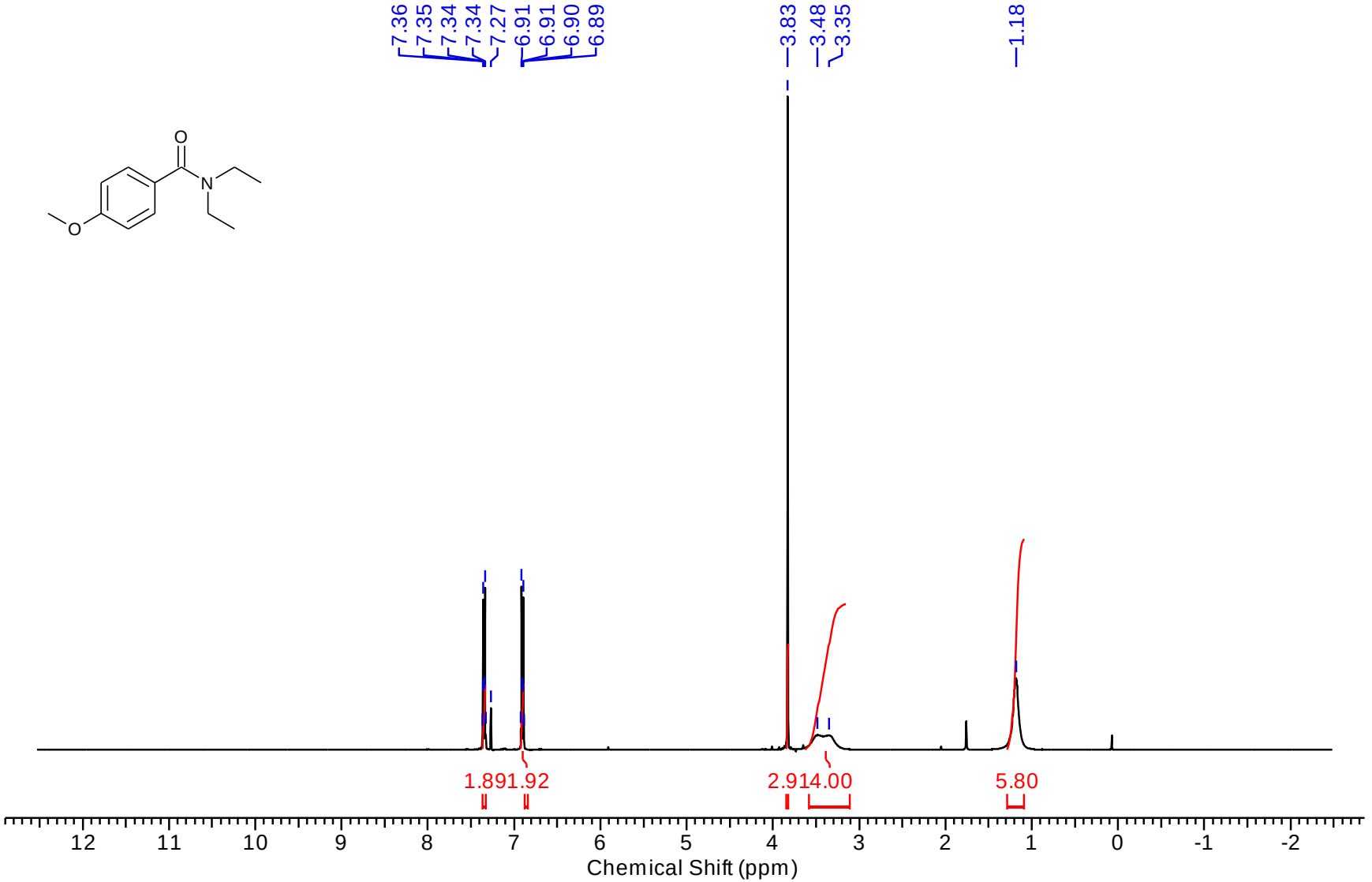

^{13}C NMR spectrum of **129** (101 MHz, CDCl

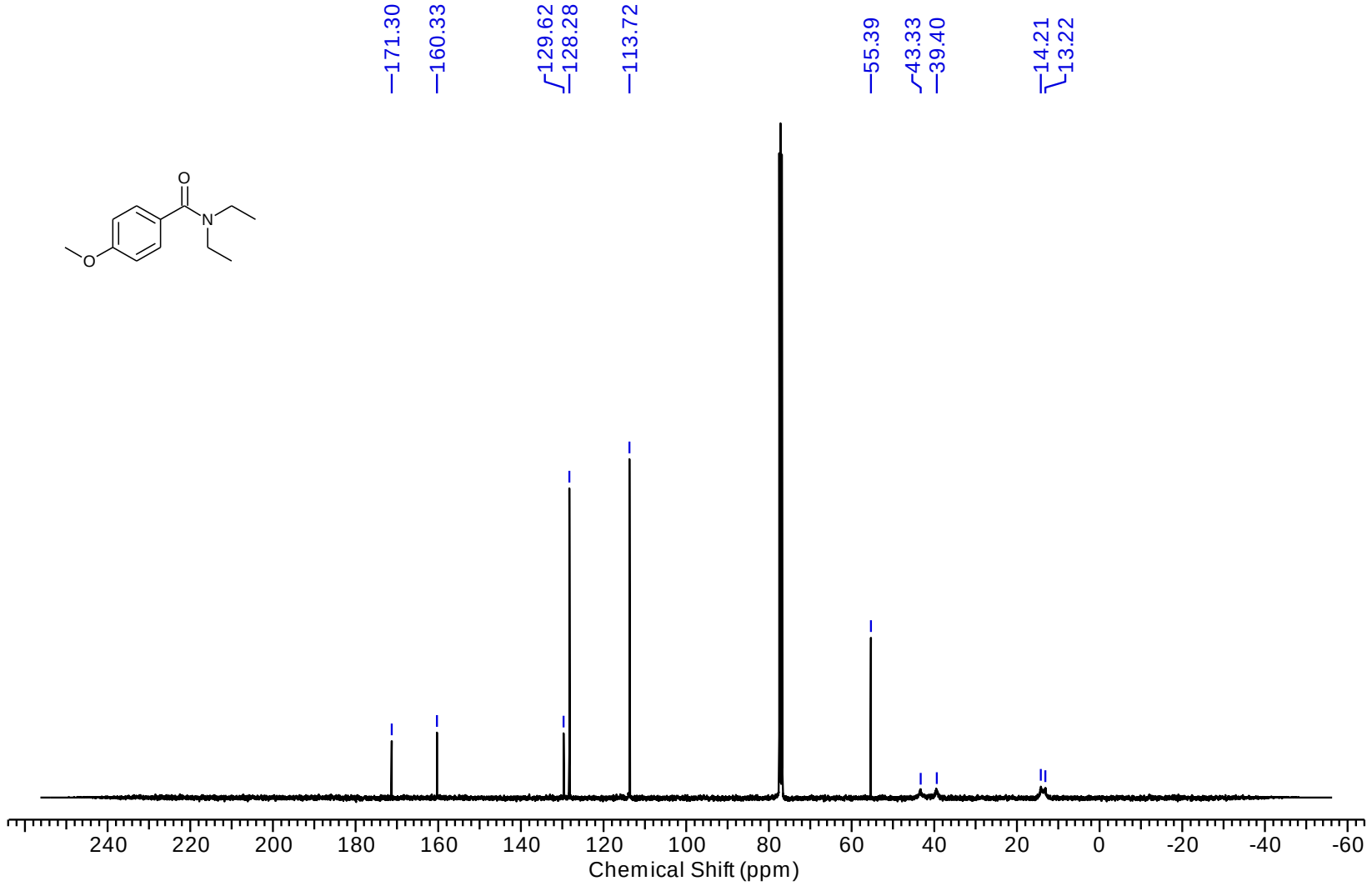

^{1}H NMR spectrum of **130** (400 MHz, CDCl

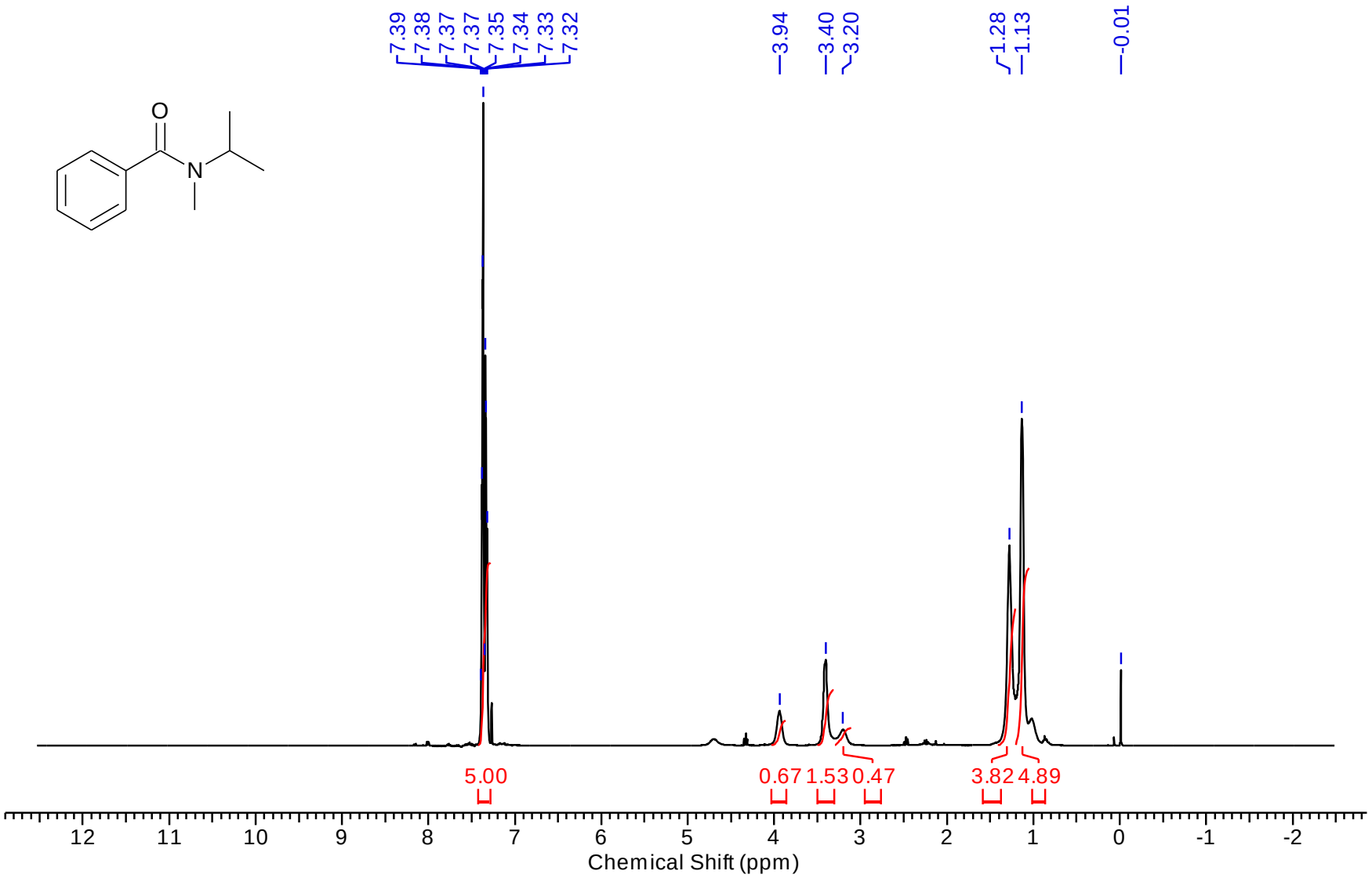

^{13}C NMR spectrum of **130** (101 MHz, $CDCl_3$)

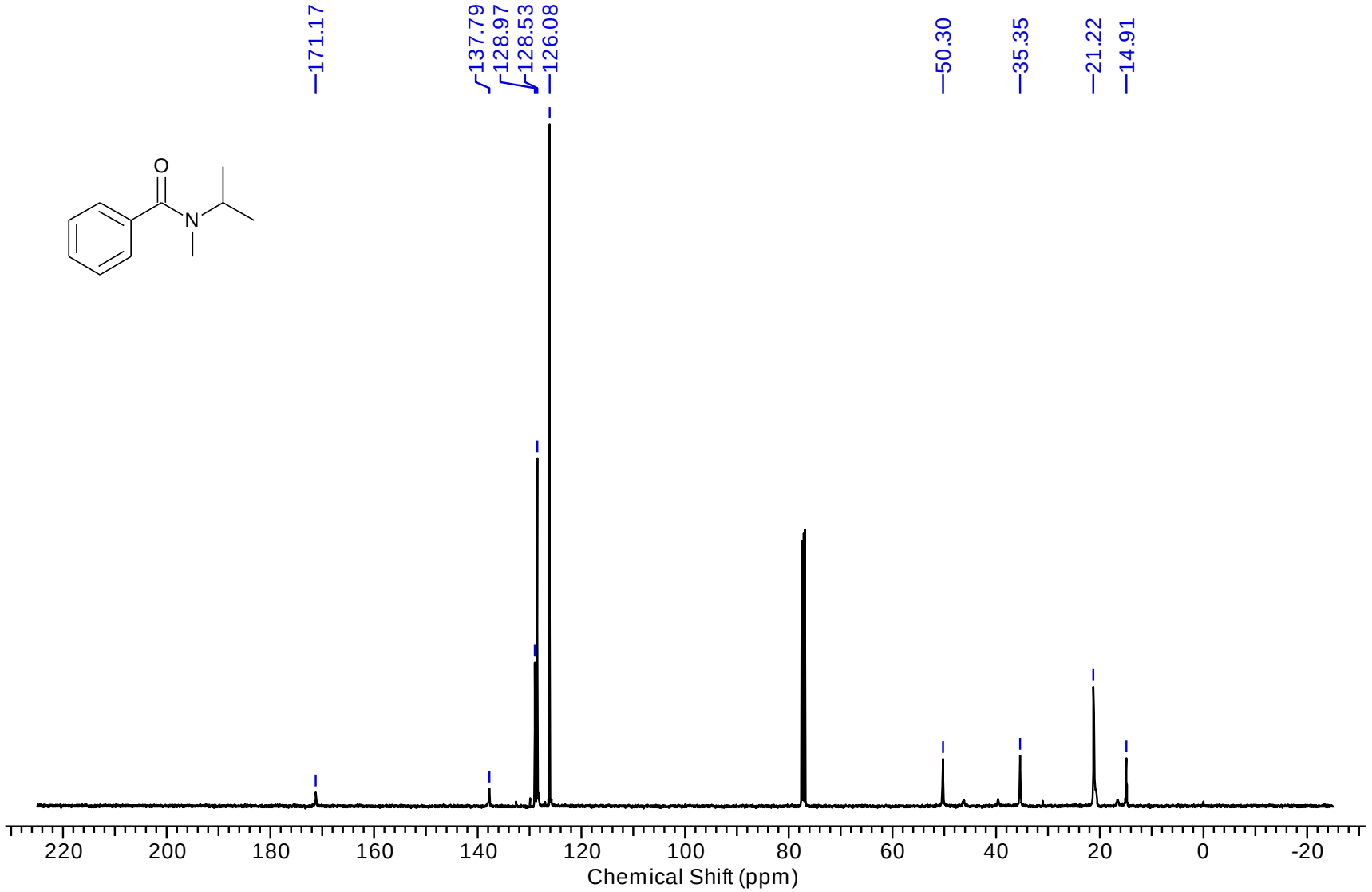

^{1}H NMR spectrum of **131** (400 MHz, $CDCl_3$)

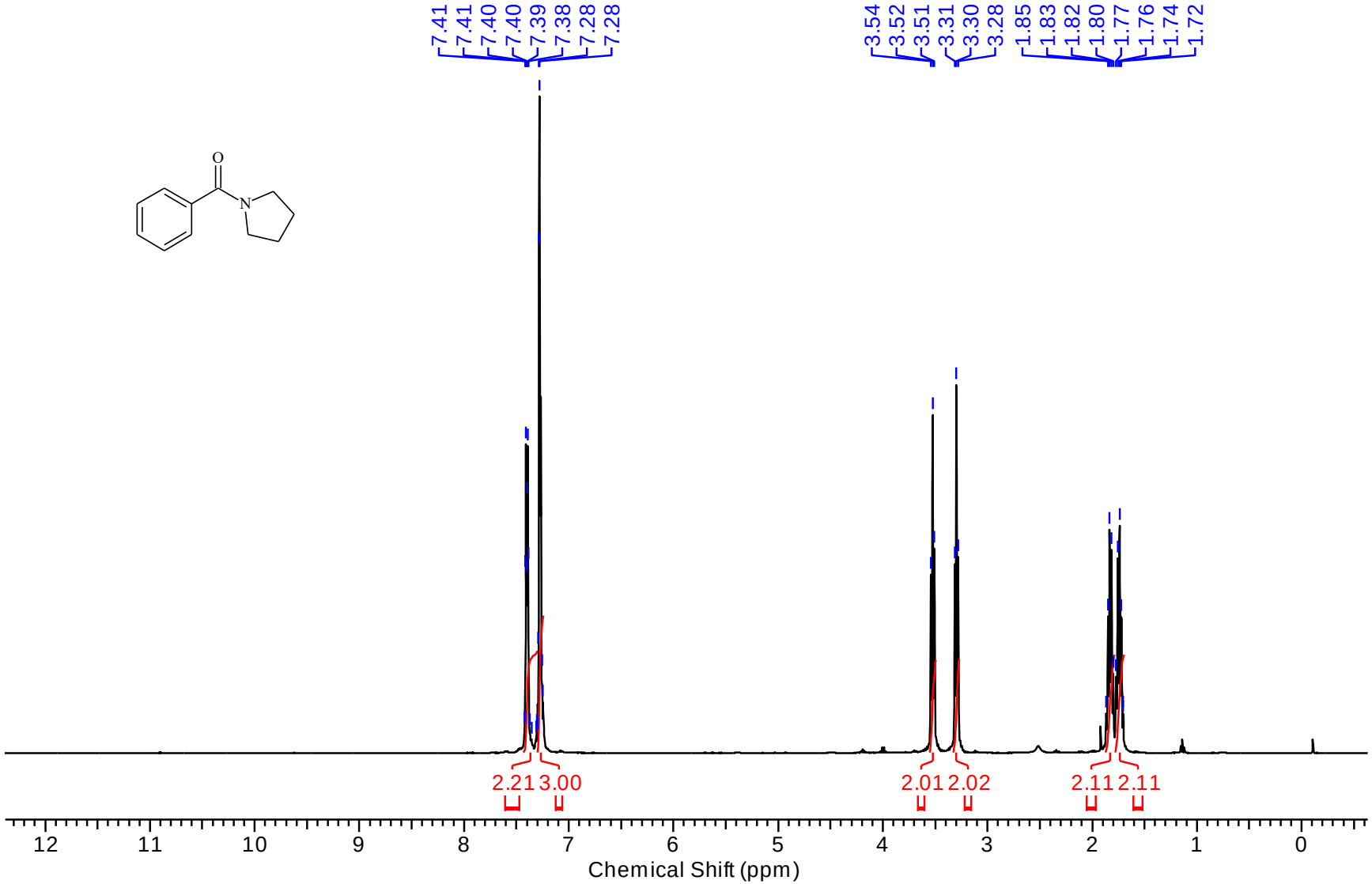

^{13}C NMR spectrum of **131** (101 MHz, $CDCl_3$)

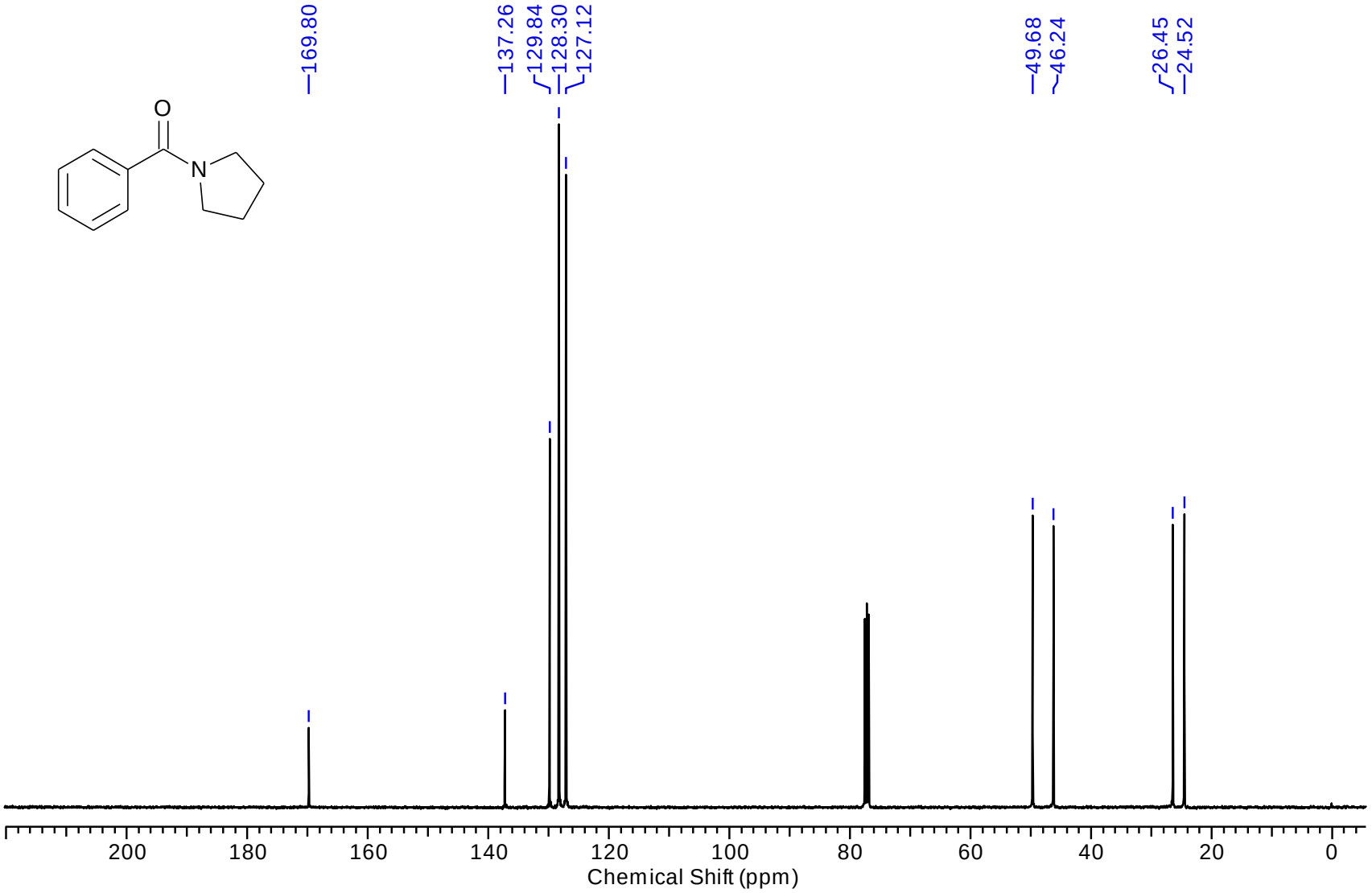

^{1}H NMR spectrum of **132** (400 MHz, CDCl

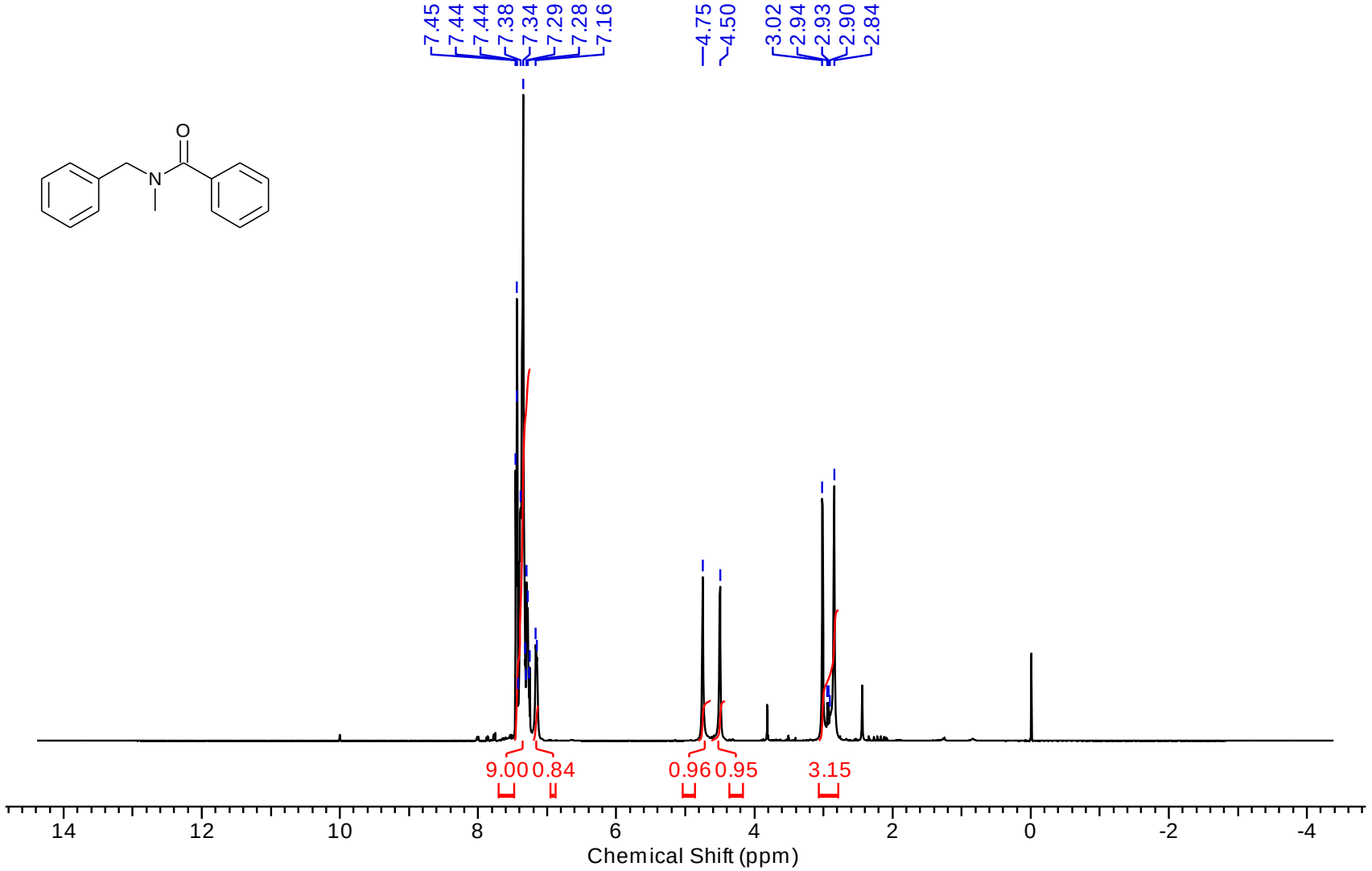

^{13}C NMR spectrum of **132** (101 MHz, $CDCl_3$)

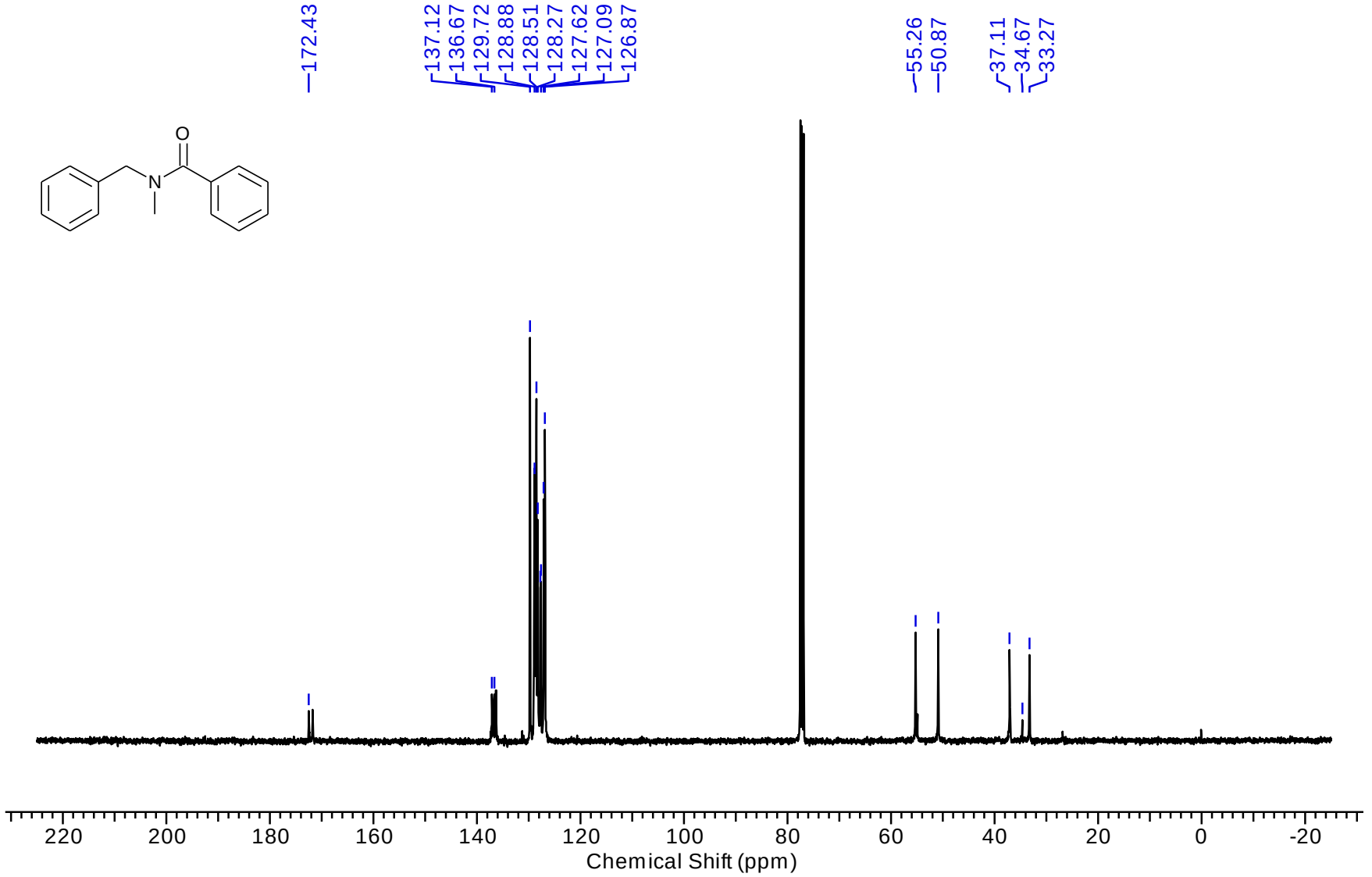

^{1}H NMR spectrum of **154** (400 MHz, $CDCl_3$

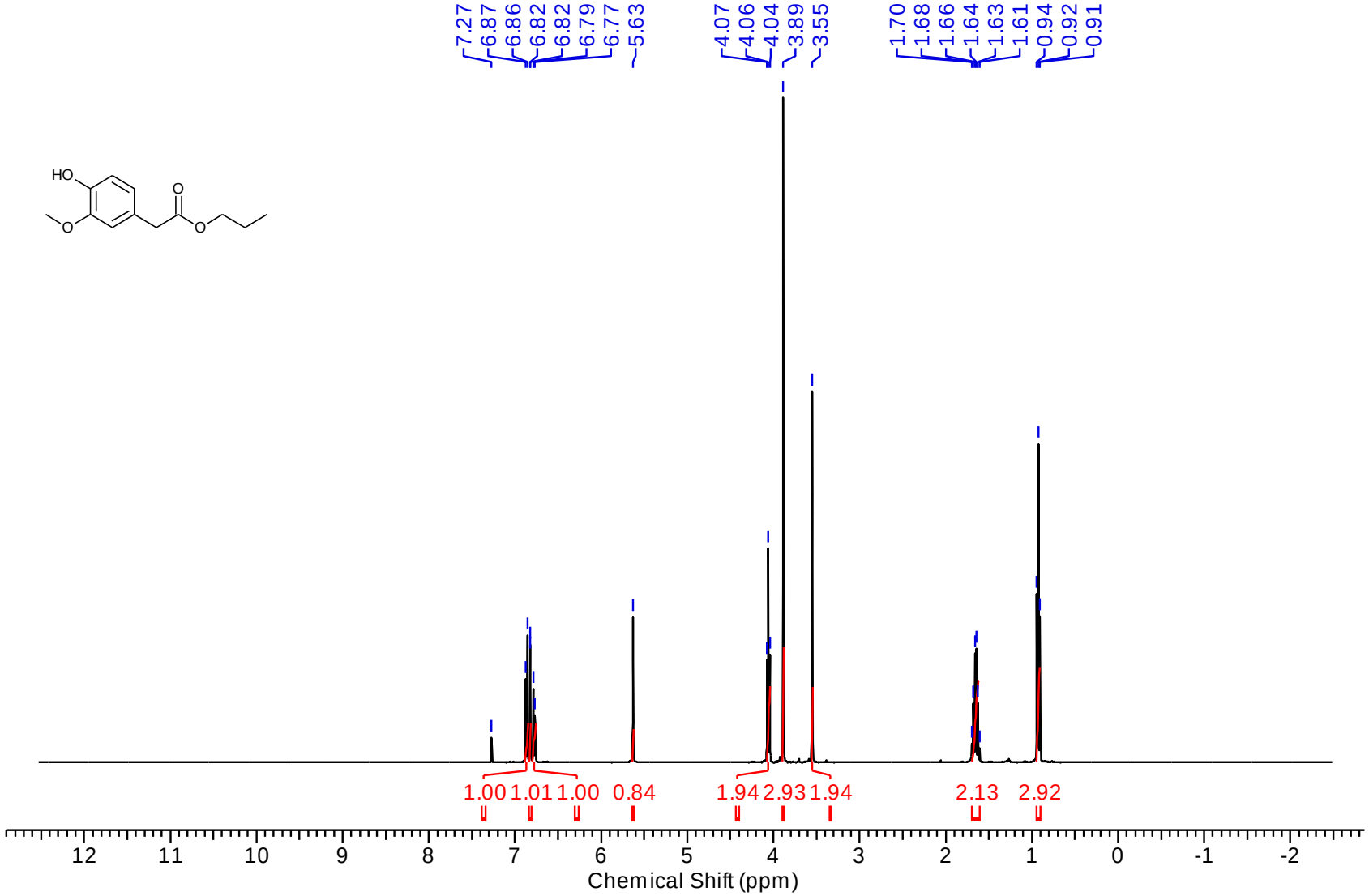

^{13}C NMR spectrum of **154** (101 MHz, $CDCl_3$)

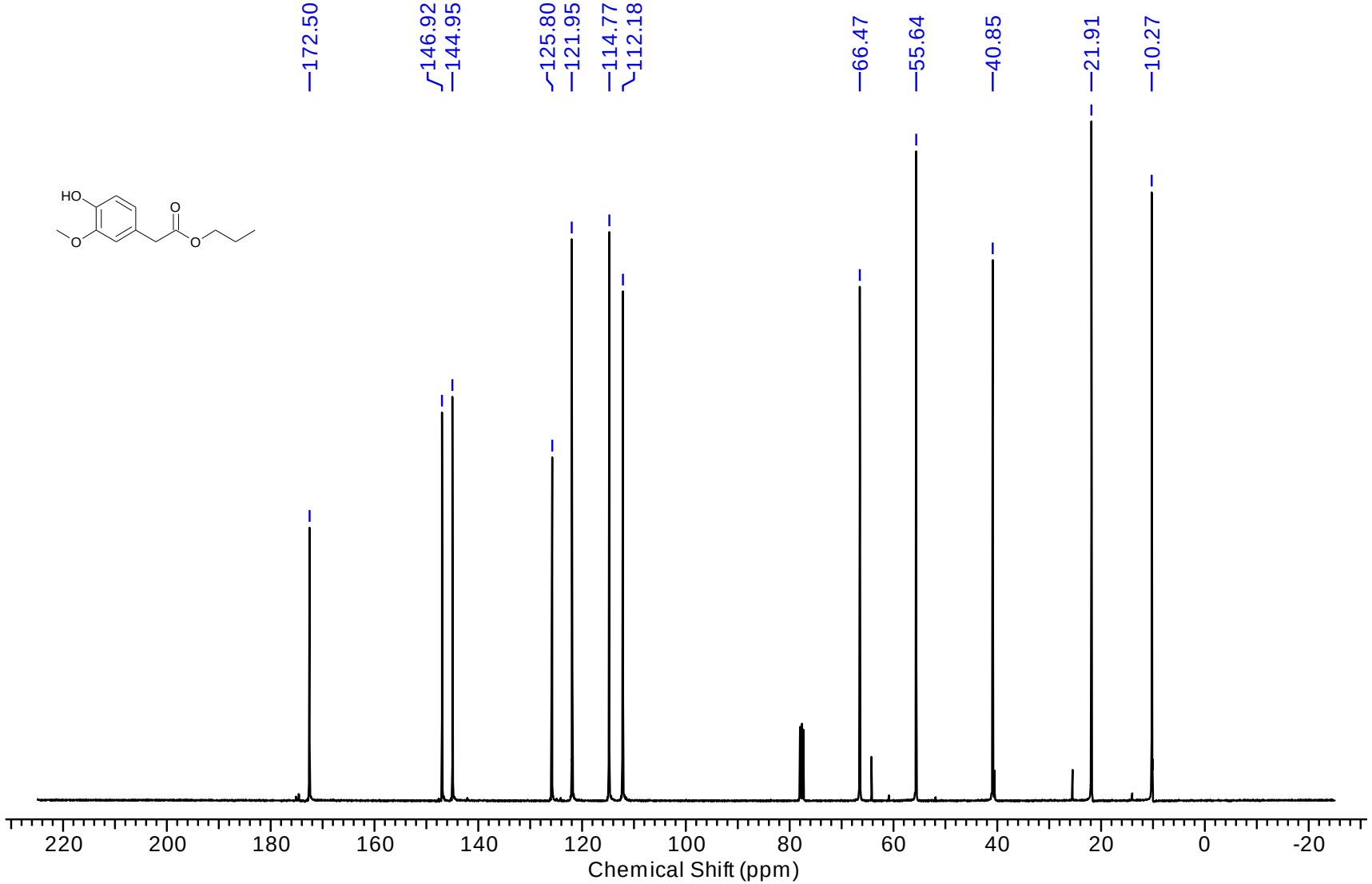

^{1}H NMR spectrum of **155** (400 MHz, $CDCl_3$)

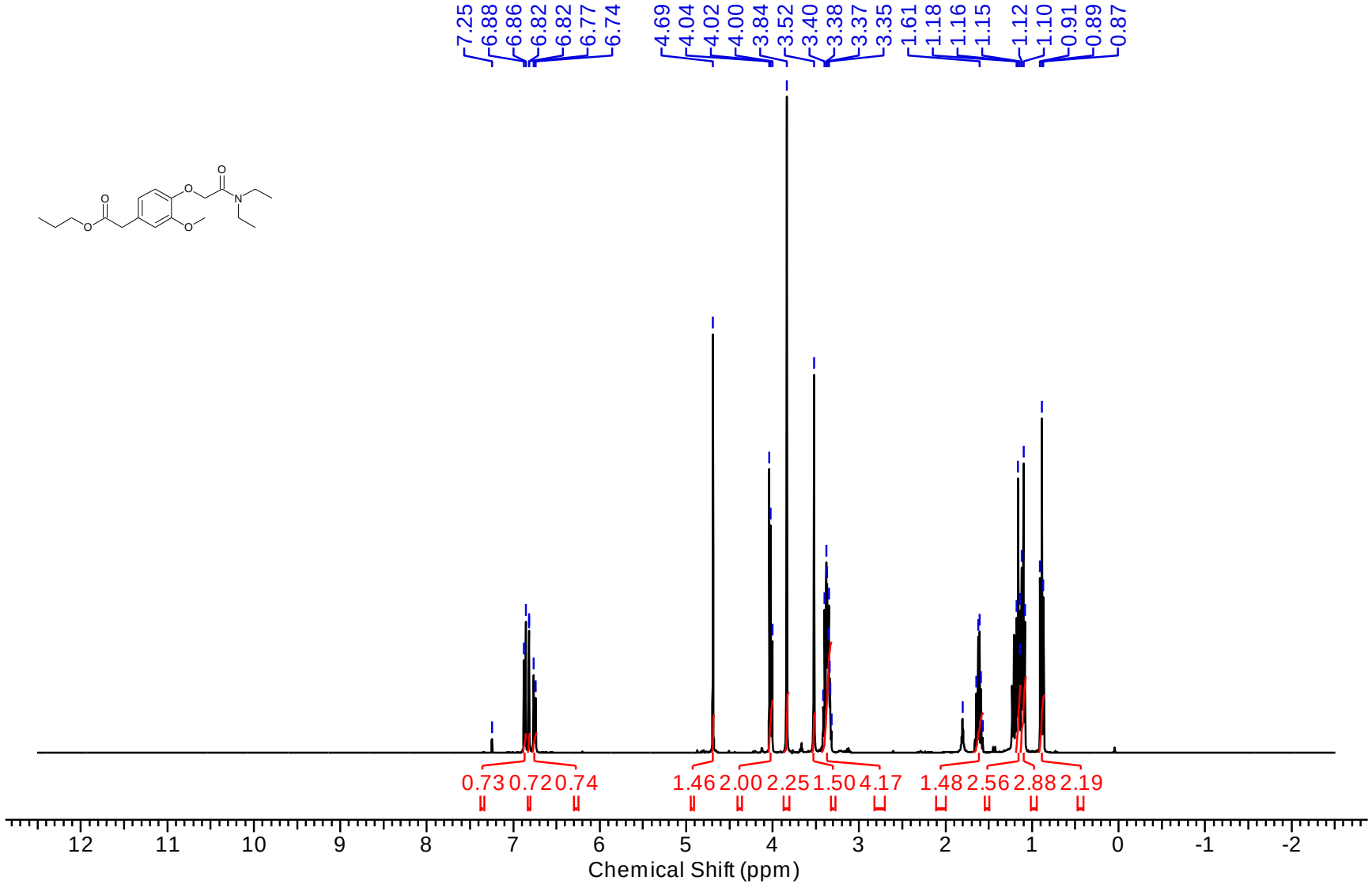

^{13}C NMR spectrum of **155** (101 MHz, $CDCl_3$)

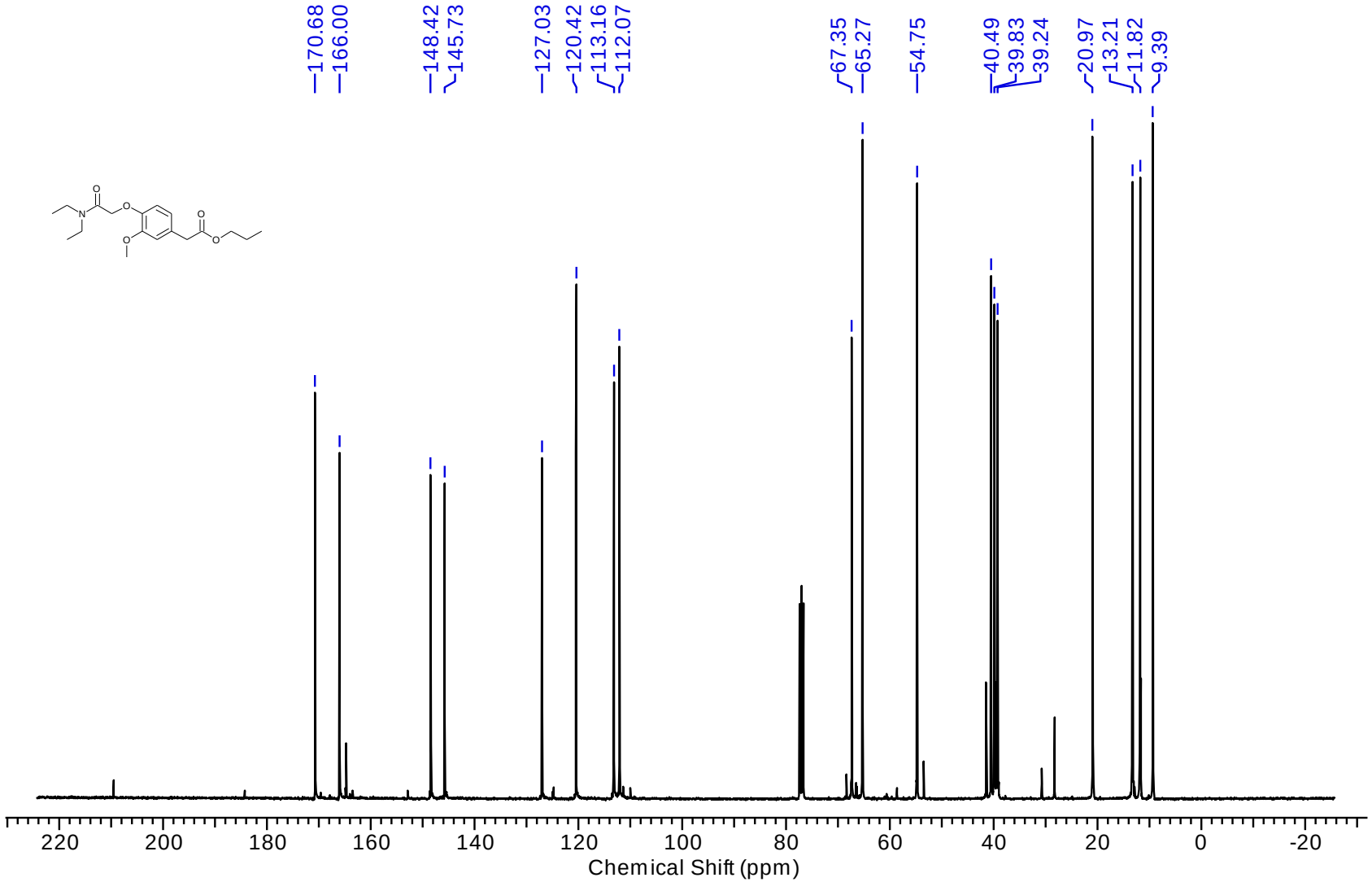

^{1}H NMR spectrum of **107** (400 MHz, $CDCl_3$)

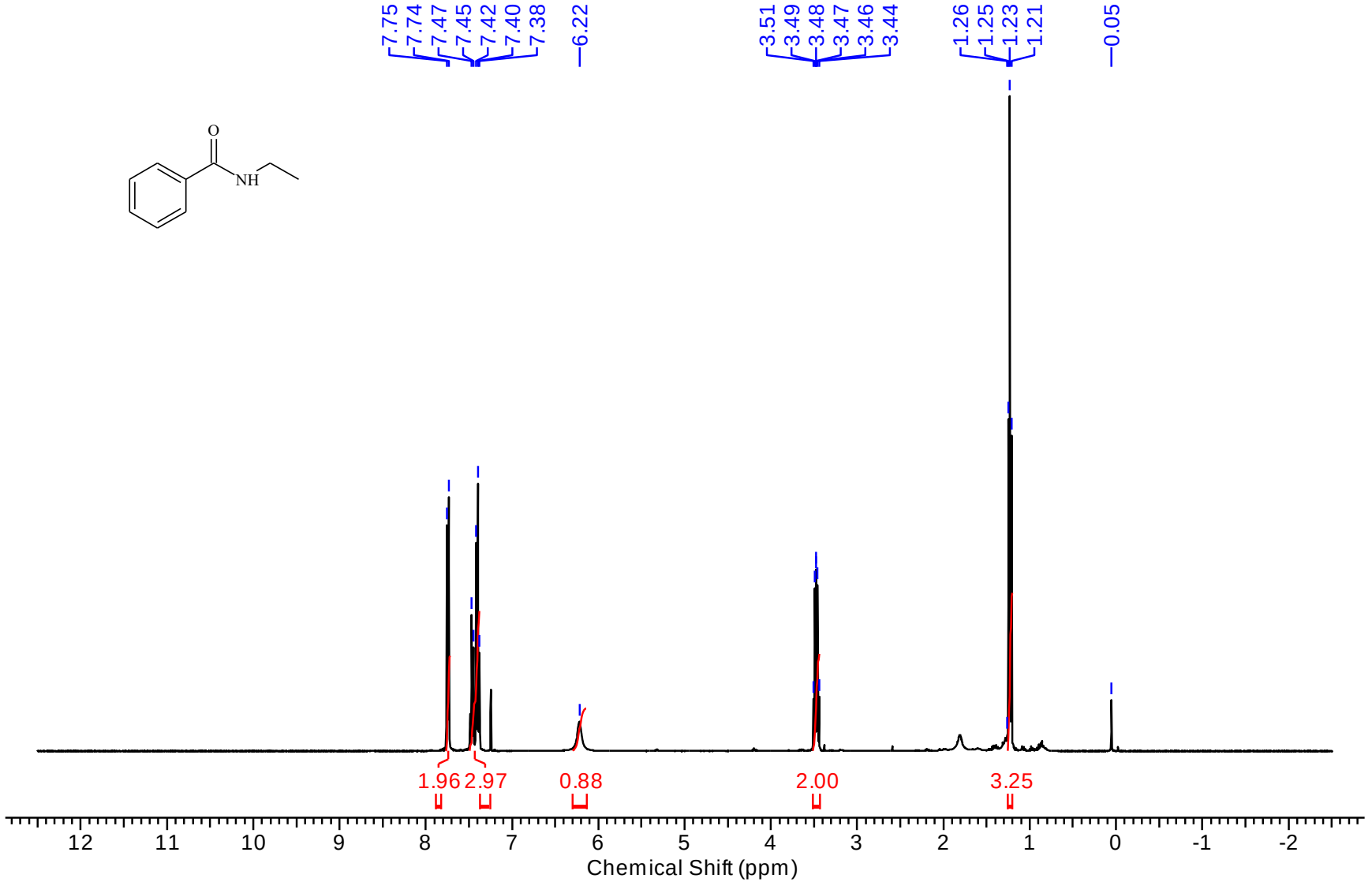

^{13}C NMR spectrum of **107** (101 MHz, $CDCl_3$)

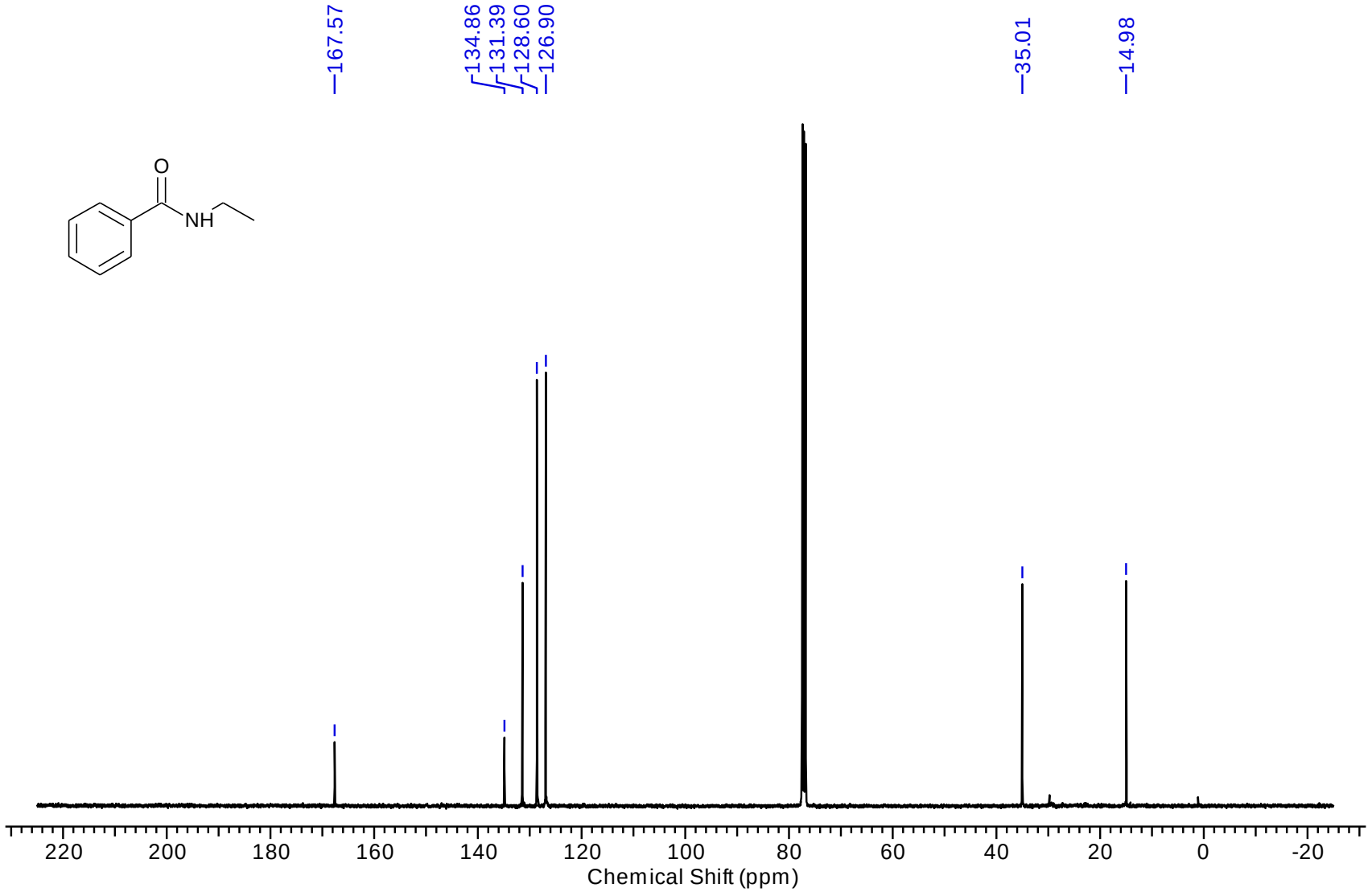

^{1}H NMR spectrum of **138** (400 MHz, CDCl

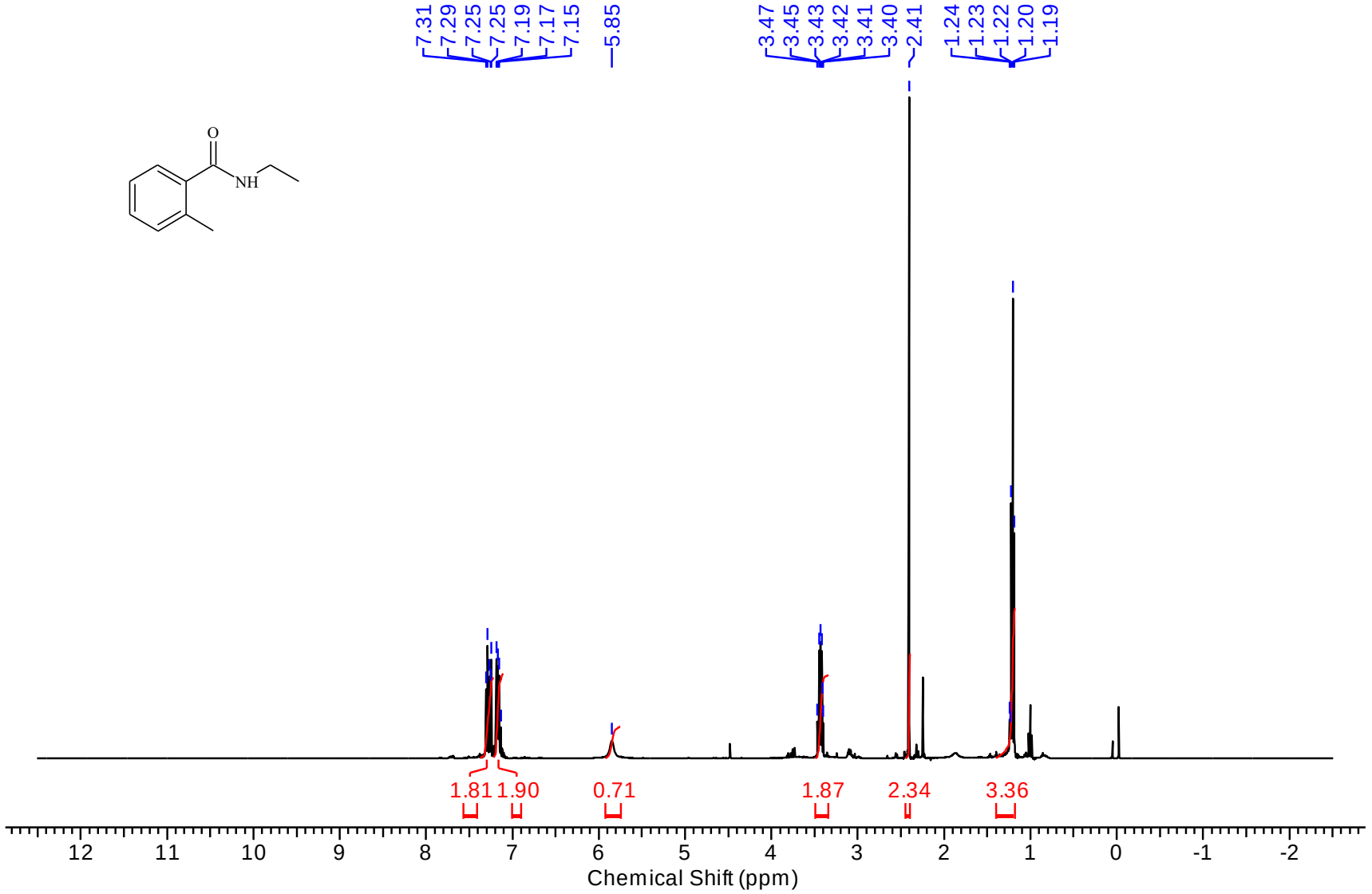

^{1}H NMR spectrum of **134** (400 MHz, $CDCl_3$)

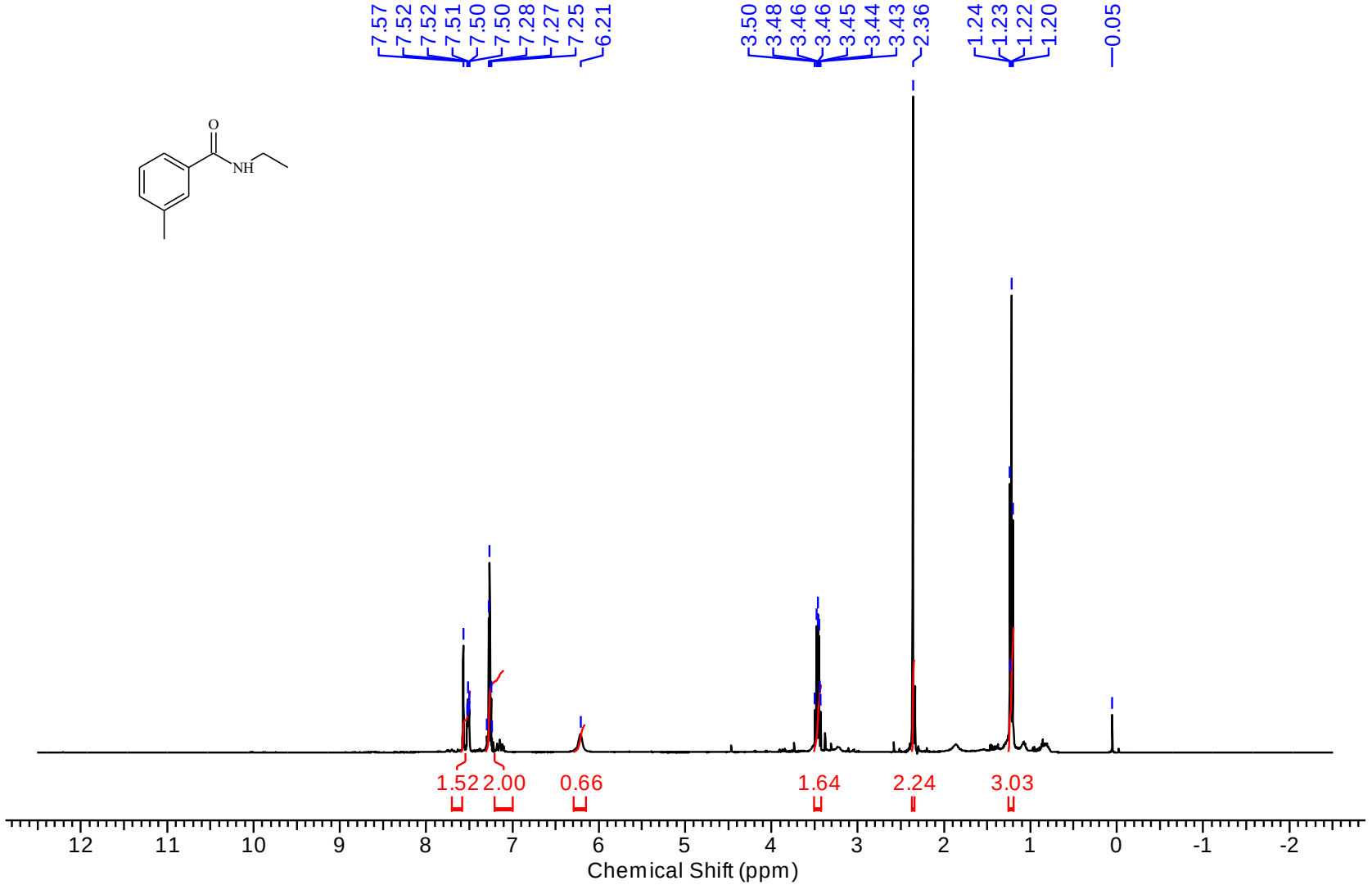

^{1}H NMR spectrum of **140** (400 MHz, $CDCl_3$)

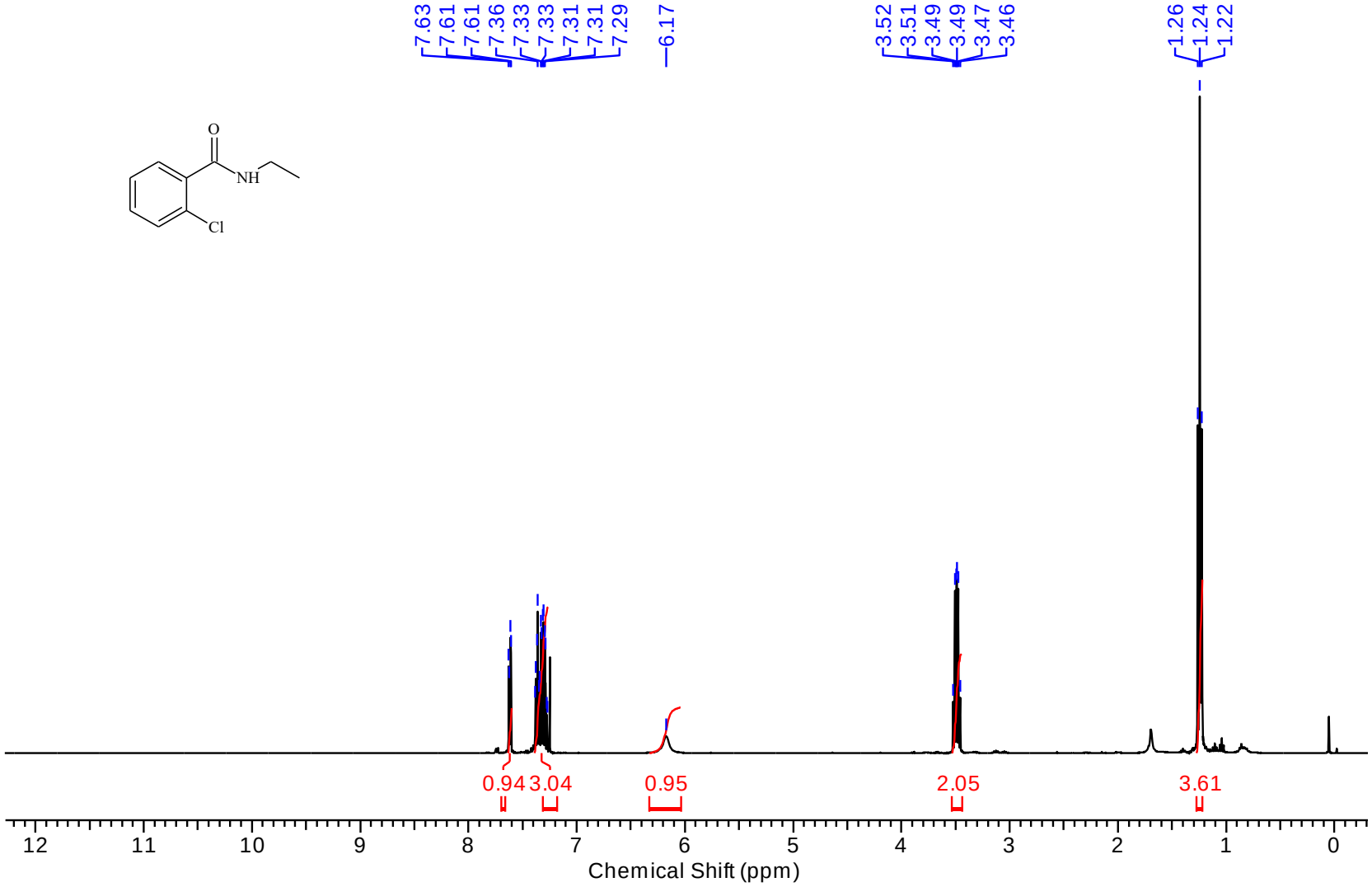

^{13}C NMR spectrum of **140** (101 MHz, $CDCl_3$)

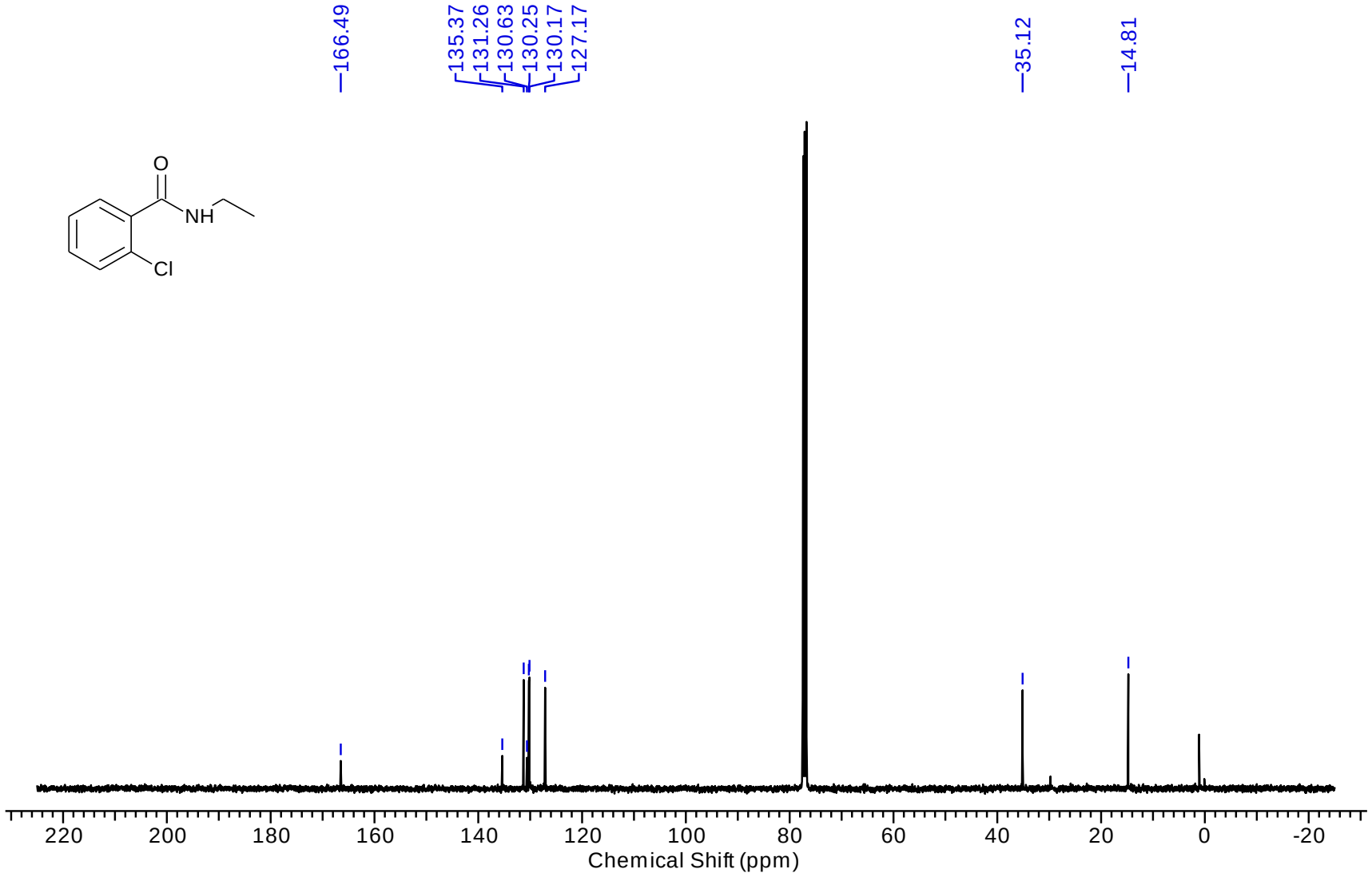

^{1}H NMR spectrum of **141** (400 MHz, $CDCl_3$)

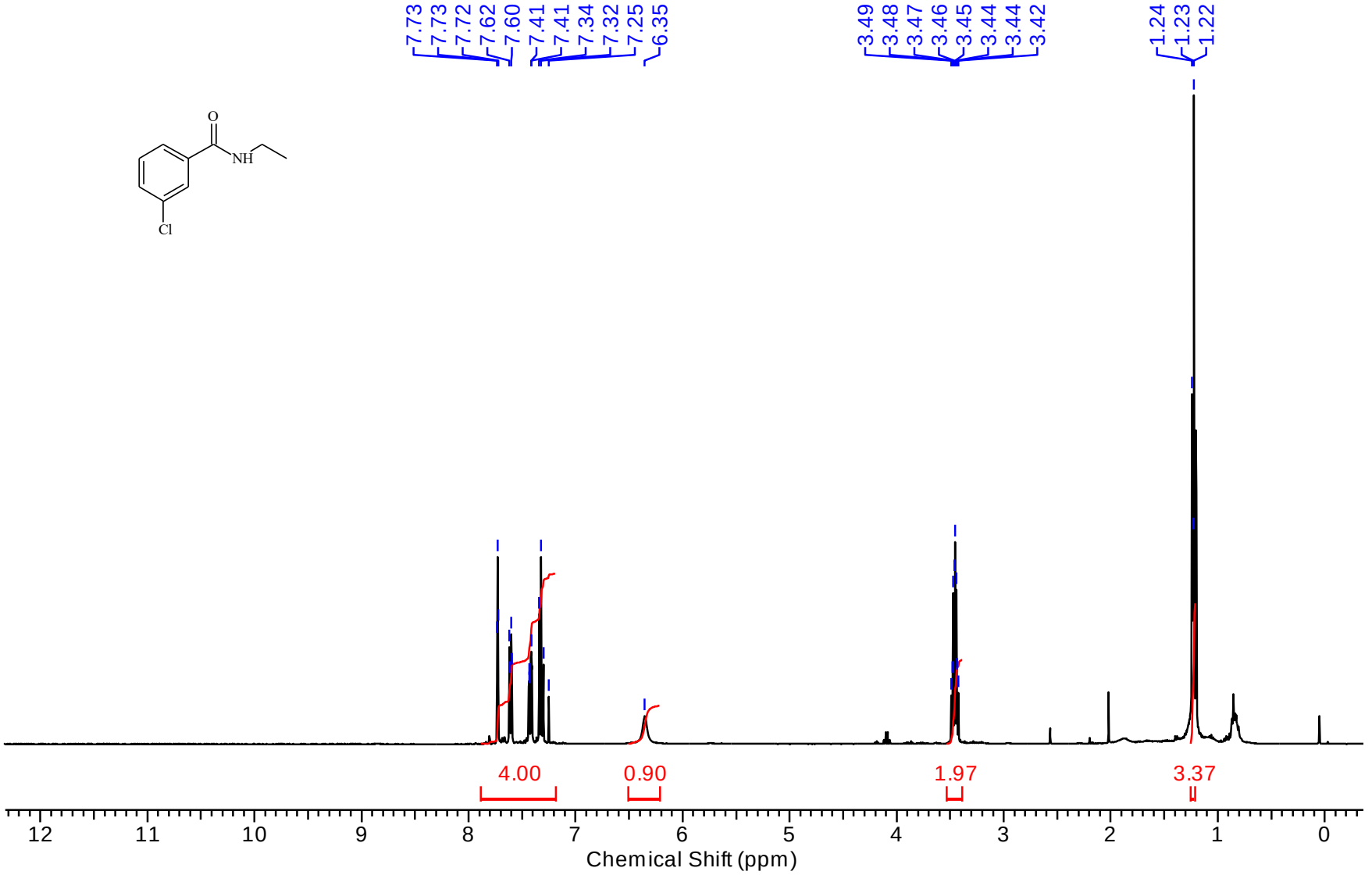

^{13}C NMR spectrum of **141** (101 MHz, $CDCl_3$)

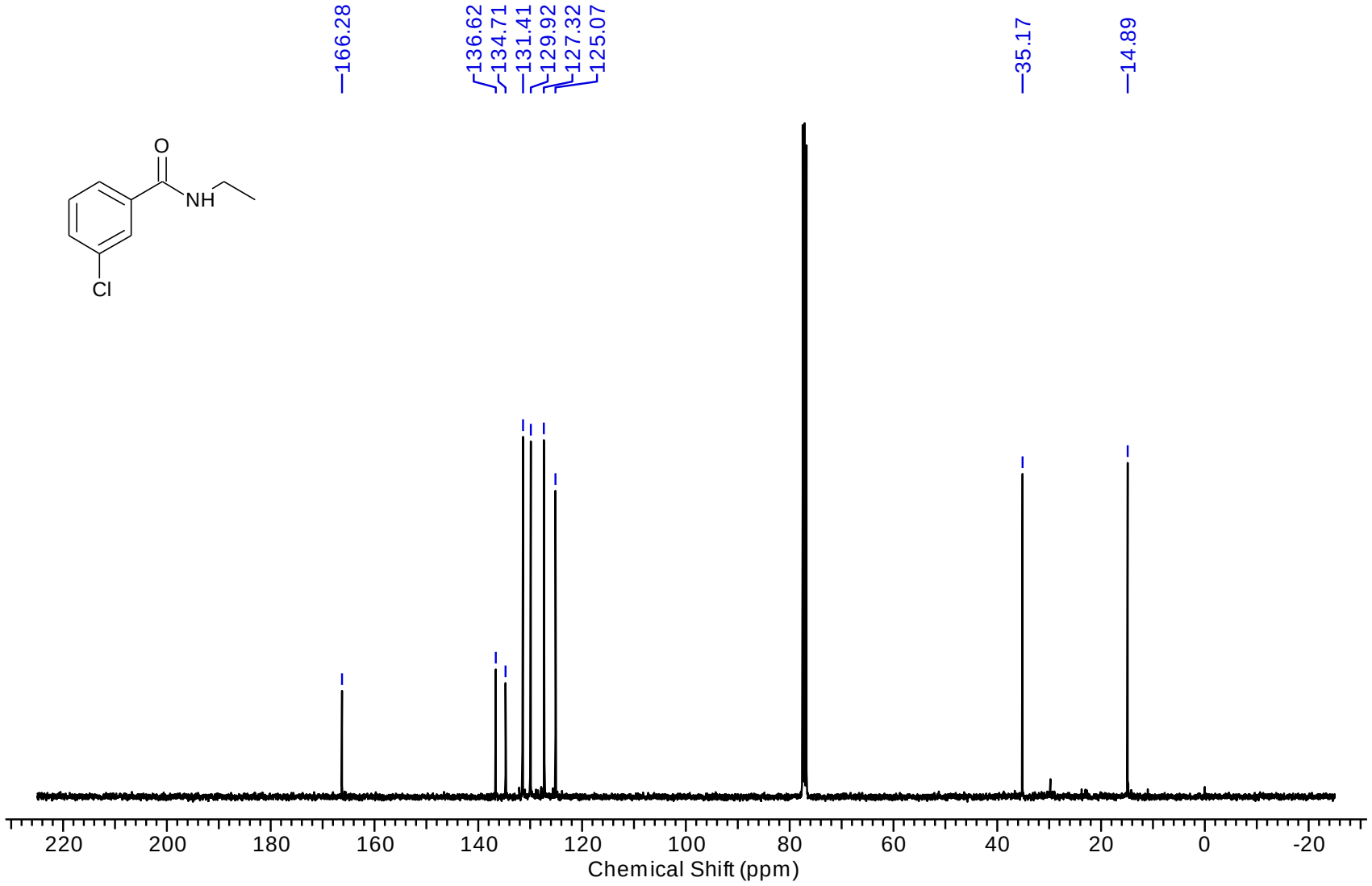

^{1}H NMR spectrum of **142** (400 MHz, $CDCl_3$)

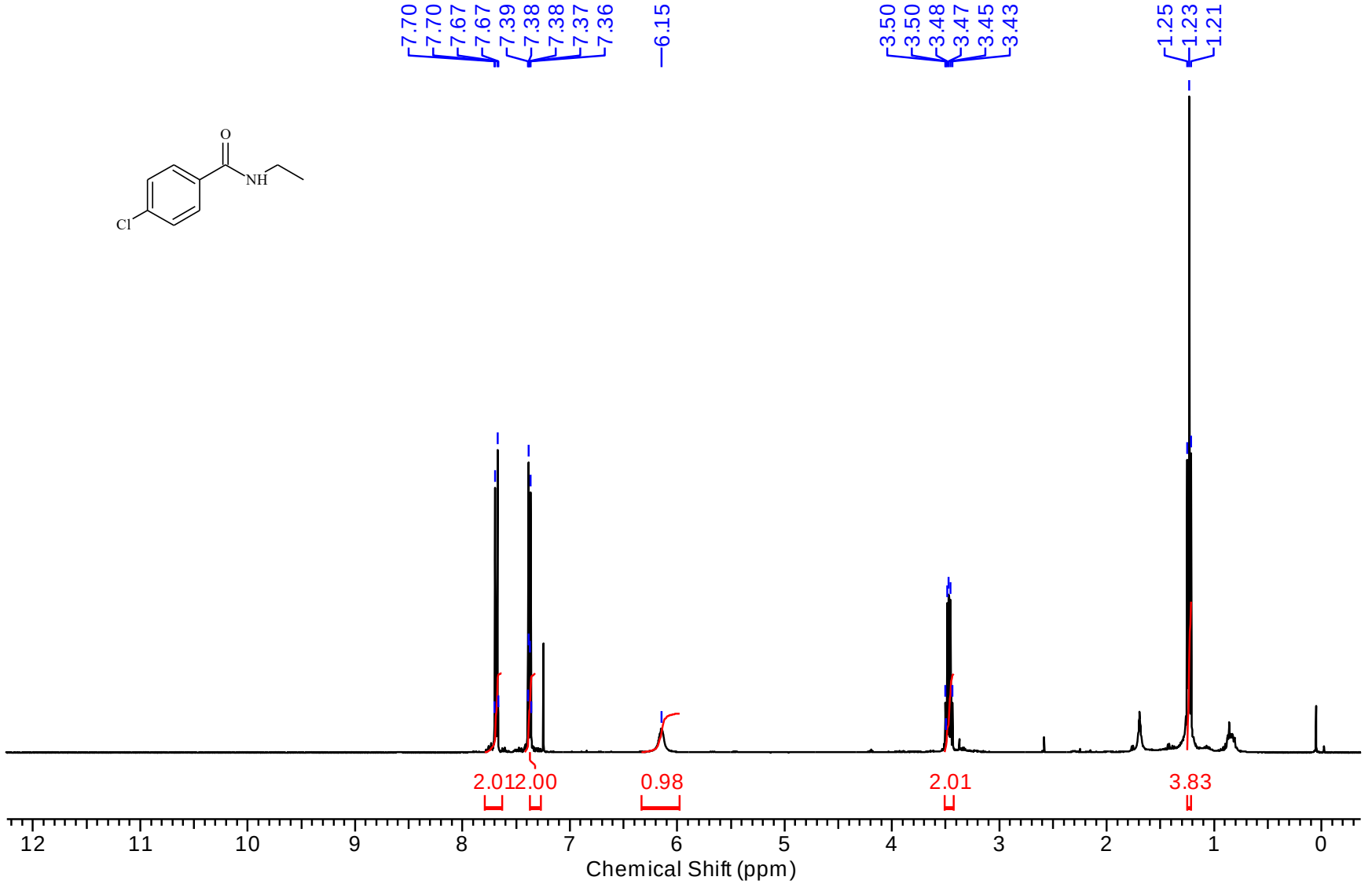

^{1}H NMR spectrum of **153** (400 MHz, $CDCl_3$)

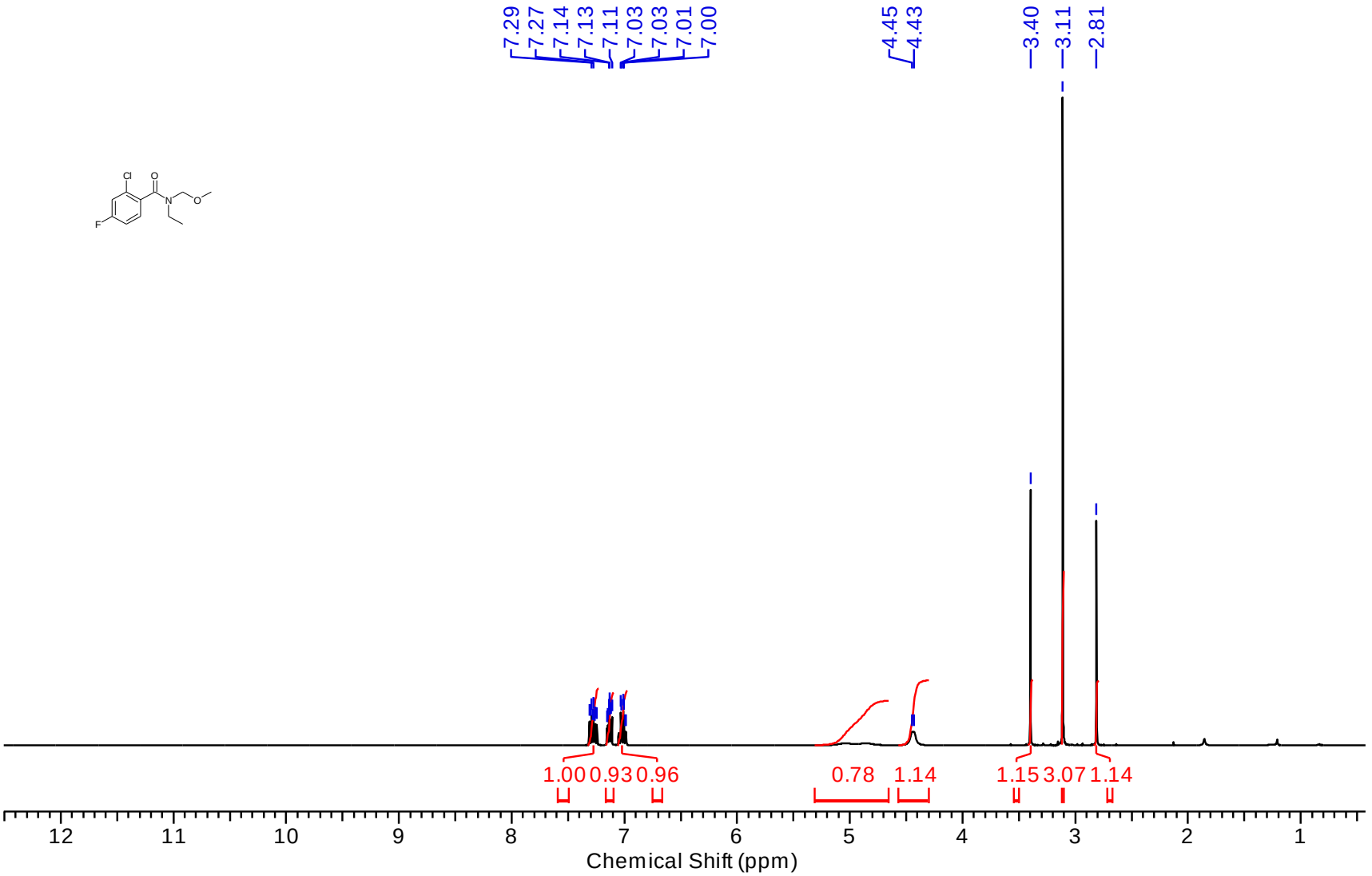

^{13}C NMR spectrum of **153** (101 MHz, $CDCl_3$)